Diagnosis of skin cancer using novel computer vision and deep learning techniques

By
Sumit Kumar Singh

A dissertation submitted for the degree of Master's of Science in Computer Science

School of Computer Science and Electronic Engineering
University of Essex

June 2022

Abstract

Recent years have noticed an increase in the total number of skin cancer cases and it is projected to grow exponentially, however mortality rate of malignant melanoma can be decreased if it is diagnosed and treated in its early stage. Notwithstanding the fact that visual similarity between benign and malignant lesions makes the task of diagnosis difficult even for an expert dermatologist, thereby increasing the chances of false prediction. This dissertation proposes two novel methods of computer-aided diagnosis for the classification of malignant lesion. The first method pre-processes the acquired image by the Dull razor method (for digital hair removal) and histogram equalisation. Henceforth the image is segmented by the proposed method using LR-fuzzy logic and it achieves an accuracy, sensitivity and specificity of 96.50%, 97.50% and 96.25% for the PH2 dataset; 96.16%, 91.88% and 98.26% for the ISIC 2017 dataset; 95.91%, 91.62% and 97.37% for ISIC 2018 dataset respectively. Furthermore, the image is classified by the modified You Only Look Once (YOLO v3) classifier and it yields an accuracy, sensitivity and specificity of 98.16%, 95.43%, and 99.50% respectively. The second method enhances the images by removing digital artefacts and histogram equalisation. Thereafter, triangular neutrosophic number (TNN) is used for segmentation of lesion, which achieves an accuracy, sensitivity, and specificity of 99.00%, 97.50%, 99.38% for PH2; 98.83%, 98.48%, 99.01% for ISIC 2017; 98.56%, 98.50%, 98.58% for ISIC 2018; and 97.86%, 97.56%, 97.97% for ISIC 2019 dataset respectively. Furthermore, data augmentation is performed by the addition of artefacts and noise to the training dataset and rotating the images at an angle of 65^0, 135^0, and 215^0 such that the training dataset is increased to 92838 from 30946 images. Additionally, a novel classifier based on inception and residual module is trained over augmented dataset and it is able to achieve an accuracy, sensitivity and specificity of 99.50%, 100%, 99.38% for PH2; 99.33%, 98.48%, 99.75% for ISIC 2017; 98.56%, 97.61%, 98.88% for ISIC 2018 and 98.04%, 96.67%, 98.52% for ISIC 2019 dataset respectively. Later in our dissertation, the proposed methods are deployed into real-time mobile applications, therefore enabling the users to diagnose the suspected lesion with ease and accuracy.

Acknowledgement

I would like to thank my supervisors Dr Vahid Abolghasemi and Dr Hossein Anisi for their invaluable advice, continuous support and patience during my master's study. Their immense knowledge and experience have not only guided me through the right path while writing this dissertation but also have encouraged me to stay motivated in my daily life and academic research. I would also like to thank my flatmates for their constant support while writing this dissertation. Finally, I would like to express my gratitude to my parents and younger brother, without their encouragement and tremendous understanding in the last few months, it would have been impossible for me to complete my study.

Table of contents

List of figures

List of tables

List of acronyms

2D	Two dimensional
3D	Three dimensional
CAD	Computer aided diagnosis
UV rays	Ultraviolet rays
MM	Malignant melanoma
NM	Non Malignant
BN	Benign Nevus
SK	Seborrhoeic Keratosis
ACS	American Cancer Society
FOV	Field of View
ROI	Region of Interest
FL	Fuzzy Logic
ANN	Artificial Neural Network
MLP	Multilayer Perceptron
CNN	Convolutional neural network
SVM	Support Vector Machine
KNN	K-nearest neighbour
FCN	Fully convolutional network
CDCNN	Convolutional-Deconvolutional CNN
YOLO	You Look Only Once
PCA	Principal component analysis
ABCDE	Asymmetrical Border Colour Diameter Evolution
CASH	Colour, Architecture, Symmetry, and Homogeneity
ELM	Epiluminescence microscopy
ISIC	International Skin Imaging Collaboration
SNR	Signal to Noise Ratio
PSNR	Peak Signal to Noise Ratio
MSE	Mean Squared Error
RMSE	Root Mean Squared Error
UIQI	Universal Image Quality Index
IOU	Intersection Over Union
TP	True Positive
TN	True Negative
FP	False Positive
FP	False Negative
ROC	Receiver Operating Characteristic
AUC	Area Under Curve

List of publications

[1] Singh, S.K, Abolghasemi, V, and Anisi, H.M, " Diagnosis of Melanoma skin lesion using Deep learning technique and fuzzy algorithm". Computer Methods and Programs in Biomedicine. [Under review]

[2] Singh, S.K, Abolghasemi, V, and Anisi, H.M, Chakraborty. A " Skin cancer diagnosis based on Neutroscopic features with a Deep Neural Network". Medical and Biological Engineering and Computing [Under review]

Chapter 1: Introduction

Scientific surgical instruments and modernised medicines have led to advancement in the field of medical science, which increases the effectiveness of treatment thereby improving the quality of life of a patient. However, researchers and medical practitioners across the globe are struggling to discover effective cancer treatments. As mentioned in the reports of the National Skin Cancer Institute, skin cancer is the most frequently diagnosed cancer [1]. Furthermore, World Health Organization(WHO) reports that skin cancer accounts for one-third of the total cancer cases, moreover the total count of cases seems to increase with time [2]. Skin being the largest and most widespread sense organ of human anatomy is vulnerable to numerous allergies and deadly diseases. Dermis, Epidermis and Hypodermis are the three sequential overlapped protective layers of epithelial tissues of human anatomy, they have individually defined functions and characteristics. The pigment that resides along the junction of epidermis and dermis is called melanin, which is responsible for the prominent colouration of hair, skin and iris. Melanocytes are pigment-producing cells, and the amount of pigment present in an individual depends on geographical location and historical exposure to the sun and/or other tanning devices. Pheomelanin and eumelanin are two major chemical forms of melanin, the former being responsible for light colour pigmentation, while the latter is responsible for dark pigmentation. Eumelanin is considered to be more photo-protective than pheomelanin due to its dark pigment. The proportion of pheomelanin present in both light and dark-toned individuals is almost akin, however abundance of epidermal eumelanin results in a highly pigmented individual. As reported by National Skin Cancer Institute, people with high pigmentation are less susceptible to defacement caused by harmful ultra-violet rays or other tanning mechanisms, thereby they are at low risk of developing skin cancer[1]. The human body is defended against harsh exposure to the sun by two protective cells of the skin: epidermal and dermal, however uncontrollable growth of these cells along with melanocytes may damage the DNA stand, and these deformities are capable of the rapid growth of epithelial cells which may result in the formation of intimidating tumours and various skin

diseases. According to studies, the unexpected rise in the number of skin cancer cases is due to the depletion of the ozone layer which led to overexposure to harmful UV-A and UV-B radiations[3]. Moreover, skin cancer can be caused due to various other factors like- genetic history of carcinogenic genes in the family, sudden growth in several dysplastic nevi and benign melanocytic nevi over various parts of the body, lack of melanin pigment or discolouration of hair and iris.

Skin cancer can be broadly classified into Nevus, Benign and Malignant types, the earliest is solely a birth mark or a mole representing as a beauty mark, while the benign type is not being noxious to an individual, the latter is injuries and deadly, because malignant types of skin cancer can rapidly spread in and over skin while draining protein and nutrition from neighbouring cell and thereby infecting the cells in this process. Squamous cell carcinoma (SCC), basal cell carcinoma (BCC) and malignant melanoma (MM) are three most frequently diagnosed skin cancerous cells. Vast range of skin cancerous cells are benign and non-melanocytic in nature, thus they are not considered to be harmful; BCC and SCC are among non-melanocytic category, while MM is considered to be most minacious and it causes highest number of deaths due to skin cancer [4]. Superficial spreading melanoma, nodular melanoma, acral lentiginous melanoma and lentigo maligna melanoma are the four generalised categories of malignant melanoma. Figure 1.1 illustrates different forms of melanoma on various parts of the body. Superficial spreading melanoma is mostly widespread type of melanoma skin cancer which appears on limbs and trunk of human anatomy. The cancerous cell seems to grow slowly but eventually, it spread over the surface of the skin. The second most regular and aggressive category of melanoma skin cancer is nodular melanoma, it emerges as bluish-black or reddish colour lesion over the neck, head and trunk of the human body and shows faster growth of lesions than other types of melanoma skin cancer. Acral lentiginous melanoma is the rarest type of malignant lesion but tends to be a regularly diagnosed lesion for darkly pigmented individuals, it appears over soft and light pigmented part of human anatomy such as soles of feet, palms of the hand

and underneath the nails. Lentmalignantigna melanoma usually is not a common type of malignant skin cancer and it majorly develops in aged adults on the overexposed parts of the body, such as the face, which are regularly exposed to immoderate sunlight for ages. Lentigo maligna melanoma type of skin cancer is also termed as Hutchinson's freckle because of its appearance like a stain on the skin. It is considered to be less harmful and noticed to grow slowly as compared to other melanoma lesions [5].

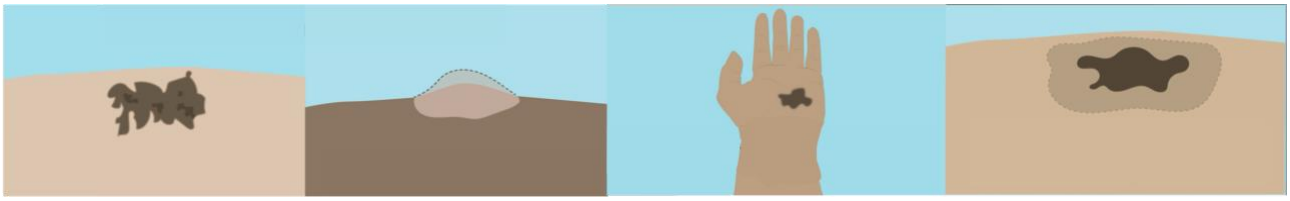

(a) (b) (c) (d)

Figure 1.1: Pictorial representation of different types of melanoma (a) Superficial spreading melanoma (b) Nodular melanoma (c) Acral lentiginous melanoma (d) Lentigo maligna melanoma

According to recent reports, both sexes are equally affected by malignant melanoma[6], however, the mortality rate in male patients arise reported to be higher. Scientists have stated that malignant melanoma emanates during its radial growth phase from the epidermis of the skin and further penetrates dermis layer of the skin when the prognosis of skin cancer turns to be increasingly poor in the course of its vertical growth phase. According to dermatologists, malignant melanoma appears as an ameboid or irregular shaped mole of diameter more than 6mm, which can originate on the dermis layer of the skin either from a pre-existing mole by changing its shape, size, texture and colour or form a new abnormal-looking lesion. Regular moles are smaller in dimension as compared to a melanoma lesion. Moreover, a melanoma lesion is in the shades of blueish-grey, black and brown which is not the colour of a typical-regular mole. Conventionally, malignant melanoma is defined as a fast-growing tumour with an irregular surface. It is explicated as an asymmetrically shaped lesion with various shades of colour contours stretching from blueish-grey to black. Various colour pigments are clustered to form a contour of colour on the lesion. As the tumour grows with time itching, ulceration and inflammation are the signs of a matured lesion. Few lesion even shows bleeding from

the tumour in its developed phase. However, dermatologists assert that a melanoma lesion might not show any regular features or signs of being malignant melanoma on the skin and it can also appear on parts of the body which are never been exposed to harmful UV rays. Figure 1.2 portrays the growth of malignant melanoma in different stages. Malignant melanoma originates from the epidermal layer of the skin in stage 0 which is often termed as 'melanoma in its situ' by medical practitioners. Furthermore, the lesion drives deeper up to 2 millimetres (mm) down the outer skin layer in stage 1 of melanoma skin cancer where it might form ulceration. Stage 2 of malignant lesion marks a deeply immersed lesion up to 4mm, although melanoma can be cured till this stage as the lymphatic nodes are not being affected by this time, thus the survival rate of a patient if diagnosed at/before Stage 2 of melanoma skin cancer is higher than being diagnosed of skin cancer at its later stages. Stage 3 marks the destruction of lymphatic nodes along with lymph channels and shows ulceration and sign of swelling over the outer layer of the skin, in some cases the malignant tumour also shows signs of bleeding over the lesion. Cancer would be spread into various organs and damaged distant lymph nodes in Stage 4 of malignant skin cancer. Additionally, these cancerous moles are capable of metastasizing from epithelial tissues to different parts of human anatomy including the cerebrum and bone marrow, thereafter the chances of survival of a patient decrease by 80% even after surgery or radiation treatment like chemotherapy. Therefore, accurate detection of malignant melanoma in its situ or early phase becomes imperative, however, diagnosis of melanoma is a more tedious task than other forms of skin cancer because of its uncertainty of features and varied complexities of a malignant lesion and intense rapidity of spreading. With the advancement in the field of medical vision and dermoscopic tools, dermatologists across the globe can diagnose a lesion with more accuracy and certainty. The proposed dissertation aims to propose an effective and novel tool for accurate, fast and easy diagnosis of a deadly melanoma lesion.

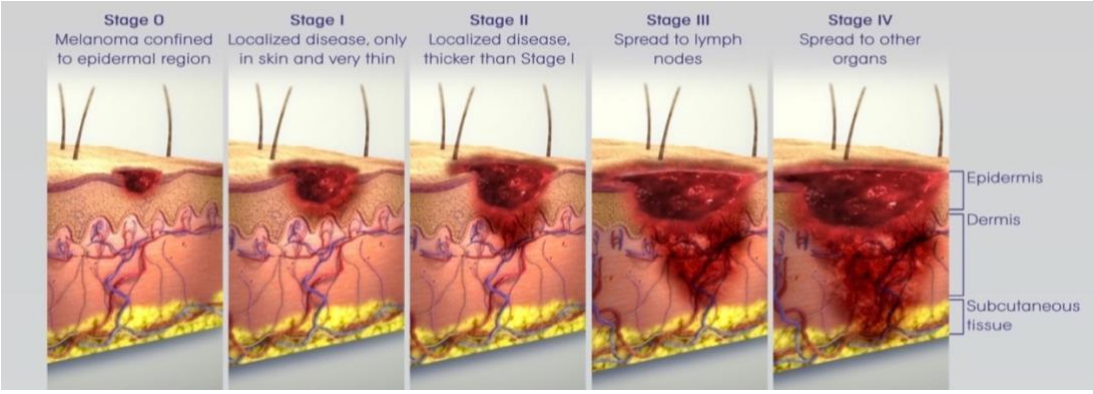

Figure 1.2: Pictorial representation of different phases of melanoma skin cancer[1]

1.1 Background

The methods of detection and diagnosis of skin cancer for an unusual growth of skin cells have evolved over last two decades. With the advent of the 20th century, diagnosis of malignant melanoma was carried out solely by visual inspection and manual screening of the lesion, depending on its conventional features and characteristics like size, colour, texture, shape, ulceration or bleeding of the tumour. If the lesion is anticipated to be malicious, it is further subjected to a pathological or dermatological method for advance analysis to validate the lesion to be malignant. A biopsy is an anatomical-pathological approach performed by a pathologist to diagnose the suspected lesion by laceration of the epidermis layer over the lesion. Thereafter the lacerated skin tissue is examined by skilled pathologists to diagnose malignant melanoma. These aciurgy techniques are not likeable to be exercised by many clinical patients because of the pain it incurs; additionally, the complete process of biopsy is time-consuming and takes around 3 to 12 weeks, which might result in fatal for patients in their later stages of skin cancer. Thereby, the early prognosis was an implausible goal during those days because of the lack of advance diagnosis methods and instruments therefore dermatologists exclusively depend on manual observation for the diagnosis of a suspicious lesion.

With the advancement in the medical field over years, diagnosis of malignant melanoma has become more economical and accurate using dermoscopic tools and methods. The next era of

[1] https://www.scientificanimations.com/3d-medical-animation-melanoma-skin-cancer-symptoms-causes-treatment

diagnosis of lesion have replaced manual inspection and pathological methods by non-invasive approaches like epiluminescence microscopy and dermoscopy which produces superior accuracy for lesion detection over visual examination[7]. Various dermoscopic tools like Epiluminescence microscopy, Dermoscopic photography, Dermlite, DermoGenius, Dermlite-II pro are pictorially represented in Figure 1.3. Transillumination of region encompassing the suspected lesion is the fundamental principle of dermoscopy, furthermore detailed analysis of meticulous features of malignant melanoma is accomplished over the intense magnified dermoscopic image. Although manual diagnosis with the use of these dermoscopic tools demands highly skilled dermatologists, moreover due to interobserver variations in the diagnosis of skin cancer: reports for a specific lesion suffers plenty of variations by numerous dermatologists. Therefore if the malignant melanoma lesion is diagnosed by an inexpert dermatologist the detection accuracy for a specified skin lesion ranges from 70% to 80%, while the accuracy mark ranges from 75% to 84% if the lesion is diagnosed by a skilled professional[8]. These methods of manual screening and visual inspection of dermoscopic lesion demand specialised dermatologist and moreover these techniques are error-prone, subjective, time-consuming and complex in nature.

In recent times, accurate diagnosis of melanoma lesions has established its path through molecular dermatopathology, which is a form of deliberation between dermatologists and pathologist. With the recent growth in the field of radiation treatment and immunopathology, orthodox diagnosis methods like descriptive morphology have been distinctively shifted to molecular histopathology[9]. Histological diagnosis of malignant melanoma is accorded by most of the dermatopathologists by considering them to analyse by classical microscope, certain melanocytic neoplasms termed atypical melanocytic proliferations call for expert consultation before they can be classified as benign or malignant. This also necessitates the evaluation of the histopathological characteristics with that of clinical and microscopic data. Improper application of molecular diagnosis for the identification of benignity or malignancy could as well be misleading and prone to loss of its utmost utility.

Gradually with advancements in recent technology and the impact of computer vision and machine learning algorithms along with medical science have led to the emergence of computer-aided diagnostics (CAD) system, which made the diagnosis process fast, accurate and more reliable than previous pathologists and dermatologists techniques. Various algorithms and methods have been incurred for precise feature extraction and faultless classification of skin lesion. ABCD (Asymmetrical shape, irregular Bordered, Colour variance and Diameter) Rule[10], seven-point checklist[11], Menzies method[12] and CASH (colour, architecture, symmetry, and homogeneity) method[13] have been introduced and practiced by researcher, these modern method of feature extraction have initiated a new dimension in the field of efficient diagnosis of malignant melanoma. Additionally these methods have surpassed the shortcomings of conventional dermoscopy technologies. The initial version of computer aided diagnosis system was embedded on desktops and workstations, thereby enabling the researchers and physicians to analyse and identify malicious cancerous lesion which are not perceptible through bare human eye. With the progress of medical vision, numerous computerized systems are employed in clinics of medical practitioners thereby helping them in early and accurate diagnosis of skin cancer.

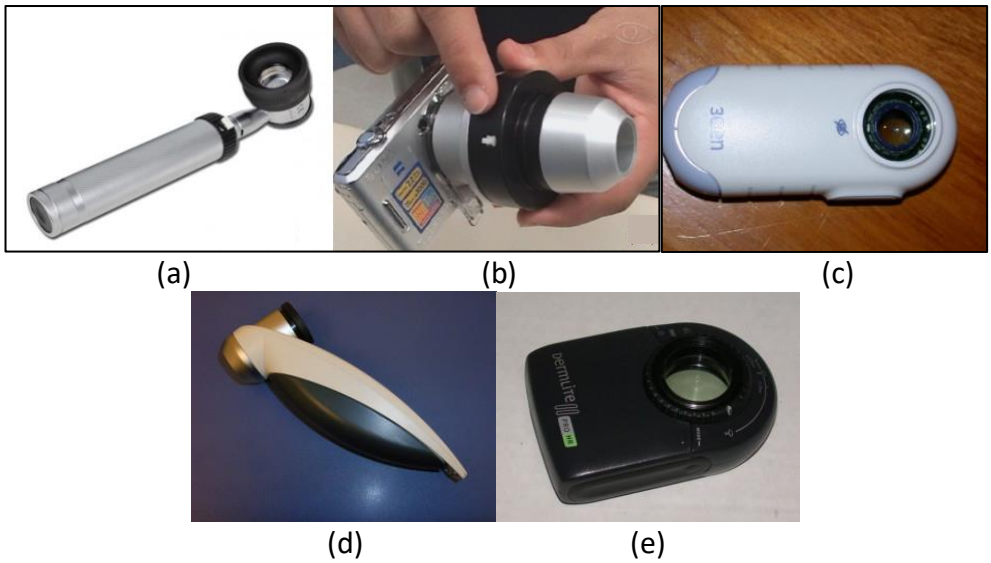

Figure 1.3: Images of different dermoscopic tools (a) Epiluminescence microscopy (b) Dermoscopic photography (c) Dermlite (d) DermoGenius (e) Dermlite-II pro

1.2 Aim and objective of research

The fundamental aim of this research is to provide novel and sustainable methods for effective and efficient diagnosis of malignant melanoma using several computer vision techniques and deep learning models. The primary goal of the proposed system is to classify the acquired image into two category: melanoma and non-melanoma. Our research not only focuses on fast and accurate diagnosis of skin lesion but also eases the accessibility and increases the intend to diagnose suspected lesion more frequently. With the ease and availability of computer-aided diagnosis system over a smartphone, the users will be more intended to detect suspicious lesion, which will increase the rate of early diagnosis of the lesion, thereby decreasing the mortality rate as melanoma can be treated and cured in its situ or early-stage more effectively than in later stages where it tends to damage vital internal organs. Moreover, the use of the YOLO (You Look Only Once) classifier has significantly reduced the processing speed, thereby producing a quick result of the diagnosis. The dissertation proposes a smartphone application which will be equipped with novel image processing techniques and deep learning models to correctly classify the lesion. Moreover, it can be available in any remote location and ease the diagnosis process without undergoing any invasive techniques. Additionally, the accurate diagnosis results will promote it to be used in clinical practice by an expert dermatologist, who might use this application as a supplementary decision-making tool or as a magnified imaging tool which might help them in visual inspection of the lesion.

Considering our major objective of the dissertation, a dependable deep learning model is being developed for computer-aided diagnosis system which will produce a segmentation of skin lesion boundary with high precision along with an accurate classification of the lesion. The dissertation aims to achieve a high score of sensitivity and specificity for the classification of skin lesions.

1.3 Significance of research

Accurate and timely diagnosis of malignant melanoma is not only a crucial but also a challenging task which will decrease the mortality rate of cancer patients. Cases of melanoma accounts to 4% of total dermatological cancers, however, mortality rate of melanoma holds a share of 80% of total deaths by dermatological cancer, and a small proportion of 14% can survive up to five years with metastatic melanoma[14].

United States of America accounts to maximum number reports of skin cancer across the globe. According to American Cancer Society (ACS), the third most deadly and widespread lesion is malignant melanoma. As mentioned in federal data, more than 63,000 individuals are diagnosed with melanoma from 2007 to 2011. The survey of last three decades proves that skin cancer holds a larger proportion than various other type of cancers. According to the published report of 2017 by ACS: 38,220 females and 57,140 males are diagnosed with skin cancer, out of which 5,940 cases females and 7,550 cases males accounts to melanoma. The same report states that a deadly malignant lesion results into death of one person in every 54 minutes [15]. Estimation of ACS rises in 2018 to 99,550 cases, where 39,940 females and 60,350 males were diagnosed with skin cancer. Additionally, 13,460 cases were of malignant melanoma, which clearly draws a picture that melanoma is most fatal and widespread dermatological disease [16]. Statistic of 2019 by ASC shows that 104,350 cases have been reported, which includes 42,030 cases of female and 62,230 cases of male [17]. From those cases related to melanoma are 11,650. The report by ACS also estimates 7,230 deaths due to melanoma in USA alone. Diagrammatic representation of MM cases and deaths due to MM (in thousand) in USA over the period of last five years is illustrated in figure 1.4, which clearly shows the ratio of number of people diagnosed with melanoma and died of melanoma are almost marginalised, which portrays the vigorous nature of the disease. China have also reported an increase in number of cases of MM from 3% to 8% and have projected to 2 times in upcoming decades [18]. According to statistical data of United Kingdom, MM was reported to be fifteenth most commonly

diagnosed cancer with 12,800 new cases in 2010 [19]. The data also claims MM to be eighteenth most common reason for death in UK due to cancer, with around 2209 deaths in 2011. The data portrays gender impartiality of MM, where 41% of female and 59% of males are effected out of total cases of MM. In Brazil, 2960 males and 2930 females were diagnosed with MM in 2014 [20]. Increasing number of cases around the major countries of the globe, clearly depicts the seriousness of the topic. MM have be statistically proven to be fatal and noxious form of cancer, thus an accurate, smart and easily accessible mode of diagnosis is the need of the hour.

From statistical figures of melanoma cases and deaths it could be inferred that early diagnosis of suspicious lesion and treatment of malignant lesion in its situ or early stage can decrease the number of deaths. However, diagnosis of a lesion is challenging and time consuming task which is not likely to be practiced in real-world, additionally, invasive modes of diagnosis, make the complete process a far-fetched dream which promote patients not to undergo diagnosis of suspicious lesion. Lack of modernised and huge machinery for diagnosis of lesion in remote parts of the globe, reduces the chances of early identification of lesion. Moreover, the reports of diagnosis are prone to errors due to indiscriminate features of MM lesion. Analysis of single lesion by several expert dermatologists might result differently, due to decision making errors which is because of visual similarities of MM lesion with skin. Visual impurities like hair follicles, blood vessels and other artifacts; which are present around ROI, might affect the results of decision makers. Thus a well-defined computer aided diagnosis system which is proposed in this dissertation will increase the rate of diagnosis of suspicious lesion. Early and efficient diagnosis of skin lesion by the proposed system will encourage patients to diagnose and treat the lesion in its early stage, therefore decreasing the mortality rate.

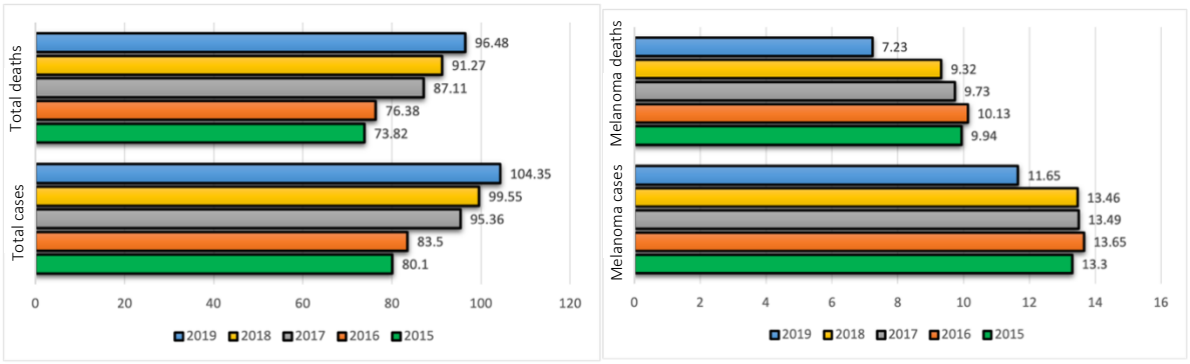

Figure 1.4 : Graphical representation to total number of skin cancer cases along with melanoma cases from 2015 to 2019 in USA

1.4 Novelty

A novel system is developed which acquires the images using proposed dermatascopy and smart phone, where alcohol or diagnosis gel is applied over the suspicious lesion to prevent the unexpected reflection in dermoscopic image. Then, the skin lesion image is pre-processed by various computer vision approaches such as histogram equalisation method which enhances the quality of the acquired image, furthermore the artefacts such as hair follicles, ruler marks, etc are digitally removed by novel artefact removing algorithms. Segmentation of the region of interest from the FOV is done in the next step, where the lesion is segmented by employing novel methods of L-R fuzzy logic and triangular neutroscopy in two proposed methods respectively. The proposed segmentation accounts for highest score of accuracy over other state-of-art algorithms. Henceforth, feature extraction is performed over the segmented image. This stage is carried out through classical mathematical methods to identify features of the malignant lesion in the segmented skin lesion. In the final phase, YOLO classifier is modified and a novel deep learning model is proposed (in two respective proposed methods) to fetch best-fit results, thereby achieving an accurate classification of suspected skin lesion. The modified classifier proves to produce superior results over well-known classifiers such as the Support vector machine, K-nearest neighbour method, and Decision trees. Encapsulation of all the stages of CAD enables the proposed system to achieve the fundamental goal of this research.

1.5 Dissertation structure

The forthcoming chapters of this dissertation are outlined as follows. A detailed literature review of state-of-art methods is highlighted in Chapter 2, where the problems related to skin lesion diagnosis along with the solutions for accurate diagnosis using modern skin imaging techniques and tools are mentioned. State-of-art approaches for Computer-Aided Diagnosis (CAD) system such as pre-processing, segmentation (both conventional and deep learning-based segmentation methods), feature extraction (handcrafted, clinical, pattern and deep learning-based feature extraction techniques) and classification (conventional and deep neural network-based methods) models are highlighted in this chapter. Additionally, a list of publicly accessible datasets of different dermatological cancers and performance evaluation metrics are also described in this chapter. Technical preliminaries of fuzzy logic along with proposed pre-processing using histogram equalisation and dull razor algorithm, followed by novel segmentation method by dynamic standard deviation calculation and L-R fuzzy logic is explained in Chapter 3, where the classification of the image is done by the trained model of YOLO classifier. A tabular and graphical representation of result analysis is illustrated in this chapter to portray and compare the top-notch mark of accuracy by the proposed system. Chapter 4 discusses another proposed method, where a novel pre-processing algorithm is proposed which includes the removal of noise and other digital artefacts like hair follicles and ruler marks. Furthermore, the image is enhanced by histogram equalisation. This chapter also proposes a novel method of segmentation using Triangular neutrosophic number. Henceforth the segmented image is classified by the proposed classifier which is employed over inception and residual blocks with a softmax layer after each residual block. The result and analysis section of this chapter portrays an edge cutting score for accuracy, sensitivity and specificity over other state-of-art methods. Additionally, this chapter also introduces a smartphone application for easy and quick diagnosis of the suspected lesion. Finally, conclusions and our future work plans are presented in Chapter 5.

Chapter 2: Overview of melanoma lesion detection

Recent evolution in the implementation of computer vision and machine learning algorithms in medical vision had led to advancements in CAD system for the detection and diagnosis of a melanoma lesion. These revolutionary detection system enables the early identification of noxious cancerous cells over the dermis layer of the skin. According to the orthodox clinical manual methods of diagnosis of skin lesion as represented in figure 2.1; the suspected lesion is primarily being examined by local medical practitioner, who further refer the patient to a pathologist or a dermatologist depending on the features and characteristics of the lesion. The medical practitioner examines any minute transformation of shape, colour, texture or size of a suspected mole on the patient's skin. Any transformation of unusual change can be contemplated to be skin cancer and for further analysis of the lesion the patient is referred to an expert pathologist or dermatologist. The pathologist performs invasive methods such as a biopsy to analyse suspected lesion. The dermis layer of the skin over the suspected lesion is gashed and tested in laboratories for 3 to 12 weeks. This method is quite slow and requires advance expertise for the accurate diagnosis of skin cancer. On the other hand, dermatologist perform diagnoses using dermatoscopy tools which is most regular imaging technology and act as an intensified magnifying glass for precise feature extraction of the lesion based on ABCD rule, seven-point checklist and several other methods. However, the accuracy of detection of malignant melanoma is not satisfactory. Both the pathologist and dermatologist method for detection of skin cancer is used to classify a lesion to be melanocytic or non-melanocytic.

The survival ratio of the last five years for the patients suffering from malignant melanoma at an advanced stage is lower than 15%, while the same statistics of survival ratio elevates to 95% if the lesion is diagnosed and treated in its situ or early phases [21]. The mathematical data of survival ratio provide clear evidence that mortality of a patient is directly proportional to timely diagnosis and treatment of the lesion. Therefore fast, reliable, accurate and easily accessible mode of diagnosis is the need of the hour which can decrease the mortality rate of the patients. Currently, dermatoscopy

devices are employed as hand-help tools along with computer vision and deep learning techniques for generating valuable information for clinicians. Notwithstanding the fact that an entirely reliable and autonomous diagnosis system for detection of malicious skin cancer remains an unachievable task in medical vision.

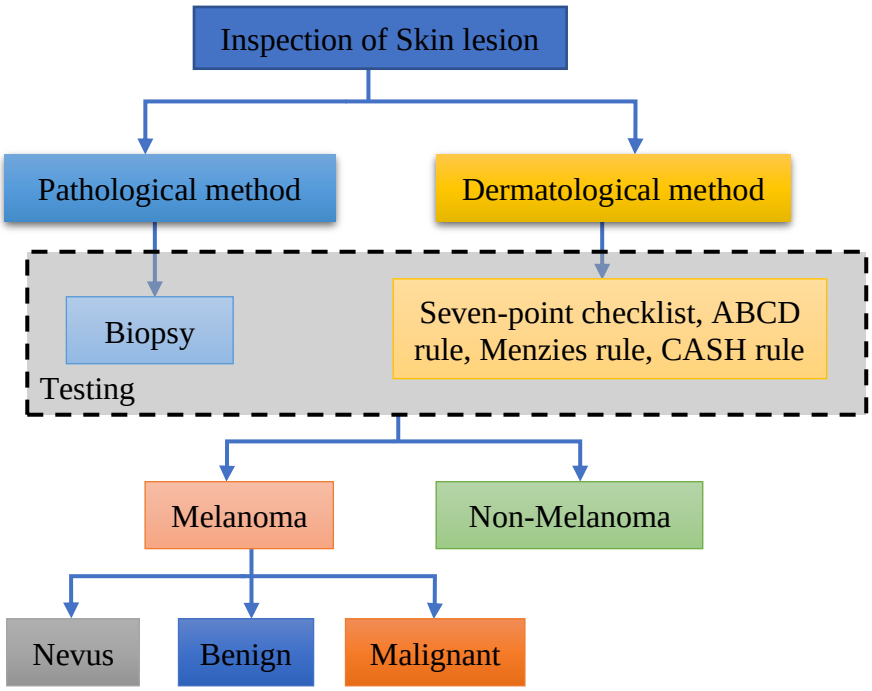

Figure 2.1: Pictorial representation of different techniques for the diagnosis of skin lesion

2.1 Skin imaging challenges

Variations in image sources and their types during the process of image acquisition led to numerous difficulties in the detection of suspected skin lesion. Dermoscopic images of skin lesion containing various deformities like hair follicles, bubbles caused due to dermoscopic fluid, blood vessels, oils and other physical artefacts; which diminishes the accuracy of diagnosis of a malignant lesion. Furthermore, the shallow contrast gap between the lesion and surrounding skin region reduces the segmentation performance, thereby limiting the accuracy of a classifier to achieve higher marks of accuracy. Moreover, the different shape, size and colour of a skin lesion makes the task of detecting of melanoma lesion more tedious and tiresome. Malignant melanoma being the most uncertain yet deadly lesion exists in innumerable dimension and various colour contrast, which makes the process

of diagnosis more challenging for manual screening by dermatologist, thereby a visual inspection by computerised diagnostic devices is of utmost importance for accurate diagnosis of lesion. This automatic diagnosis device is employed on the method of digital image processing and deep learning thereby it is not only equipped to digitally remove the artifacts and enhance the dermoscopic images of the lesion but also have specified algorithms for lesion classification which will support the dermatologist in quick analysis and decision making about a suspected mole. Such a convenient system will aid the clinicians in accurate and fast decision making about a lesion to be either classified as malignant melanoma or non-melanocytic lesion.

Prodigious disparity in the visual appearance of the skin of different individual compels skin diagnosis to be a tedious and strenuous task. Complex visual attributes of dermoscopic skin lesion is illustrated in figure 2.2, where various challenges in the process skin lesion diagnosis is highlighted. The list of all the physical artifacts and visual challenges are encapsulated below, where complication of dermoscopic images like multi-dimension of skin lesion, presence of artefacts and visual noise, fuzziness of lesion boundary, low contrast and brightness of dermoscopic image, illumination of colour and variation of human skin colour is briefly explained[22].

1. *Multi-dimension of skin lesion* : Massive diversity of skin lesion have led to increase in visual complexity of dermoscopic images thereby decreasing the rate of accuracy for identification of skin diseases. Due to the immense variability and uncertainty of lesion location, shape and size efficient manual diagnosis have become a far-fetched dream. Therefore, a modern approach of digital pre-processing of the lesion is performed by many image analysis algorithms to surpass the challenge of uncertainty in the measurement of the suspected lesion, thereby this pre-processing method increases the accuracy of skin lesion diagnosis.
2. *Presence of artefacts and visual noise*: Visual noise is the unwanted pixels which are introduced in the dermoscopic images during image acquisition. Detection of malignant melanoma from a dermoscopic image might be affected due to the presence of physical artefacts like mark of a

ruler or dermoscopic frame; along with these artefacts, existence of noise is also a major reason for diminishing detection accuracy. These artefacts and noise are defined as the hindrance in the dermoscopic image introduced during image acquisition, which is not a part of the primary lesion but they can affect the results of diagnosis by visual inspection and can also deviate the outcome of computer-aided segmentation techniques on various skin lesion. The presence of hair follicles, bubble marks, blood vessels, rulers and frame marks are considered to be physical artefacts of dermoscopic image.

3. *Fuzziness of lesion boundary* : Uncertain and ameboid borders are the characteristic of malignant melanoma lesion, this attribute of malignant lesion makes it difficult to produce efficient accuracy mark for computer based segmentation and classification techniques. Accurate localization of lesion boundary and efficient refinement of contours are affected due to fuzzy boundary of malignant melanoma lesion. Pre-processing of dermoscopic image to fetch accurate lesion boundary becomes a laborious task, thereby prediction of asymmetrical nature of lesion becomes a difficult assignment.
4. *Low contrast and brightness of dermoscopic image* : The low contrast and brightness of the lesion image make the segmentation and location detection process difficult, as the pixel difference of primary melanoma lesion and local field of view of dermoscopic images is negligible. Due to low brightness of image along with low contrast the region is underexposed thereby decreasing the segmentation outcome.
5. *Illumination of colour* : Colour texture of the image of skin lesion, light ray captured during image acquisition and reflections around the dermoscopic image can deviate the illumination result of the lesion image thereby providing a multi-resolution image.
6. *Variation of human skin colour* : Human skin consist of numerous tones of colour due to the varied quantity of Eumelanin and Pheomelanin present in the epidermis of the skin. Thus

sometimes, it is difficult to differentiate the FOV and ROI from a dermoscopic image due to visual similarity of malignant melanoma lesion and dark skin tone.

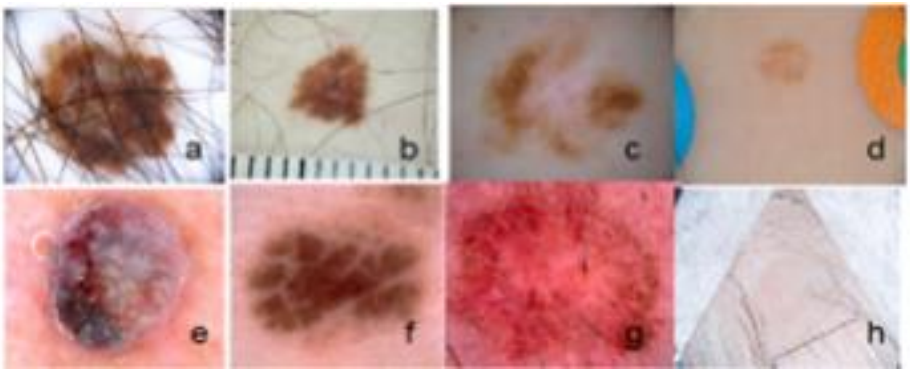

Figure 2.2: Presence of various artifacts in skin lesion image : a) presence of hair follicle, b) presence of artifacts like ruler mark, c) low contrasted image, d) illumination of colour, e) presence of bubbles, f) irregular border, g) blood veins,h) presence of artifacts like frame [23]

2.2 Skin imaging tools and technology

With the aim to overthrow the painful invasive methods like biopsy and achieve better diagnosis results for malignant melanoma, a new field of "Dermatoscopy" was innovated in 1920 by a German dermatologist named Johann Saphiera. Epiluminescence microscopy (ELM), well known as dermatoscopy is a skin acquisition approach used for analysis of skin lesion by a dermatologist, this techniques is non-invasive in nature, therefore it is likely to be more acceptable by the patients. Dermatoscopic tools are equipped to fetch a magnified image of the skin lesion, the acquired magnified image is termed as dermoscopic image. Image of the suspected skin lesion is acquired by the dermatologists from dermoscopy, thereafter the various existing dermoscopic or clinical methods are employed over the fetched images to investigate the suspected skin lesion.

With advancement in technology and medical vision, numerous non-invasive image acquisition tools and skin imaging techniques are introduced in state-of-art [24]. Multi-spectral imaging, digital camera photography and dermatoscopy are few of the popular non-invasive skin imaging techniques used for magnified image acquisition. Optical coherence tomography (OCT), Confocal laser scanning microscopy (CLSM) and Magnetic resonance imaging (MRI) are the modern laboratory-based approaches to non-invasive mode of diagnosis for skin cancer. Laser-based systems and multiphoton

tomography are a few of the low penetrating, infrared methods for diagnosis of skin lesion. Ultrasound is one of the effective yet high penetrating waves to identify malignant melanoma from a suspected skin lesion [25]. Table 2.1 encapsulates various skin imaging tools and techniques in tabular format.

Table 2.1: Various techniques of skin image acquisition

Techniques	Merits	Limitations	Penetration depth
Dermatoscopy	• Magnified image of high quality. • Deeper degree of visibility. • Strong lighting system enable the device to remove total surface reflection.	• Operates over skin superficial layer only.	2mm
Laser Doppler perfusion	• Provided functional information about the flow of blood. • Non-ionizing radiation is passed without any physical contact with the human anatomy. • The device is portable and of low cost.	• Cannot provide in depth information. • Unable to produce skin imaging in Z-plane.	0.2mm
CLSM	• Provides high resolution imaging outcomes. • Result is produced in 3-dimentional structures.	• The structures created are of micro scale.	0.3mm
MRI	• Eligible to measure both thickness and volume of the lesion. • Provides information about depth of the lesion. • Provide other vital information about the tissue covering the lesion.	• Impossible to practice over patients with metal plate inside them.	Whole body penetration
Ultrasound	• Provides real time observation. • high frequency ultrasound of 100MHz.	• Can measure penetration depth and thickness of the skin for macro structures only.	1mm
OCT	• Provides outcome result of higher resolution of 5 to 15 macro metre. • Low coherence in 3D imaging.	• Limited to small tumours which are scattered over epidermis tissue. • Provide outcome in low resolution.	0.5 to 1.5 mm
Digital camera	• provides high quality magnified images. • High resolution.	• produces limited morphological data over top layer of the skin.	0.1mm
Multispectral imaging	• Provides consistent outcome based on narrow frequency over reflector band.	• Lack imagining information about depth of the lesion. • Lack values of Z-axis plane.	0.1 to 1 mm
Multiphoton tomography	• Provides high resolution sound with the effect of second harmonic generation (SHG).	• Minute penetration depth	0.2mm

2.3 Fundamentals of analysis of skin lesion

Huge potential in the field of diagnosis and detection of skin cancer is marked through dermoscopic images, which was never achievable using ordinary lenses or even a digital camera. Image acquired through the dermoscopy devices undergoes different methods of dermoscopy like CASH, seven-point checklist, ABCDE rule and Menzies method. These methods are performed by a skilled dermatologist for diagnosis and detection of malignant melanoma lesion, however, they lack a few major areas of diagnosis. The process of manual detection of skin cancer by visual imaging of dermoscopic images is time-consuming and slow process. Moreover, it is sometimes difficult to fetch accurate diagnosis results due to low contrast between FoV and ROI. Additionally, it is a challenging task to make visual difference between melanocytic and non-melanocytic lesion based on its appearance. Notwithstanding the fact of the presence of physical artefacts like ruler marks, air bubbles and the existence of variable skin conditions such as skin colour, presence of hairs and blood vessels over FoV and marginal difference in contrast of lesion and skin makes the diagnosis process tiresome and decreases the rate of detection of skin lesion. Presence of these ambiguities on lesion image forces the dermoscopic images to undergo numerous digital pre-processing steps to fetch overall accurate detection result. Therefore to overcome these anomalies, several computer-aided diagnosis (CAD) methods are employs which enable automatic diagnosis of malignant melanoma from skin lesion.

Several computerized methods have been adopted over the years for diagnosis and identification of skin cancer. The traditional techniques of medical imaging is performed through a sequence of low level pixel processing approach. Usually, the whole series of computational methods for diagnosis and detection of malignant melanoma can be well encapsulated into five vital processing stages i.e. Image acquisition, pre-processing of the image, segmentation of pre-processed images, feature extraction and classification of skin lesion, these stages are collectively termed as CAD method [26]. The complete series of computer-aided diagnosis of skin cancer in five major stages is highlighted in figure 2.3 using flow diagram, where the digital image of the surface of the epidermis

of skin is captures and it undergoes through pre-processing stage, where physical artifacts and noise from the image is removed to improve the quality of the image. The pre-processing step employs image enhancement and restoration algorithms along with digital artefact removal functions to enhance the standard of dermoscopic image. Thereafter the processed image is segmented, where the relevant and necessary lesion region is outlined and cropped out of the complete dermoscopic image, thus enabling the subsequent stages to only focus of region of interest, thereby enhancing the accuracy. Feature extraction and Classification of the image are the subsequent stages where the dermoscopic image lesion is classified as melanocytic, based on the features of the lesion image.

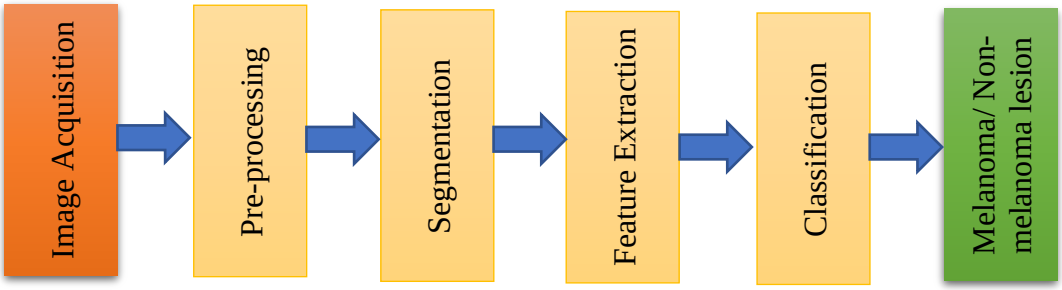

Figure 2.3: Representation of computer-aided diagnosis

2.3.1 Pre-processing

Pre-processing is aimed at enhancing images for efficient processing to fetch accurate detection score in the next stage. Dermoscopic image is acquired from an image acquisition device and further, it undergoes pre-processing stage, which includes grey scaling of the acquired images, binarization and noise filtration of the generated image. These methods include adjustment of intensity which enables the dermoscopic image to modify its intensity value of each pixel, thereby generating a high-quality output image which will further assist to fetch a better segmentation score. Moreover, the pre-processing methods are equipped with contrast adjustment algorithms which provide histogram extension to achieve better visibility, contrast adjustment also helps the image to efficiently mark the outline of the lesion [27]. Histogram equalization is one of the vital methods of pre-processing where pixel intensities are evenly distributed over the entire pixel metric of the image, thereafter entire pixel range of intensities is enhanced to produce a global contrasted dermoscopic image. Morphological

operations are used for localisation and feature extraction of malignant melanoma lesion are performed by employing dilation and erosion methods on dermoscopic image. Binarization of image is operated to fetch morphological results, it is a process to convert a digital image to a binary image by changing the intensity value for each pixel. A dermoscopic image is in three planes which is reduced to a single plane of grayscale with 256 shades of colour grey in the process of grey-scaling, furthermore, the grayscale image is converted into a binary image depending on the constant threshold value which forces the pixel intensity value to be either black or white depending on the threshold value [28].

Pre-processing techniques can be broadly classified into four major categories; First, the transformation of pixel brightness for correction in brightness level is one of the major methods of pre-processing where the image is enhanced by the local-pixel modification method, and all the pixels in the image matrix are modified according to the value of the global metric. Brightness correction method where the pixel intensity value is modified according to surrounding pixels; and greyscale transformation methods where three plane image is reduced to a single plane; are the two sub-categories of brightness transformations. Sigmoid stretching, gamma correction or power-law transform and histogram equalization are the three types of operation for pixel brightness transforms. Second, geometric transformations are used to rectify shape and de-skew image into its corresponding two dimensional and three-dimensional planes. Geometric transformations are performed either by the Spatial transformation method where pixels of the dermoscopic image metis are physically rearranged to modify the image; or by interpolation of grey level which is done by assigning levels of grey colour into the transformed image. Third, the Image filtration method is a pre-processing technique used for smoothing the image and finding the sharp edge of the dermoscopic lesion image by using the low pass filtering method for smoothing the image pixels by generalising pixels of image metrics; the high pass filtering method for sharpening the image and produce accurate edge detection of the lesion thereby assisting segmentation process for the dermoscopic image; Directional filtering

method and Laplacian filtering are two method edge detecting filtering methods. The prior is an edge detection algorithm which calculates the first derivatives of image metrics. When the value of the adjacent pixel shows the large difference it is reflected in the first derivatives or slope. Directional filtering methods are capable of plotting in multi-direction within a provided space. Unlike the Directional filter, the Laplacian filter computes over the second derivatives of the image, while calculating the rhythm of change in the first derivatives. This filter analyses the change to determine whether the deviation of pixel values is from continuous progression or adjacent edge; Finally the fourth major pre-processing technique is the Fourier Transform method which decomposes the input image of spatial domain into cosine and sine components to generates output of the image in frequency domain, thereby enhancing the quality of image.

Notwithstanding the fact that melanoma skin cancer diagnosis and detection is a perplexing task with naked eyes therefore skilled medical professionals are shifting towards dermoscopy devices which enable them to fetch high resolution images of skin lesion, although it is an expensive alternative and the cost of the devices forces dermatologist to compromise with their efficiency. Recent research and development in the field of high resolution image acquisition have developed an economical alternative for dermatoscopy, which is able to produce dermoscopic images with same quality and resolution as dermatoscopy. Blum have introduced a 'Tape dermatoscopy' methods for image acquisition, this techniques is not only simple and portable but also effective. Tape dermatoscopy [29] method involves application of immersive fluid over suspected area and thereafter covering of suspected lesion with transparent adhesive tape, which prevents formation of air bubbles and diminishes surface reflection over the ROI. The lesion images is recorded at an angle of 45° from the region of diagnosis and a distance of 7.5 to 8.5 cm is maintained between the image acquisition device and the lesion to acquire high quality dermoscopic image of the mysterious lesion. Image is captured in presence of adequate natural or artificial light to ensure a dermoscopic image with proper

contrast and intensity. Therefore tape dermatoscopy is proved to be one the most efficient, user friendly and cost effective mode of dermatoscopy.

Along with pre-processing methods like morphological operations, binarization, data augmentation and adjustment of intensity and contrast of the image, removal of noise and other artefacts from the dermoscopic image are one of the vital aspects of pre-processing. Several noise removal algorithms are introduced to reduce the noise present in the dermoscopic image, however, removal of artefacts like blood vessels, hair follicles, rulers and frame marks are still a challenging task. Researchers around the world has tried to invent various methods and algorithms for Digital hair removal from the dermoscopic image which will increase the accuracy of the diagnosis of malignant melanoma lesion [30]. According to research, accuracy of detection of skin cancer is decreased by 13%-23% for the same set of dermoscopic images when the classification is done without digital hair removal, thus this feature is of utmost significance. Table 2.2 provides a detailed analysis of various hair removal methods and draws a clear conclusion about the publicly available methods for hair detection and removal from a dermoscopic image. Moreover, standardization of images along with image enhancement is an important subject which is achieved by rescaling dermoscopic images, which helps the system to decrease the computational complexities.

Table 2.2: Detailed analysis of various hair removal technique

Method	**Dull Razor [31]**	**Xie et al [32]**	**E.shaver [33]**	**Abbas et al. [34]**	**Fiorese et al. [35]**	**Huang et al. [36]**	**DHR [37]**
Hair detection method	Generalized morphological closing	Top-hat operator	Prewitt edge detector	Gaussian derivative theorem	Top-hat operator	Multiscale matched filters	Gap detection by multiscale skeletons
Image inpainting	Bilinear interpolation	Anisotropic diffusion	Averaging of colours	Coherence transport	PDE based inpainting	Median filtering	Fast marching method
Test data	5	40	5	100	20	20	300
Implementation	Yes	No	No	No	No	Yes	Yes

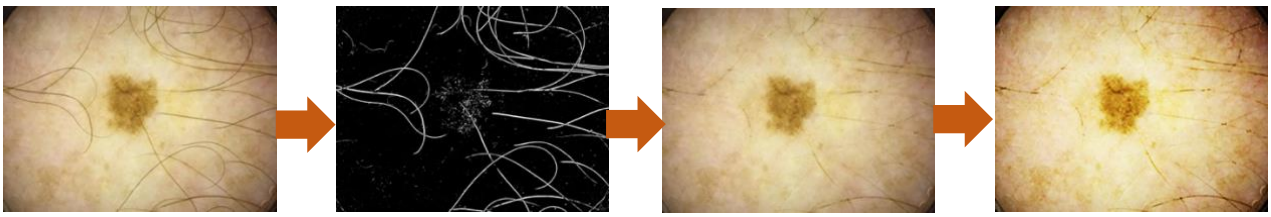

Figure 2.4: Illustration of pre-processing of skin lesion (a) Input image (ISIC_0599605) (b) Threshold image (c) Digitally hair removal (d) Image enhancement

2.3.2 Segmentation

Segmentation is the process of fetching a region of interest out of a field of vision from a dermoscopic skin lesion image. It is a vital process of the CAD system where analysis of dermoscopic skin lesion image is performed with an efficient accuracy based on the segmented region of the lesion. In this process the diseased lesion is segregated from the healthy dermoscopic image, in this stage, the normal epidermal tissues are segmented out, and the feature of the region of interest is extracted, therefore a precise feature is being calculated which promotes the classifier to achieve high score of accuracy of diagnosis and detection of malignant melanoma. According to computer aided diagnosis pipeline, segmentation is performed over pre-processed image of dermoscopic lesion, which increases its accuracy because of enhancement of the dermoscopic skin lesion image.

Clustering, thresholding, region and edge based technique are few of the conventional segmentation approach, however these methods experience difficulties in edge detection and segmentation of skin lesion for a complex image, thereby the method is unable to fetch accurate segmentation outcome for region of interest of melanoma lesion[38]. Intelligent based segmentation approach developed by recent researchers using genetical algorithm, artificial neural network (ANN), fuzzy logic and deep learning techniques [22]; have proved to be more reliable and accurate mode of segmentation of dermoscopic skin lesion. Various approach for segmentation of dermoscopic skin lesion includes traditional segmentation methods based on handcrafted features such as region and edge based segmentation and threshold value based segmentation methods; and modern methods of segmentation incudes Intelligent based segmentation technique which consists of deep learning methods and algorithms of artificial neural network. Basic comparison between traditional and modern methods of segmentation is illustrated below in table 2.3.

Table 2.3: Various techniques of segmentation of skin lesion

Methods	Reference	About the method	Merits	Demerits
Threshold and clustering	[39], [46]	• It is a partitioning technique to distinguish foreground from background image • Initial value of threshold is determined for segmentation of original image	• Fast and easy to implement • Spatial characteristic knowledge is not required	• Hypersensitive to noise thus it undergo inhomogeneity of intensity.
Region and Edge based	[48] [49]	• Search based techniques are used to execute region detection and edge identification for demarcation of RoI on skin lesion image.	• Homogeneity criteria is satisfied • Hybrid approach of Split and merge is employed to fetch enhance segmentation result.	• Manual initialization is required at seed point for processing some regions • Sensitive to noise
Conventional intelligence based method	[50] [51]	• Based on artificial intelligence to execute analysis of images by training large dataset. • Both supervised and unsupervised models • Example : Fuzzy C-Mean, Genetic algorithm and ANN	• Sensitivity and specificity better than threshold and region based methods.	• Spatial modelling is not considered • Sensitive towards noise • Uncertainty in specific data processing is observed.
Deep learning	[52]	• Multiple processing layers are used for data representation and training. • Range of supervised and unsupervised feature learning algorithms along with hierarchical probabilistic models and neural networks are the example of deep learning	• Representation of features is done from pixel to high-level semantic features. • Intricate structures of big sized data are implicitly captured; better than conventional methods.	• Computationally expensive • Computational time for training is high • Large storage is required

2.3.2.1 Conventional segmentation method

These are methodologies with the capability of performing region segmentation based on pixel analysis. Conventional segmentation methods employs intensity, HSV and different local or global pixel values for categorising the pixels into different clusters. Similar pattern of pixel are merged together, while uneven pixels are discarded from the ROI. A detailed explanations of conventional segmentation methods and algorithms are as follows:

1. Thresholding methods

Segmentation of skin lesion by thresholding method can be classified as Local or Global thresholds depending on the proportion of input image; that is whether it's a complete pixel matrix or a fragment of it. The dermoscopic image is segmented by segregating intensities of grey colour using a fixed threshold mark by current thresholding approaches. Otsu threshold(OT)[39], Renyi Threshold (RT) [40], Bradley Threshold (BT) [41], Iterative Threshold (IT) [42] and Huang Threshold (HT) [43] are the few popular thresholding method for segmentation of skin lesion.

For bi-level or multi-level general purpose segmentation on grayscale images OT,IT and HT methods are introduced which are evaluated by visual inspection over various classical images. Whereas RT method was developed on two additional techniques by efficiently employing the concept of entropy of images in various manner. For real-time segmentation during processing of augmented reality or live video streaming BT method has been proven to be highly efficient. It marks pixels into black or white by analysing the spatial variation in brightness of image, thereby producing efficient and rapid results. Figure 2.5 represents the results of applying OT over dermoscopic image. It shows that OT methods is able to fetch an accuracy of 89.76%, when we have applied it over ISIC 2017 dataset under normal condition.

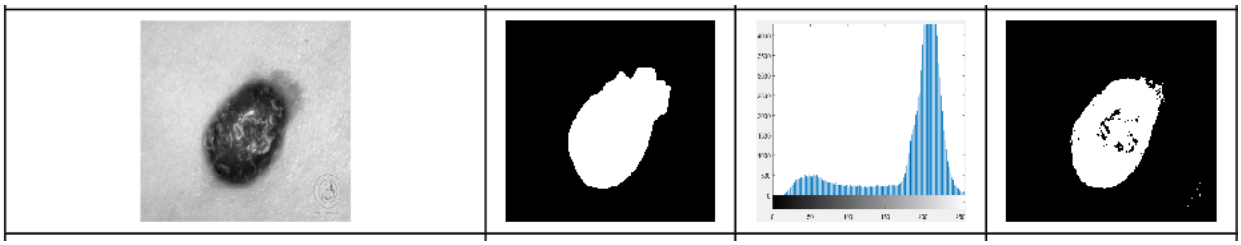

(a) (b) (c) (d)

Figure 2.5: Pictorial representation of otsu threshold method. [39] (a) Input image (b) Ground truth result (c) Histogram representation (d) Segmented output

2. Clustering methods

Clustering method is an approach of grouping an akin set of pixels into a cluster using specific similarity metric. Image pixels which share identical pixel value for specified metric are enclosed into similar group thereby forming different clusters of specific type. This approach is frequently used by researchers for proposing different applications for segmentation of skin lesion. Mean-shift colour (MC) [44], Mean-shift colour and Spatial (MS) [45], K-Mean Colour (KC) [46], and K-Mean Colour and Spatial (KS) [47] are four different methods of clustering, which are employed for segmentation. Figure 2.6 pictorially represents the KC method. MS and KS are the expansion of classical algorithms like MC and KC respectively. These modified methods are evolved to employ spatial information of the image, to produce enhanced results.

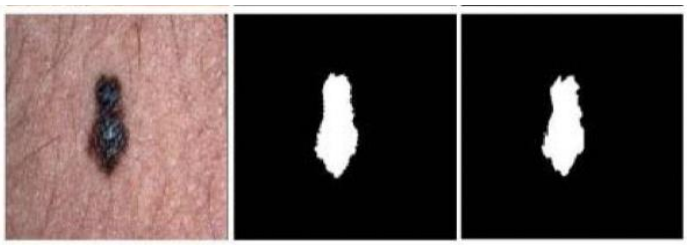

Figure 2.6: Pictorial representation of KC method [46] (a) Input Image (b) Segmented outcome (c) Ground truth value

2.3.2.2 Deep learning based learning-based segmentation technique

Though the technique of deep learning is a tedious job in the field of computer vision, it has still achieved significant heights in the domain of segmentation of the dermoscopic image. Several models based on deep learning have been suggested by researchers. The techniques bring about

magnificent performance for the purpose of segmentation of skin lesion [22]. Few of the deep models which are significantly examined in this dissertation include Deep convolutional neural networks, Convolutional DE- Convolutional Neural Networks (CDCNN), Fully Convolutional Network (FCN), and U-Net.

The algorithms discussed so far are categorized as traditional approaches, which have been continuously evolving towards modern methods based on recent technologies. A new type of algorithm has emerged taking on count the advantages of present developments in the domain of machine learning. A few among such machine learning techniques were specifically designed for the segmentation of skin lesions. A comparison of five different algorithms of the deep convolutional neural network is structured as follows:

1. Fully convolutional networks (FCN): Based on Convolutional Neural Networks, FCN was developed to demonstrate as a validation of principle that represents complex networks by oneself, furthermore they are trained pixels-to-pixels and end-to-end by numerous layers of convolutions. Thereafter a high level of semantic information is stored to produce detailed and accurate segmentation. The information about the appearance in fine or shallow layers is combined with semantic information in deep or coarse layers to form a skin architecture by resorting to several convolutional layers. Figure 2.7 illustrates the architecture of FCN with a block diagram. A group of pooling and convolutional is utilized to develop FCN. The parallel integration (PI) technique was introduced by [48] where PI was employed to develop a multi-stage FCN for segmentation of skin lesions, and it was employed for advancement in intensifying the edges of the partitioned skin lesions. When evaluated on the dataset of the International Symposium on Biomedical Imaging 2016 (ISBI 16), the system scores the trailblazing performance of 91.18% dice coefficient score and 95.51% accuracy for the segmentation of skin lesion images. A Deep Full-Resolution Convolutional Network is

developed by [22] which is a modified FCN for segmentation of skin lesion. FCN architecture deems to show the possibility of overfitting of segmentation which might result in producing an output of coarse segmentation with the restricted dataset for training.

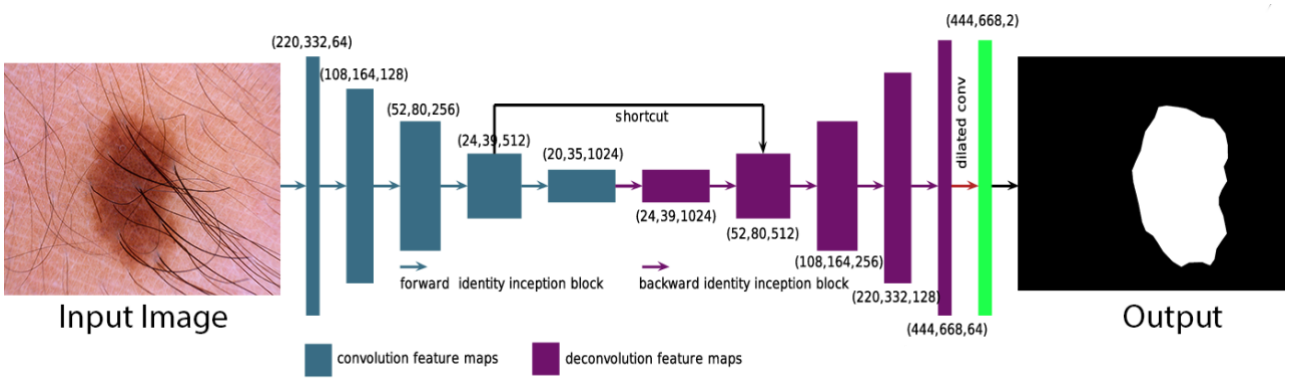

Figure 2.7: Architecture of FCN

2. Convolutional-Deconvolutional Neural Network (CDNN): It is an entirely computerized segmentation technique of dermoscopic images by strengthening a neural network of nineteen layers of deep convolutions. It incorporates a group of schemas to clinch efficient and effective learning with restricted data for training, along with an original loss function which operates on Jaccard distance to remove the necessity of weighing the sample again (while applying cross-entropy because of the high uncertainty of total count of background and foreground pixels); Significantly, this architecture can be classified into two proportions: Networks of Convolutional and Deconvolutional. CNN's that works in the process of reverse convolution are known with the term Deconvolutional networks. To extract discriminative features, both networks are used. The architecture of CDNN is represented in figure 2.8. To obtain the final high-resolution output, with smoothening maps of segmentation the deconvolution layers are employed. This model was developed by [49] on skin lesion images of different colour spaces. High computational cost is what a system with CDCNN requires. With insufficient training data set, limited and coarse results are obtained by techniques based on CDCNN. These techniques have attained improved results for segmentation and detection of diseased portion of dermoscopic image. Although dense tuning over vast number of

parameters is applied along with various pre-processing algorithms by these above listed approaches to fetch enhanced result of segmentation, which increases the consumption of computational resources.

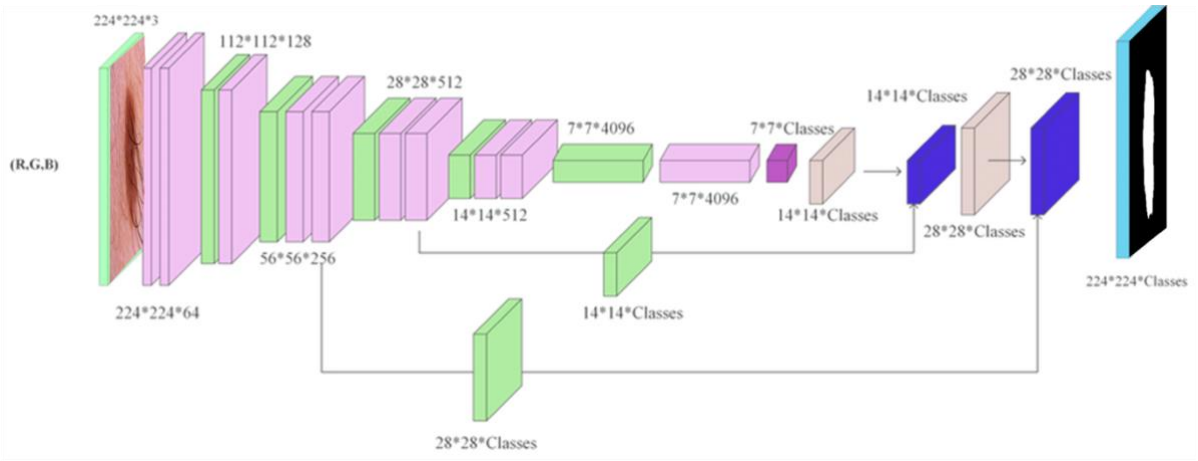

Figure 2.8: Architecture of convolutional deconvolutional neural network

3. Enhanced CDNN (ECDNN) [50]: To enhance the discriminant capacity, an expanded model of the former method [49] is developed, which is a deep network framework with kernels of smaller size. A deep network framework along kernels of small convolution has the potential to operate over extensive variations of dermoscopic image with adverse image acquisition conditions. Additionally, the ECDNN architecture aims to achieve efficient training of images along with supervising of over-fitting conditions by investigating the operations of channels in various color space, like CIELAB color space and Hue Saturation value (HSV) space.
4. Densely Linked Convolution Neural Network (Dermo-Net) [51]: Various neural networks with the aim of segmentation of lesion are encapsulated by a deep network of neurons to achieve higher score of segmentation. Residual propagation along with dense blocks of convolutions and funneling of network by autoencoding techniques are used as encompassing techniques to develop Dermo-Net. Dermo-Net is a recently published work which have proved to fetch high score for segmentation of skin lesion. Architecture of Dermo-Net is represented in Figure 2.9.

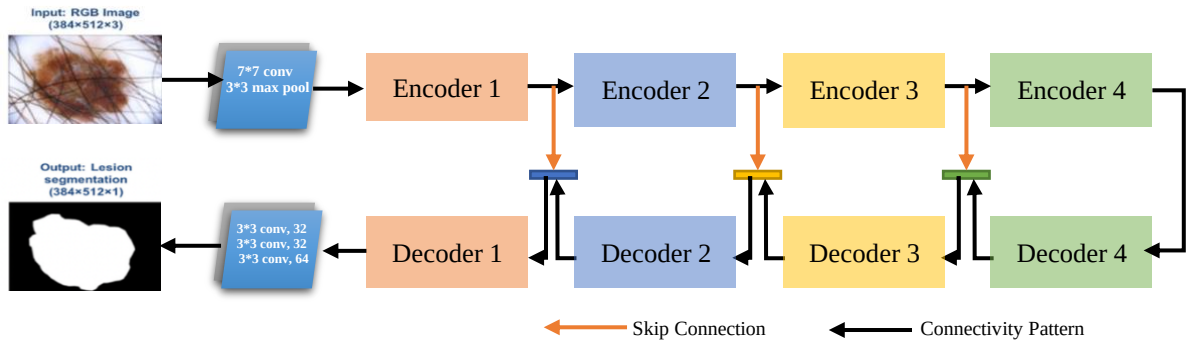

Figure 2.9: Pictorial representation of Dermo-Net, which is developed of 4 consecutive blocks of encoder and decoder .

5. U-Net**:** It is an encoder-decoder network, originated from fully convolutional network, where both decoder and encoder network are based on convolutional layers. While the decoder layer is equipped with sampling layers along with convolutions, on the other hand the encoder layer employs pooling layers. A shortcut skip connection is established between encoder-decoder modules. Architecture of U-Net is illustrated in Figure 2.10 with the help of block diagram. The U-Net model is especially developed for biomedical purposes and it extensively used by researchers. U-net model was modified by [52] to form a novel technique called skin-Net, where the encoder module of U-net architecture is modified by applying dilated convolutional changes into lowest layers of convolution. Although its shortcomings are a weak decoding module for revieing feature maps and a fragile shortcut skin connection of U-Net which losses the details of dermoscopic image.

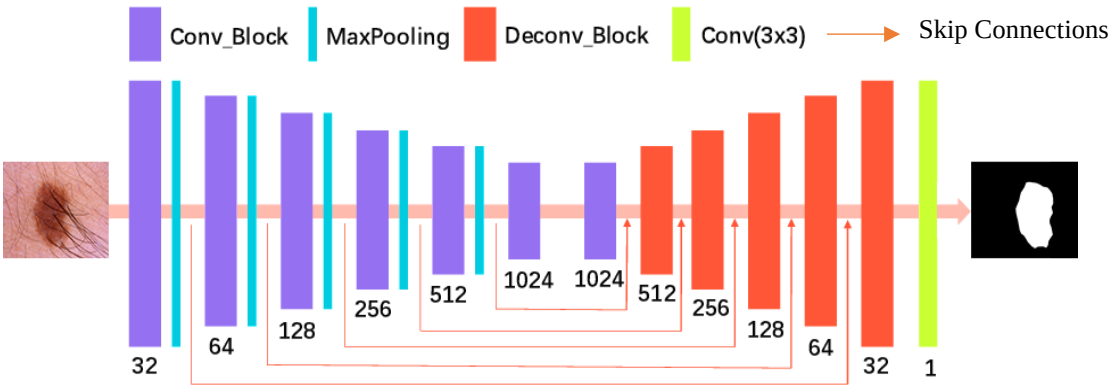

Figure 2.10 : Diagrammatic representation of architecture of U-Net

2.3.3 Feature extraction

Feature extraction approaches are employed to achieve attributes of suspected lesion in order to detect the category and degree of skin-cancer. Gabor features, Gradient feature, Fourier descriptors technique, Contour methods, Projection Histograms, Graph based analysis, Transformation of image, and Template matching are extensively used techniques for extraction of features from skin lesion image[53]. Inevitably, the inspection by hand-crafted features such as shape, texture and colour of skin lesion is necessary for diagnosis of premature melanoma lesion [54]. Several analytical attributes like contour, histogram, shape, texture and colour along with clinical methods of features extraction such as global and local pattern, ABCD rule, CASH , seven-point checklist, and Menzies method; are employed for diagnosis of malignant melanoma, however the primary difficulty is while selecting the minimal set of feature which will be able to produce high marks of accuracy and performance along with low score for computational time and complexity. Additionally, a definite and effective set or list of features of malignant melanoma is not mentioned in the current literature for segmentation or detection of melanoma lesion. A huge variation of dermoscopic images is observed in various datasets, thus distinct results are fetched on different dataset for different features. According to [55] high accuracy value of specificity and sensitivity is achieved while testing the method on 206 dermoscopic images for high-level features such as texture, colour, border and asymmetry. According to comparative research of 2017, which includes the minute features in its set such as thirty-six colours and fourteen shape features which were tested by 250 classification images. However this process takes high computational time [56].

Conclusively, numerous modern methods and algorithms are introduced yet they are incapable to operate for multiple features. Therefore a generalised method which could be manifested for extraction of important features from the lesion image is the need of the hour. Several researchers have come up with efficient feature extraction methods for the specified datasets, however the literature lacks feature detection of malignant melanoma report from dermoscopic images. Apart from

extraction and detection of traditional features such as texture, colour and shape the feature extraction techniques should focus on identification of dermoscopic structures like streaks and globules, which would be especially specified for melanoma lesion. Additionally, an association between pixel colour of lesion and colour of general malignant lesion will advance the results of image processing because the intensity of colour will represent the texture of the lesion and the depth of malignancy inside the skin. The prior knowledge about the depth of damaged skin will alarm the patient as the penetration of malignancy is directly proportional to mortality. A detailed review about the hand-crafted, clinical, pattern and deep learning based methods of feature extraction for melanoma skin lesion is summarised in forthcoming sub-parts.

2.3.3.1 Hand crafted feature extraction techniques

In the past decade, image classification and object detection techniques of computer vision have marked an extensive use of handcrafted features like LBP and SIFT[57]. As time passes, and the urge to fetch efficient accuracy increases, researchers across the globe have developed several feature extraction techniques to overcome different challenges of digital image. Hand crafted features can be broadly classified into Colour, Texture and Shape based features.

2.3.3.1.1 Colour based features

Previously, numerous researchers have worked in the field of medical vision, and several methods were introduced to enhance the performance of automatic and semi-automatic detection of melanoma skin lesion based on various criteria for evaluation. Texture and colour of the image are the most prominent features of a skin lesion image [54]. While the latter being most dominating attribute for detection of diseased portion from dermoscopic image. Any sudden change in the colour of a lesion is a premature indication of lesion being benign or malignant. As mentioned in the literature, chromatic feature well-known as ‘colour feature’ are widely utilised for analysis of image in the field of medical vision, as a healthy skin can easily be distinguished with malignant lesion due

to variation in colour [58]. Two methods were introduced by [59] which were based on local and global features, where texture and colour based features were used for identification of malignant lesion from acquired image. Additionally, the literature also consist of quantified analysis of texture and colour based features, and it claims that features based on colour produces more effective outcome than texture based features.

Accurate recognition of colour along with appropriate distribution is necessary for efficient diagnosis of diseased dermoscopic image. Precise spotting of pigment, degree of pigmentation and diffusion of colour in the dermoscopic image are the primary module for diagnosis of malignant melanoma [54]. One of the fundamental challenges of colour based feature extraction is appearance of epidermis layer of the skin as colour white in dermoscopic image decreases the accuracy score for diagnosis. Therefore presence of melanin colour is a fundamental requirement as it helps in visual segregation of chromatic and structural patterns within dermoscopic images.

The effected region of skin might be visually discriminated on the basis of localization of melanin pigment deep into the various skin layers. Usually the top layer of epidermis turns into black pigment of melanin, while the underneath layers of skin appears in slate blue and steel blue colour for papillary dermis and reticular dermis respectively, and the junction of dermo-epidermal seems to be light to dark brown depending on the degree and stage of malignant melanoma. When the lesion appears with shades of red, it is generally implies bleeding from the effected region, increase in count of capillary vessels or it is related to excessive vascularization within the malignant tumour. [60] introduces a method of detection of hue of dermoscopic image to detect blueish black to reddish black colour which signifies continuous internal bleeding and development of crust over the lesion.

2.3.3.1.2 Texture based features

Texture of lesion being an indigenous feature of a dermoscopic lesion which have pattern or structural aligned information of the skin. A correlation between grey values and spatial

neighbourhood pixel in image space is presented by texture feature. Analysis of texture feature of dermoscopic image is classified into four different methods, namely; transform-based method, structural method, model-based method and statistical method. The first method based on transform utilises properties of spatial frequency for translating the acquired picture to a latest form like wavelet, Gabor and Fourier transforms. The structural method are extensively employed by applications for pattern recognition on the basis on geometrical and topological attributes. Whereas, the stochastic and fractal model are employed by model based methods, which uses fractional Brownian motion (fBm), Gaussian Markov random field (GMRF), and autoregressive (AR) model. The last method being the statistical methods which includes descriptors of second-order statistics classical method such as gray level co-occurrence matrix (GLCM), gray level histogram, run- length matrices (RLM), and edge frequency. The latest method is employed for random texture and for the condition where identification of texture elements or texture primitives are challenging [61].

To diminish the repetition of data, scientist across the globe employs Fourier power spectrum, wavelet packet transform (WPT), Gaussian derivative kernels, principal component analysis (PCA), decision boundary feature extraction and gray level co-occurrence matrix (GLCM) for generation of skin based texture feature [62]. Geometric and standard properties exists in skin texture, therefore texture of skin cannot be effectively determined by solo method. A pattern-based classification approach is employed by [63] which used texture and colour based features. Employing features of multiscale texture and uniform colour space the method achieves a specificity mark of 93.75% and sensitivity score of 89.3%. Additionally, Regional average binary grey level difference (RABGLD) co-occurrence matrix is a new method which was introduced by amalgamation of structural parameters and second-order statistics for extraction of patterns based on texture. [64] proposed a new SFTA technique for extraction of features based on texture and have fetched accuracy score of 96%. However the conventional SFTA is able of fetch a accuracy mark of only 94%.

2.3.3.1.3 Shape based features

Determination of shape of a diseased lesion is based on diameter and border rule, where six different attributes are considered; Area and perimeter being the first two features that are employed to quantify the dimension of diseased lesion, whereas aspect ratio and perimeter to area ratio are two set of features which are used to define relation between the width and height of the smallest rectangle that covers the region of lesion. Solidity ratio is another feature of the list, where the area of convex hull is utilised to divide the area of skin lesion to draw boundary across the lesion. Extent ratio is the last set of feature where the area of diseased terrain is disintegrated by area of smallest bounding boxes. A composite technique is introduced by [65], who employed additive law by extraction of texture, colour and shape features, and the proposed system have performed well on PH2 dataset, additionally it have produced an accuracy of 97.5%, and a mark of 96.7% and 97.7% for specificity and sensitivity respectively, and 97.5% for F-score.

2.3.3.2 Clinical based feature extraction techniques

Various clinical based feature extraction based approaches such as seven point checklist, Menzies method, Asymmetry-Border-Colour-Diameter-Evolving (ABCDE) rule and CASH rule are utilised for identification of malignant melanoma from dermoscopic image. This section deal with different feature extraction techniques which are well discussed in details in further sub-sections.

2.3.3.2.1 Seven point checklist

According to the suggestions of National Institute for Health and Care Excellence (NICE), seven point checklist should be used as pin point evaluation factor for extraction of features from dermoscopic image [66]. Diagnosis of skin lesion based on ELM seven point checklist depends on four minor and three major scoring standards. The major attributes are atypical vascular design, the blueish white mask, and atypical pigment network. Whereas the list of minor attributes are formations of regression, irregular dots/drops, irregular pigmentation, and irregular streaks. Tabular

representation of attributes of seven point check list is mentioned in Table 2.4. EML seven point checklist is a new method of machine learning, which was introduced by [11] in mid of 2010, which automated the melanoma diagnosis process. The method defines a series of seven attributes on the basis of colour and texture of dermoscopic lesion. Additionally this method suspects a lesion to be malignant only if the score is three or more. Pictorial representation of extraction of features by seven point checklist is shown in Figure 2.11.

Table 2.4: Tabular representation of attributes of seven point checklist

Major criteria for ELM	**Score**	**Minor criteria for ELM**	**Score**
Atypical Vascular Pattern	2	Regression pattern	1
Blueish Gray areas	2	Irregular globules and dots	1
Atypical network of pigment	2	Irregular diffused pigment	1
		Radial streaks	1

Sample skin image:
Irregular and prominent pigment network (Score: 2)
Irregular dots and globules (Score: 1)
Blotches (Score: 1)
Streaks (Score: 1)

TOTAL SCORE: 5 (Classified as malignant lesion)

Figure 2.11 : Pictorial representation of extraction of features by seven point checklist

2.3.3.2.2 Menzies method

Menzies method of scoring was introduced by Menzies in the year 1996. This method of evaluation was on the basis of positive attributes and negative attributes [12]. Where whitish blue mask, expended network, multiple dots of grey or blue, existence of more than 4 colours, depigmentation like scar, radial streaming, pseudopod and multiple brown dots are the list of positive attributes; whereas single colour lesion with symmetrical pattern constitute to negative attribute. The circumstance under which a malignant lesion is identified as melanoma is, when more than one positive attribute are detected in the dermoscopic image. While the circumstance for a lesion to be identified as non-malignant is absence of any negative attribute in the skin lesion image. Positive and Negative attributes are tabulated in Table 2.5, which encapsulates the list of attributes for scoring a

lesion. The method states that number of positive attributes for melanoma lesion can be more than one, but there should not be any negative attribute for non-melanoma lesion.

Table 2.5 : List of positive and negative attributes of menzies method

Positive attributes for malignant tumor	Negative attributes for malignant tumor
De-pigmentation like scar	Single colour
Pseudopods	Symmetrical pattern
Broadened network	
Various dots of brown colour	
Various dots of blueish grey colour	
Radial streaming	
Blueish white veil	
Presence of Multiple colour (5-6)	

2.3.3.2.3 ABCD Rule

Dermoscopic method of Pattern analysis was succeeded by ABCDE rule which was developed by Friedman [10]. The ABCDE rules stands for Asymmetry in boundary, irregular Border, variation in Colour, enlarged Diameter and continuous Evolving. The first component of ABCD rule is asymmetry which resembles non-malignant lesion incline to be circular and symmetrical, whereas malignant lesion visually appears to be ameboid shaped and asymmetrical in nature. While the second component resembles irregularity of lesion border which appears to be blurred, notched and ragged. Colour being the third component describes that malignant melanoma mole contains variable colour and shades of lesion, it constitute of huge range of colour from brown, black to tan. The lesion might show a pigment of blueish black or even shades of white. The fourth component being diameter of lesion indicates that if a lesion is of diameter more than 6mm than it might be noxious and claimed to be malignant. Concluding component is evolving, which marks the rate of change in visual appearance of a mole which might gradually grow to be malignant in nature over specified weeks or months. Figure 2.12 pictorially represents the ABCDE features over dermoscopic images. Rule of ABCDE which is popularly known as ABCD in context of medical vision. ABCD rule results to be less computationally expensive when compared with Menzies method and seven point checklist for extraction of features from the dermoscopic image, thus it compels to be more favourable and usable

among researchers for feature extraction. Additionally, for clinical based diagnosis, ABCD rule is proved to be more consistent. [67] proposes a approach based on both classical and modern ABCD rule and conventions which are directed by skilled dermatologists for recognition of pattern over the lesion. To decrease the computational time for feature extraction a quantitative feature based on inner pattern of skin lesion images are evaluated by simple operative method, thereby fetching an accuracy of more than 85%. Illustration of scoring conditions, factors and values are well summarised in Table 2.6. Whereas Table 2.7 describes the classes and respective results after employing rule of ABCD.

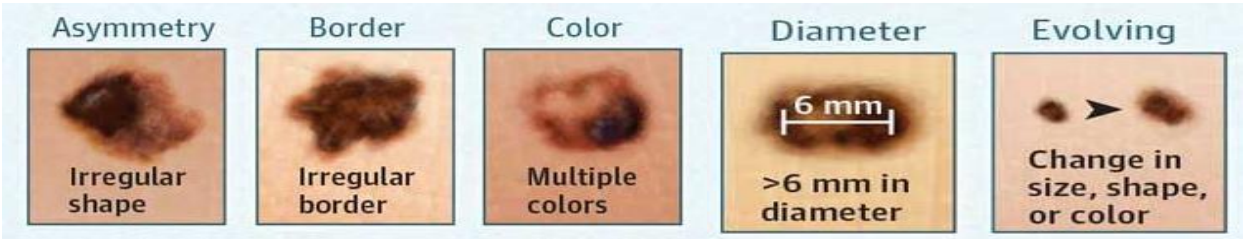

Figure 2.12: Pictorial representation of ABCDE rule

Table 2.6: Illustration of scoring conditions and factors of ABCD rule

Conditions	**Asymmetry**	**Border**	**Colour**	**Diameter**
Description	Structure, colour and contour	Eight Segments	Light-brown/tan, blueish grey, reddish black, white and dark brown	More than 6mm
Factor	1.3	0.1	0.5	0.5
Scoring	0-2	0-8	1-6	1-5

Table 2.7: Classification of lesion based on respective score of ABCD rule

Type of class	**ABCD Score**
Benign (Not dangerous)	Less than 4.67
Suspicious tumor	Ranges from 4.67 to 5.45
Malignant melanoma	More than 5

2.3.3.2.4 CASH Rule

The CASH rule is used to extract features of a skin lesion on the basis on colour, architecture, symmetry, and homogeneity. Architecture is one of the characteristic used in the CASH rule, which was not prior used but well-known feature extraction methods [13]. The scoring parameters are represented in Table 2.8. Total CASH score is calculated on the basis of scoring criteria, thereafter if

the total score is more than 7, the lesion is considered to be melanoma. The CASH system is merely a feature extraction method and not intended to be used for clinical diagnosis. Moreover, It could aid the decision making process by clinicians before performing biopsy on suspicious lesion. Figure 2.13 pictorially represents classification of various dermoscopic lesion by employing CASH method.

Table 2.8: Classification of lesion based on respective score of CASH rule

Parameter	**Points**	**Conditions**
Colour	1 point for each condition	Blue, White, Red, Black, Dark brown, light brown.
Architecture	0	None/mild
	1	Moderate
	2	Marked
Symmetry (Shape and structure of dermoscopic lesion)	0	Biaxial symmetry
	1	Monaxial symmetry
	2	Biaxial asymmetry
Homogeneity (based on structure)	1 point for each condition	Polymorphous blood vessel: presence of irregular or dotted lines
		Blotches: Covering 10% area of lesion
		Regression structures: Gray region without/ with peppering
		Blue-white veil
		Streaks/pseudopods
		Dots/ globules
		Network

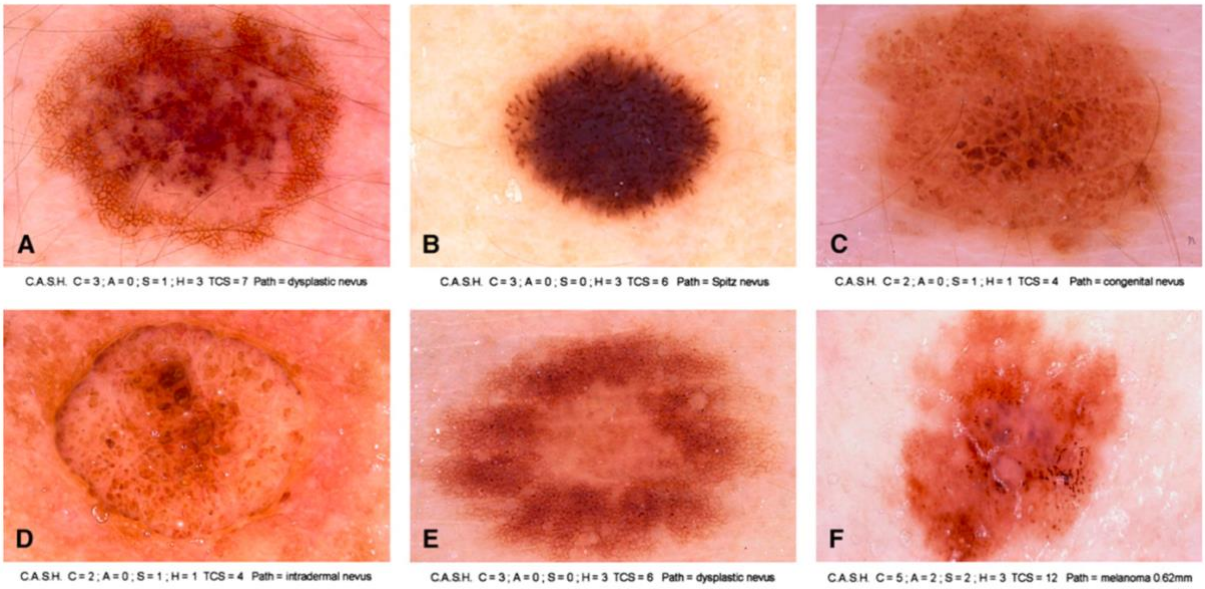

Figure 2.13: Classification of lesion using CASH rule [13]

2.3.3.3 Pattern analysis based feature extraction techniques

As stated by Consensus Meeting of Dermoscopy (CMD), the technique of pattern analysis including both local and global features was upgraded in early 2000's. Although diagnosis of malignant melanoma can be done by both global and local features [54]. While the Local feature constitute of information about features of atypical nevi, recurrent nevus, blue nevus, Spitz nevi, intradermal nevus, congenital nevus, junctional nevus, compound nevus and formation of lesion by generation of pigmented network and dots over the skin. Contradictorily, the global features constitute of complete assessment attribute, which contains cobblestone, Stardust, parallel, homogeneous, globular, reticular, multi-component, and unspecific patterns. Global pattern technique of feature extraction is proved to be better than Menzies method, seven point checklist and ABCD rule for classification of lesion, thereby it produces a maximum performance of malignant detection [68].

An approach by amalgamation of global and local features is proposed by [70]. A bag of features is acquired under local features from the original image, and the global features are the geometry or shape based features those are extracted from the dermoscopic image. Both these features are amalgamated into two fusion class named as early fusion and late fusion. The literature of the paper claims that the late fusion is a novel idea and is never utilised before, moreover it produces enhanced results of classification for PH2 dataset.

2.3.3.4 Deep learning based feature extraction techniques

Algorithms of machine learning can be classified into supervised and unsupervised based techniques, where the prior deals with labelled data and the latter is a model of unlabelled data. Regression methods such as logistic, linear and polynomial, Decision tree, Random forests and classification methods such as ANN's and naïve Bayes are the types of Supervised learner. Whereas hidden Markov model and clustering methods like PCA and k-mean are example of unsupervised approach of machine learning. The layered structure being the primary feature of deep learning model

as first introduced by Geoffrey E. Hinton in 2006. As years passed it have developed various approaches to implement deep learning model. A deep learning model is not only used for computation of hierarchical features but also for higher level features, which is not possible to be extracted efficiently by classical machine learning methods.

Artificial neural networks have being employed in recent years for extraction of deep features from dermoscopic images. In recent literature by [57] the methods based on deep neural networks for feature extraction have shown significant results with a sensitivity mark of 97% and specificity score of 96%. It also proves to be most reliable and significant contender in the list of various feature extraction techniques by producing an accuracy mark of 97% when tested over PH2 dataset.

2.3.4 Classification

According to CAD method, classification of dermoscopic image is considered to be most important stage for detection of skin lesion into specific category. Classification of dermoscopic image do facilitate the method of digital diagnosis of malignant lesion. Various categories of skin cancer could be diagnosed and identified from dermoscopic image. A dermoscopic image is classified majorly into malignant or benign by employing various classification techniques. Henceforth they are classified into Vascular, Melanoma, Nevi, Dermatofibroma, Solar Lentigo, Seborrheic Keratosis, Squamous Cell Carcinoma, Actinic Keratosis, or Basal Cell Carcinoma lesion.

Artificial Neural Network (ANN), Fuzzy Classification methods, and Decision Tree are the classical method of classification of dermoscopic image. In recent times, deep learning based approaches have fetched significant results for analysis of dermoscopic skin image, moreover deep learning have enable detection of dermoscopic lesion by simple image acquisition methods [71]. Upcoming subsections have investigated about various conventional and deep neural network based classification methods in detail. It further scrutinises every state-of-the-art technique to draw a clear conclusion about different classification techniques.

2.3.4.1 Conventional classification method

Conventional classification methods of skin lesion identification are fundamentally based on classical methods by employing region or pixel based techniques for feature extraction, thereafter the extracted features are passed to classifier for classification of dermoscopic image into specific category of skin cancer. Different models of conventional classifications are summarised as follows:

1. ***Traditional intelligence based techniques*** are developed on the basis of intelligent computing by making inferences. These techniques have ability to process uncertain, vague and null-valued information which will be of great help in the medical science where uncertain data is available. Although these models are not extensively used as they are sensitive to inhomogeneities of intensity and noise of the image, additionally these models cannot work efficiently with spatial modelling. Swarm intelligence, genetic algorithms, fuzzy based inference system and artificial neural networks are the instances of traditional intelligence bases technique.
2. ***Support vector machine (SVM)*** is an architecture of supervised learning which performs analysis and classification of image. Rule-based architecture is applied for identification of patterns by the classifier in order to execute binary classification, where decision boundary is employed as a right hyper-plane to achieve maximum separation. All the cost functions are optimised by SVM, thereby making it an ideal classifier. Although SVM tends to produce a biased outcome during unavailability of probable class membership function [72].
3. ***Instance based classifiers*** were proposed by Khalid and Jamil [72], where they compared instances of new pattern with identified instances while training the system, additionally it does not employ generalization such as various other classifiers. Implementation of this technique is simple and training phase is not required, which saves a lot of computational energy. However, these classification methods do require high computational time and sometimes it turns up to be complex and insensitive. RBF networks, kernel machines and K-Nearest neighbour (KNN) algorithms are examples of this technique.

4. ***Decision trees*** were proposed by [73], these are tree-like structures where attributes are represented as a tree. Each node is a representation of an attribute and the optimum attribute is set as root node, which creates directives for classification of image samples. Major advantage of using decision tree is its features, which allows to bypass parameter setting. Notwithstanding the fact that noise can influence the outcomes and they are unable to classify data beyond their training set. Random forests are instances of decision tree.

2.3.4.2 Deep neural network based classification technique

Rapid growth and progression in computing resources like SSD and GPU's have led to significant development in the field of computer vision by introducing several models of deep learning like Convolutional Neural Network (CNN) [71]. Evolution of CNN with well-formed formulas of deep convolutional network have marked magnificent results for processing and classification of dermoscopic images by state-of-the-arts. Method based on Deep neural network have been proved to perform better than traditional method for classification of dermoscopic images. However, the deep learning based approach also faces few challenges which can be subjugated to fetch best-fit results by making modifications in convolutional layers.

2.3.4.2.1 Overview of CNN

CNN is a category of artificial neural networks which is fundamentally employed for investigating images and to produce meaningful results. These CNNs are network of neurons which can optimize by themselves through regressive learning. It is originated as a group of convolution layers which are equipped with several functions to process and classify the high dimensional vector image into its significant category. The pictorial representation of CNN is shown in figure 2.14 which includes all of its major modules such as hyperparameters, activation function and layers. Optimizers, learning rate, padding, batch size, and filter kernel are a few of the criteria of Hyperparameters. Optimizers are employed to generate maximum outcomes from a convolutional model. Nesterov and

Sobolev gradient-based optimizers, rmsprop and Adam are a few of the examples of optimizers. The activation function module is used as a transformation unit which is used to map the acquired signals into resultant signals for operating the deep neural network. Softmax, Exponential Linear Unit, Rectified linear units (ReLU) which is also termed as piecewise linear functions, Sigmoid functions (hyperbolic tangent and logistic functions), and linear activation function are few of the popular types of activation functions. Fully connected, pooling and convolutional layers are primary categories of layers in CNN [72].

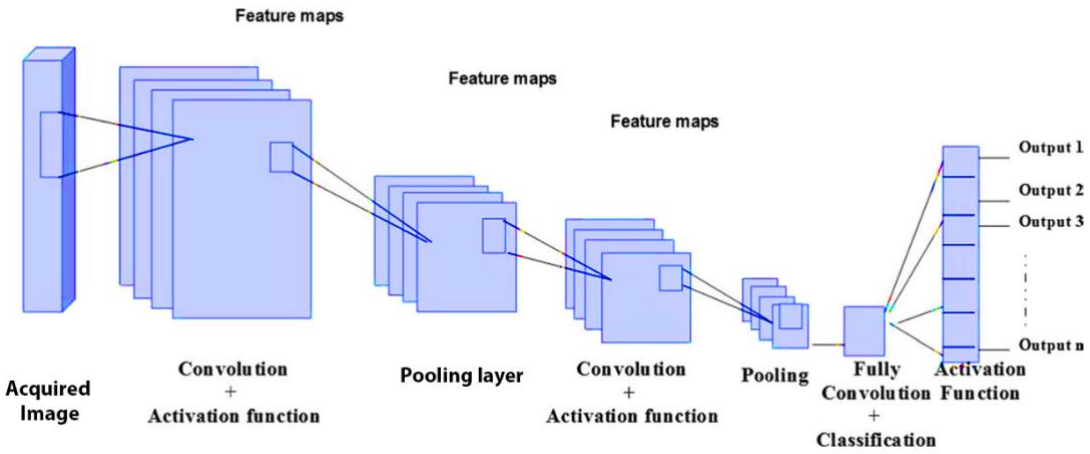

Figure 2.14: Generalised architecture of CNN

2.3.4.2.2 Different architecture to CNN

Several models of CNN are present in literature. These models are prime reasons for constructing algorithms of deep learning. The models are briefly explained below:

1. ***AlexNet*** *:* It is elementary yet powerful CNN model which contains pooling and convolutional layers. Henceforth these layers, a network of fully connected layers is present in this architecture. For extraction of features it employs filters of both large and small size, with initial layer being of 5X5 and 11X11 in dimension while the end layers are 3X3 in size. Due to larger dimension of filters it tends to generate artifacts from feature map which are already being trained. The fundamental advantage of AlexNet [74] is the presence of the scale which

enable the parallel utilization of GPU while training and classifying the data, therefore it act as an accelerator to deal with complex models. It is still employed as initial stage for most of the models of deep neural networks specifically in the field of speech recognition and computer vision. Pictorial representation of architecture of AlexNet is shown in figure 2.15.

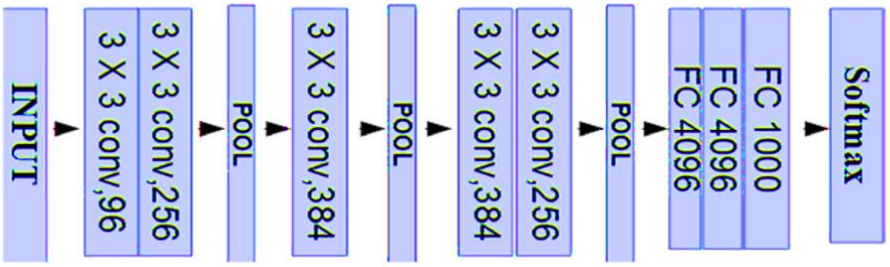

Figure 2.15: Generalised architecture of AlexNet

2. ***VGG Net*** : VGG Net is specified by pyramidal shape. This deep learning architecture was developed at Oxford University by researchers of Visual Graphics Group. It is constituted by sequence of convolutional layers which is succeeded by pooling layers, these pooling layers are narrowing the shape of the layers [72]. It is well illustrated in figure 2.16, where the complete model is described. The architecture is well-formed for processing which makes it favourable for setting it as benchmark for certain task. Pre-trained models of VGG net is extensively used by several popular state-of-art technologies. Although the fact that it takes a lot of time and computational resources while training the system makes it unfavourable among researchers.

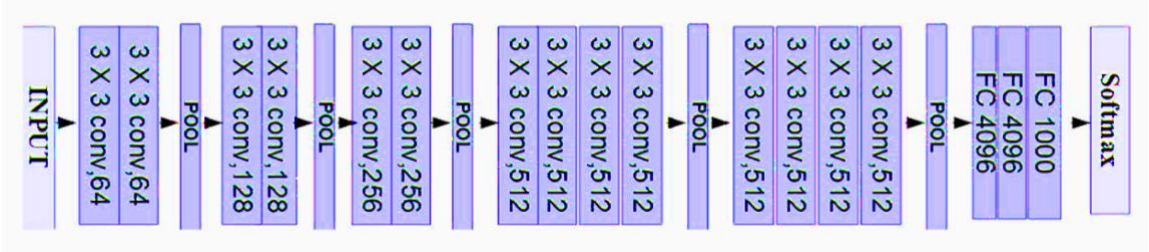

Figure 2.16: Architecture of VGG net

3. ***Google Net*** : It is developed at Google by several well-known researcher. It is also termed as Inception network as the model is formed by multiple inception modules which are stacked

over each other as represented in figure 2.17. These stack of inception layers enables both parallel and joint training. This neural network is constituted by twenty-two layers, and it utilises a method of split, transform and merge processes. Additionally, this network is able to pool the input or convolve an input. The major advantage of using google net is its high speed training of data with limited resource. Limit of divergence is increased by an Xception network which is present in inception module. Use of bottleneck layer reduces the count of parameters which is an advantage for researchers but it also losses important information due to narrowing of the layers. The convergence rate is improved by the use of auxiliary classifiers. Although the use of heterogeneous topology makes customization of parameters a challenging task [76].

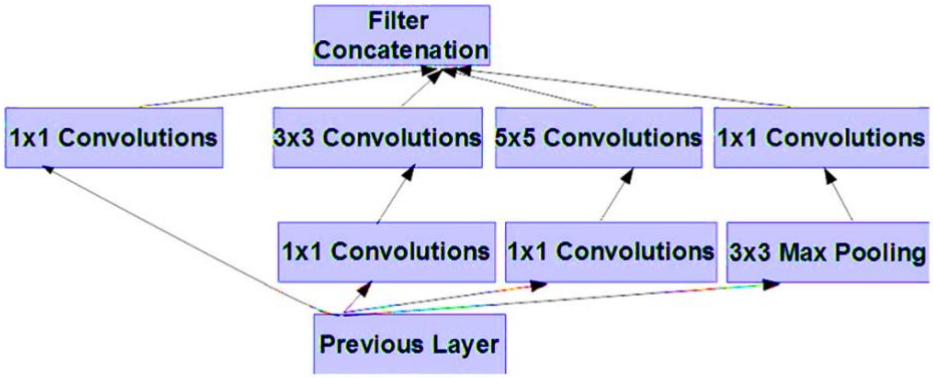

Figure 2.17: Diagrammatic representation of the inception model

4. ***ResNet*** : An architecture of ResNet is also termed as residual network as it is designed by several successive residual modules, which are fundamental units of this network [77]. It is deep CNN architecture of 152 layers of residual blocks. A complete end-to-end network is formed by stacking these residual modules. The major advantage of ResNet is its ability to be developed from several residual layers which can be employed during training the network thereby it increases its accuracy. Additionally, this network is 8 and 20 times denser than VGG and AlexNet respectively. Computational complexity of ResNet is also minimum when

compared with previous proposed networks. ResNet with 50, 101 and 152 layers are examples of ResNet architecture.

5. ***ResNeXt*** : ResNeXt, also is termed as Aggregated Residual Transform Network is a modern and advance method for object detection which is assembled by encapsulating architecture of ResNet and GoogleNet. It is an advance version of GoogleNet that utilizes the idea of split, transform and merge in a significant yet easy way by proposing cardinality. The amount of set for transformation is called Cardinality, which is employed by combining architecture of GoogleNet and VGG topology by modifying spatial resolution to 3X3 filters in the split, transform and merge blocks. Furthermore, to enhance the convergence of wide and deep network, residual learning is employed by ResNeXt [78]. Several transformations are used in a split, transform and merge block, thereafter these transformations are defined by cardinality. Significant rise in cardinality enhances the accuracy and develops a new and modified architecture, although the computational cost is very high.
6. ***Deep reinforcement learning*** : Reinforcement learning systems are created and trained from the basic roots, from the randomised behavioural set to knowledge based set which is gained from past experiences while training the datasets. It is an encapsulated version of deep learning and reinforcement learning which uses less amount of computational data and resources. The agent is capable of learning from its stimuli, thereafter it uses the learning for decision making problems for random series including analysis of image. AlphaGo Zero and AlphaGo are the examples of deep reinforcement learning [79]. The prior mentioned model requires less computational resources than the latter, additionally it also produces efficient results at higher level because of the adaptation of several state-of-art techniques.
7. ***DenseNet*** : Architecture of DenseNet is same as ResNet, it was introduced to resolve the problem of vanishing gradient. It employs cross-layer connectivity thereafter it connects every layer to its succeeding layers in a feed-forward manner to resolve the complexities that arises

in ResNet, which specifically saves details by transformation of additive identity which led to increase in complexity of the network. DenseNet model employs dense blocks thereafter the feature maps of prior layers are used as the inputs for all successive layers [80]. The diagrammatic representation of the network is shown in figure 2.18.

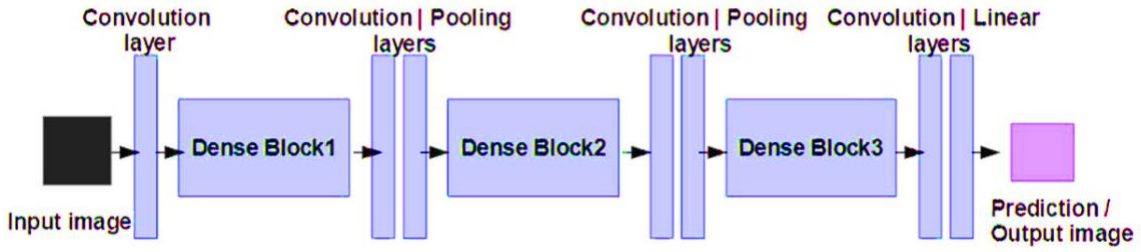

Figure 2.18: Architecture of Dense-Net

Table 2.9 summarises the performance of the above stated CNN models and project light into the strengths and weaknesses of each model.

Table 2.9: Evaluation of various CNN models on the basis of strength and weakness

CNN model	Strengths	Weakness
AlexNet	• Regularization in CNN • Uses GPU parallelly to accelerate the process.	• Generates artifacts due to large filter size
VGG	• Uses efficient receptive field with homogenous and simple topology	• Uses computationally expensive fully convolutional layers
GoogleNet	• Bottleneck layer reduces parameter count. • Convergence rate is improved by the use of auxiliary classifier.	• Parameter customization is difficult • Information might be lost due to representational bottleneck model.
ResNet	• Residual learning is employed	• Complex design • Degrades information quality during processing
DenseNet	• Remove redundant feature-map	• Large number of parameters at each layer
ResNeXt	• Customizable parameters • Grouped convolution	• High computational cost

2.3.4.3 Recent application of CNN

In recent years, CNN models are utilized significantly in numerous fields especially for classification of dermoscopic images. A computer aided automatic diagnosis technique was introduced by [81], for detection of malignant melanoma from dermoscopic image at an elementary stage. InceptionV3, MobileNet, VGG16 and VGG19 are the four different models which employs dilated convolution for training, validating, and testing of the models over HAM10000 dataset. It fetched an accuracy mark of 89.81%, 88.02%, 87.42% and 85.02% respectively for each model. Ensemble of deep learning architectures like ResNeXt, SENet and EfficeientNets, are employed to perform classification of skin lesion by [82]. A modified architecture of deep learning is used by [83], where 12,378 skin lesion images are used to train the CNN model for digital diagnosis of malignant melanoma. The researchers used the model to diagnose hundred dermoscopic images and evaluate the results in terms of hand drawn ground truth segmented images by 157 dermatologist from twelve hospitals in Germany. The model proposed by [83] seems to be more effective than an expert dermatologist, as their decision making is based on visual inspection which is prone to errors.

Adaptive momentum learning rate (ADAM) by gradient descent and transfer learning were used by architectures of AlexNet and GoogleNet for skin lesion classification by [84]. Classification performance of the system was calculated and compared over ISIC dataset of dermoscopic images. Seborrheic keratosis, melanoma, and benign are the three classes that are classified by the system. The system performed classification over both segmented and non-segmented dermoscopic images and fetch the accuracy score of 92.2% and 89.8% respectively for each testcase. [85] have introduced a framework of deep learning which is integrated with information's of deep features to produce significant feature vector. Entropy-Controlled Neighborhood Component Analysis (ECNCA) was used for reduction of dimension and selection of discriminant features. Specific layers of popular CNN's such as Inception-V3, Inception-ResNet-v2, and DenseNet 201 are utilized for classification by the above mentioned system. ISBI-2017,ISIC UDA, ISIC MSK, and PH2 datasets are employed

to evaluate the performance of the system, the accuracy score for diagnosis of skin lesion for these dataset are 95.9%, 97.1%, 99.2% and 98.8% respectively.

Inception- ResNet-v2, VGGNet and SVM are the three deep network models which are compared for classification of seven different category of dermatological disease from dermoscopic image by [86]. The Architecture of Inception-ResNet-v2 was evaluated to fetch highest score for classification of skin lesion images. Modern method of diagnosis of dermoscopic images by deep learning approach was introduced by [87], where the model employs feature–based methods and deep neural networks for classification. Pretrained models of NasNet-Large, ResNet-101 and GoogleNet were used in their proposed architecture, these models were trained over dataset from Places356 and ImageNet. Furthermore, SVM was employed for detection of lesion, and it fetches high score of accuracy. Thereafter the classification the system was capable of discriminating skin lesion images into two classes: benign nevus and melanoma.

An amalgamation of ABCDE rule along with deep learning models is proposed by [88] to fetch effective results of pre-processing, feature extraction, and classification of dermoscopic images. Along with extraction of handcrafted feature by ABCDE rule, deep learning based features are also extracted by employing CNN model. The proposed system was calculated over ISIC 2018 dataset and compared with state-of-art frameworks such as Relevant Vector Machines (RVMs), SVMs and Linear Regression (LR) models. The system yields an enhanced values of sensitivity, specificity and accuracy over other existing models. A Deep Supervised Multi-scale network (DSM network) is proposed by [89] which is used on dermoscopic images to perform automatic segmentation of skin lesion. To execute segmentation of skin lesion, the proposed framework employs side-output layers within the convolution to incorporate information from superficial to dense layers with a block of multi-scale connection. A model of Conditional Random Field (CRF) is also employed to enhance the outcomes of segmentation. Conclusively, deep learning methods of classification and analysis of

images and videos have been proved to perform extensively better than classical machine learning algorithms in several field of medical vision.

2.4 Dataset and evaluation metrics

This section contains most vital information about the dissertation, it reflects the dermoscopic dataset available on internet for free. This section highlight on easily accessible and reliable datasets along with its ground truth results, which are published and accepted by expert dermatologist. Additionally this section also throws light on essential evaluation metrics which are used to evaluate each step of the proposed method in upcoming sections.

2.4.1 Overview of publicly available datasets

Publicly available and easily accessible datasets are used in our research work, which not only increases the speed of research but also enable us to employ large set of data for training the classifier and thereafter testing the proposed methodology. Table 2.10 gives a summarized figure of total number of dermoscopic images for each dataset for training, testing and validation respectively. Few of the well-known and extensively accepted datasets are mentioned below:

Table 2.10: List of skin lesion dataset

Dataset	Training	Testing	Validation	Total
Dermofit	1300	0	0	1300
PH2	0	0	200	200
HAM10000	8695	1320	0	10015
ISIC 2016	900	379	0	1279
ISIC 2017	2000	600	150	2750
ISIC 2018	8695	1320	0	10015
ISIC 2019	20251	2530	2530	25311
ISIC 2020	33126	0	0	33126

1. ***Dermofit dataset*** [90] was developed by University of Edinburgh. It comprises of 1300 dermoscopic skin images, which are acquired by Canon EOS 350D SLR camera and a controlled flash ring light is used to ensure proper lighting conditions. It consists 46 skin lesion image of Melanoma, 65 Dermatofibroma, 96 Haemangioma, 24 Pyogenic Granuloma, 78 Intraepithelial carcinoma, 257 Seborrhoeic Keratosis, 88 Squamous Cell Carcinoma, 331 Melanocytic Nevus, 239 Basal Cell Carcinoma and 45 Actinic Keratosis image. These 8-bit RGB skin lesion images which ranges from 177x189 to 3055x1630 pixel in dimension. Ground truths are generated by using a statistical technique which works on framework of level-set.
2. ***Pedro Hispano Hospital(PH^2) dataset*** [91] is obtained from Hospital Pedro Hispano. It comprises 200 skin lesion images which are captured using 20x magnification lens with a Tubingen Mole Analyzer system. It consists of 40 melanoma lesion, 80 atypical nevi and 80 common nevi image. These are 8-bit RGB dermoscopic images which ranges from 761×570 to 769×577 pixel in dimension. Ground truths are generated by manual annotation by skilled dermatologists. According to various literature reviews, PH2 dataset is most used publicly accessible dataset for dermatological disease detection.
3. ***The EDRA-Interactive Atlas of Dermoscopy (Atlas) dataset*** [92] is a illustrative group of pictures which allows comparison of samples of histopathology, dermoscopy and clinical. It contains 8-bit RGB images of dimension 700x447 pixel, which are captured by Optotechnik/ Dermaphot dermoscopy. However, it does not contains ground truth results, but few researcher in the literature are manually drawing segmentation borders for the lesion by consulting skilled dermatologist. Due to lack of ground truth images in the dataset, segmentation results cannot be compared or considered to be optimum, thus this dataset is rarely employed by researchers.

4. ***Human Against Machine or HAM 10000 dataset*** [93] comprises of a set of 10000 dermoscopic image from various set of population. Several modalities are used to acquired and store the images. This dataset is generally employed for training the classifier. This dataset is widely employed for machine learning, where 10015 skin lesion image are used. ISIC archive provide an easy accessibility of HAM10000 dataset.
5. **ISIC 2016 dataset** [94] is developed by International Symposium on biomedical images(ISBI) in the challenge of Skin lesion analysis towards Melanoma detection. The dataset for segmentation comprised of 900 training and 379 test images. To validate the results of segmentation and classification the ground truth images were provided along with the dataset and were compiled by a panel of the dermatologists. Distribution of dermoscopic images in ISIC 2016 dataset is illustrated in table 2.11.

Table 2.11: Detailed description of ISIC 2016 dataset

	CATEGORIES	M	B	TOTAL
ISIC 16	**TRAINING**	173	727	900
	TESTING	75	304	379

6. ***ISIC 2017 dataset*** [95] is also complied by ISBI in 2017, it constitute of 2000 images for training, 600 lesion images for testing and 150 images for validation. The dataset consists of 3 classes namely: Malignant melanoma (MM), Seborrhoeic Keratosis (SK) and Benign Nevus (BN). Image resolution of both training and testing images is ranging from 1022x767 to 6748x4499 pixels, these are 8-bit RGB images. It contains 1450 of BN, 296 of SK and 404 MM images in training and validation section, where as it constitute of 393 BN, 90 SK and 117 MM images for testing. Table 2.12 briefly illustrates the division of dermoscopic images for ISIC 2017 dataset.

Table 2.12: Tabulated description of ISIC 2017 dataset

	CATEGORIES	MM	SK	BN	TOTAL
ISIC 17	**TRAINING**	374	254	1372	2000
	TESTING	117	90	393	600

	VALIDATION	30	42	78	150

7. ***ISIC 2018 dataset*** [96] is originally sourced by HAM10000, it contains 10015 training images of various skin diseases along with their ground truths. To improve the accuracy of melanoma diagnosis, ISIC along with International society for Digital imaging of skin (ISDIS) have accumulated largest dataset of skin lesion images which is available publicly. ISIC 2018 dataset contains seven classes of different skin diseases. Table 2.11 have encapsulated different classes along with total number of training files present in the dataset.

Table 2.11: Tabulated description of ISIC 2018 dataset

Class	**No. of images**
Melanoma	1113
Melanocytic nevus	6705
Basal cell carcinoma	514
Actinic keratosis / Bowen's disease (intraepithelial carcinoma)	327
Benign keratosis (solar lentigo / seborrheic keratosis / lichen planus-like keratosis)	1099
Dermatofibroma	115
Vascular lesion	142
Total	10115

8. ***ISIC 2019 dataset*** [97] is sourced from MSK, HAM10000 and BCN20000 Datasets. It is constituted of 25,331 RGB images of 8-bit for training along with ground truth images and 8238 test data images of skin lesion. The dataset contains ground truth images and corresponding metadata about sex, age and general anatomic site of the lesion. The dataset is derived of eight different classes: Squamous cell carcinoma(SCC), Vascular Lesion(VL), Dermatofibroma(DF), Benign Keratosis (Lichen planus-like keratosis, seborrheic keratosis and solar lentigo)(BKL), Actinic Keratosis(AK), Basal Cell Carcinoma(BCC), Melanocytic Nevus(NV) and Melanoma (MM). A detailed description of these classes shown in Table

2.12. Complete analysis of total number of dermoscopic images present in ISIC 2019 dataset is illustrated in table 2.13.

Table 2.12: Detailed description of different lesion categories present ISIC 2019 dataset

ISIC 19	CATEGORIES	MM	NV	AK	DF	VL	SCC	BCC	BKL	TOTAL
	TOTAL	4522	12875	867	239	253	628	3323	2624	25331

Table 2.13: Illustration of total number of images for training, testing and validation phase

ISIC 19	CATEGORIES	M	NM
	TRAINING	3622	16649
	TESTING	450	2080
	VALIDATION	450	2080
	TOTAL	4522	20809

M→Malignant NM→Non-Malignant

9. ISIC 2020 dataset [98] is the recently published dataset with 33126 dermoscopic images for training and 10982 test images. The dataset is developed by ISIC by accumulating skin lesion images of over 2000 patients from University of Athens Medical School, University of Queensland, Melanoma Institute Australia, Memorial Sloan Kettering Cancer Centre, Medical University of Vienna, and the Hospital Clínic de Barcelona. Along with skin lesion images and respective ground truths the dataset also consists of metadata of each lesion which stores the patient personal details like age, sex and site of lesion. Ground truth images are drawn by expert histopathologist by mutual agreement among the panel, which increases the legitimacy of the result. Table 2.14 illustrates the division of dermoscopic image of ISIC 2020 dataset.

Table 2.14: Detailed description of ISIC 2020 dataset

ISIC 19	CATEGORIES	MELANOMA	BENIGN	TOTAL
	TRAINING	584	32542	33126

2.4.2 Data augmentation

Data augmentation is a process of increasing the size of training dataset such that it would increase the reliability of prediction model. Moreover, deep learning models requires huge size data which might not be available, thus data is augmented to develop a generalised model.

Notwithstanding the fact that it can be applied in different domains (specially data analysis), it is extensively employed for computer vision. Position and colour based augmentation are few of the most common techniques for data augmentation of images. Rotation, translation, padding, flipping, cropping, scaling and affine transformation are the different methods of position based data augmentation, where the dataset is physically transformed such that the model produces enhanced output. Whereas, for the colour based augmentation, the contrast, brightness, hue and saturation of the image is modified to generate more training data. Generative Adversarial Networks (or GANs) are the deep learning based approach of generation of new sample images for training. These images are generated from noise by a series of convolutional layers. Another modern approach of data augmentation is, Neural style transfer, where the content of an image is combined with the style of other to generate new image which is used as training dataset.

2.4.3 Performance of evaluation metrics

This section specifies different evaluation metrics that are used to validate and evaluate each stage of CAD system: Pre-processing, localization, segmentation and classification. These metrics are accepted and employed globally by well-known researchers in similar domain.

2.4.3.1 Evaluation metric for pre-processing of lesion

The accuracy of pre-processing stage is evaluated by employing universal image quality index (UIQI), peak signal to noise ratio (PSNR), signal to noise ratio (SNR), root mean squared error (RMSE) and mean squared error(MSE). These matrices are used to calculate the enhancement capacity of the dermoscopic image in pre-processing stage, which might increase the accuracy of lesion detection in later stages. These parameters also measures the accuracy of pre-processing method by measuring its capacity to remove artifacts digitally.

The quality of image is widely measures by peak signal to noise ratio (PSNR) and signal to noise ratio (*SNR*). Where, P_{I_s} is the peak signal of the image and P_I is the noise level in it. Quality of

image enhancement is marked by high score of SNR and PSNR. If the empirical score of PSNR is higher than 20 dB it is considered to be a well-enhancement image. The quality of information sustained in the pre-processed image is portrayed by PSNR, higher values of PSNR depicts more sustained valuable details in the pre-processed image. Mathematical representation of SNR and PSNR are given below in eq. 2.1 and 2.2 respectively.

$$SNR = 10 \times log_{10}(\frac{P_{I_S}}{P_I}) \quad (2.1)$$

$$PSNR = -20 \times log_{10}(\frac{I_{S(max)}}{MSE}) \quad (2.2)$$

The mean difference between acquired image with noise I(i,j) and pre-processed image I_S(i, j) is calculated by MSE. The square root of MSE is calculated in RMSE. A low value of MSE and RMSE signifies to robust image enhancement. The loss of energy in pre-processed image is depicted by value of RMSE. It evaluates the difference in intensity of pre-processed and acquired image. Low value of RMSE portrays less distortion of processed image. Size of the input image is considered to be m and n in the equation. The equations for both MSE and RMSE is given as follows:

$$MSE = \frac{1}{mn}\sum_{i=0}^{m-1}\sum_{j=0}^{n-1}[I_s(i,j) - I(i,j)]^2 \quad (2.3)$$

$$RMSE = \sqrt{\frac{1}{mn}\sum_{i=0}^{m-1}\sum_{j=0}^{n-1}[I_s(i,j) - I(i,j)]^2} \quad (2.4)$$

UIQI is the estimation of linear correlation of acquired dermoscopic image along with pre-processed image, based on luminance, contrast and structure features in pre-processing stage. Mathematical representation UIQI is illustrated below:

$$UIQI = \frac{4\sigma_{I_P,I}\bar{I_P}\bar{I}}{\sigma_{I_P}^2+\sigma_I^2\,[\bar{I_P}^2+\bar{I}^2]} \quad (2.5)$$

$\bar{I}$, $\bar{I}_P$, σ_I and σ_{I_P} represents mean of input image, mean of pre-processed image, standard deviation of the acquired image and standard deviation of the pre-processes image respectively. The value of UIQI ranges from -1 to 1, which is used to ensure the image quality after enhancing the image. This matrix is used to express the evident change of removal of digital artifacts such as hair and thereafter refining the image from natural and clinical artifacts like clinical colour swatches, clinical ruler marks, black frame, etc. Image quality is measured by UIQI with respect to human vision by employing parameters like structural information, contrast and luminance. The value of UIQI is independent of RMSE, SNR and PSNR. UIQI value ranges from 0.4 to 0.7 for twenty test images of pre-processed lesion, this range is perceptible human vision range. Thus it is used to measure the capacity of pre-processing method to remove the artifacts of images along with enhancing the image by modifying its contrast and sharpness, without lowering the image quality.

2.4.3.2 Evaluation metric for localization of lesion

The performance of an algorithm is visualized by a 2x2 table which is known as Confusion matrix or error matrix. It encapsulates a detailed report of prediction results on classification problem. Each row represents occurrence of predicted class and each column indicates occurrence of actual class. It is employed for localization and classification of malignant lesion. Pictorial representation of confusion metrics is shown in figure 2.19. If a malignant lesion is predicted to be malignant it is defined as true positive (TP) value, where as if it is predicted to be non-malignant it is referred as False negative (FN). If a non-malignant lesion is predicted to be melanoma: it is classified to be false positive (FP), as it raises a false malignant flag, where as if it is predicted as non-malignant, the classification is termed to be True negative(TN).

Actual / Predicted	Melanoma	Non-Melanoma
Melanoma	True Positive	False Positive
Non-Melanoma	False Negative	True Negative

Figure 2.19 : Pictorial representation of confusion metrics

Evaluation of melanoma lesion localisation is executed by overlapping predicted region over ground truth region to find intersection area, this greedy method is termed as Intersection-over-union(IoU) which is represented in equation 2.6. The acceptable range of detection of melanoma area lies from 0.5 to 1. This matric is used to compare the predicted area with the ground truth which are generated by expert dermatologist, in order to calculate the accuracy of localisation.

$$IoU = 2 * \frac{TP}{TP+FN+FP} = \frac{Area\ of\ overlap}{Area\ of\ union} \quad (2.6)$$

Mean average precision(mAP) is used for evaluating localization phase by computing the mean precision of detection of melanoma area. Equation 2.7 shows the detailed mathematical representation.

$$mAP = mean\frac{TP}{TP+FP} \quad (2.7)$$

2.4.3.3 Evaluation metric for segmentation of lesion

Segmentation accuracy is evaluated by matrices such as Jaccard Index (JI), False Positive Rate (FPR), True Detection Rate (TDR), Hausdorff Distance (HD), and Border Error (BE). High score value of TDR and JI represents efficient performance by proposed segmentation method, whereas, low value for other metrics indicates better performance. Sørensen-Dice metric can be directly calculated from JI, equation 2.8 shows a mathematical representation for the same.

$$Dice = 2 * \frac{JI}{1+JI} \quad (2.8)$$

Segmentation algorithms are assessed broadly by BE, it is illustrated in equation 2.9. BE calculates percentage-area of segmented portion(SM) which are non-overlapping (exclusive-OR) in ground-truth(GT) and proposed segmentation result. BE is the measure of false detection of area in comparison with ground truth.

$$BE(SM, GT) = \frac{Area(SM \oplus GT)}{Area(GT)} \quad (2.9)$$

HD metric is the measure of distance between two non-null entity in open space. Equation 2.10 shows mathematical representation of HD, where # indicates count of pixels which are present in segmented image. From the equation, we understand that two entity are said to be close to each other if each pixel of both the entity is near to same pixel in the image.

$$HD(SM, GT) = \frac{\#(SM \cup GT) - \#(SM \cap GT)}{\#(SM \cup GT)} \quad (2.10)$$

The ratio of truly detected pixels of lesion image is calculated by TDR, which is represented in equation 2.11. On the other hand, the ratio of false detected pixels of lesion is calculated by FPR, which is represented in equation 2.12.

$$TDR(SM, GT) = \frac{\#(SM \cap GT)}{\#GT} \quad (2.11)$$

$$FPR(SM, GT) = \frac{\#(SM \cap \overline{GT}}{\#(GT)} \quad (2.12)$$

Similarity between two entity is calculated by JI index, which divide the intersection area over union area for a segmented mask to calculates the accuracy of segmentation. JI metric is termed as intersection over union index as it enhances common area over ground truth lesion image, this feature is used to measure the segmentation performance. JI is considered to me most efficient metric for comparison of proposed segmented results with ground truths, which help to analyse the accuracy of the method.

$$JI(SM, GT) = \frac{|SM \cap GT|}{|SM| + |GT| - |SM \cap GT|} \quad (2.13)$$

2.4.3.4 Evaluation metric for classification of image

For evaluating the performance of skin lesion classification, evaluation metrics such as: Sensitivity (Sn) , Specificity (Sp) , Accuracy (Ac) , Dice index coefficient (Dc) and Jaccard score (Js)

are used. These standardised criteria of evaluation are utilised for validation of segmentation and classification performance in ISBI challenge, which is considered to be standard platform for publishing practical implementation of diagnosis of melanoma lesion.

Sensitivity (Sn) represents the ratio of accurate detection/segmentation of dermoscopic lesion, whereas Specificity (Sp) indicated the proportion of accurate detection/ segmentation of non-melanoma pixels. Overall performance of diagnosis is quantified by measure of Accuracy(Ac) metric. The dice index coefficient (Dc) is used to measure the performance of detection/segmentation by comparing ground truth results. Similarly, Jaccard score(Js) is an measure of intersection over union of segmented lesion with ground truth results. The Matthew correlation coefficient (MCC) quantifies the correlation between segmented and annotated area of lesion, the outcome of MCC ranges from -1 to 1. Larger value of MCC represents efficient detection/segmentation of skin lesion. Mathematical representation of all these matrices are shown as follow:

$$Sn = \frac{TP}{TP+FN} \tag{2.14}$$

$$Sp = \frac{TN}{TN+FP} \tag{2.15}$$

$$Dc = \frac{2*TP}{(2*TP)+FP+FN} \tag{2.16}$$

$$Js = \frac{TP}{TP+FN+FP} \tag{2.17}$$

$$Ac = \frac{TP+TN}{TP+FN+TN+FP} \tag{2.18}$$

$$Mcc = \frac{TP*TN-FP*FN}{\sqrt{(TP+FP)(TP+FN)(TN+FP)(TN+FN)}} \tag{2.19}$$

Receiver operating characteristic (ROC) graphs are plotted using True positive rate and false positive rate in Y and X axis respectively. ROC curve is used to analyse the performance of proposed method. Area under curve (AUC) metric is used for assessing performance by calculating the area of ROC curve for each state-of-art method, where area of curve is directly proportional to segmentation performance. The probabilistic curve of ROC and AUC depicts the measure or degree of separation.

It indicates the capacity of classifier to differentiate different classes. High value of AUC represents better classification architecture for prediction of true values as true and false entities as false. Pictorial representation of ROC curve is shown in Figure 2.20.

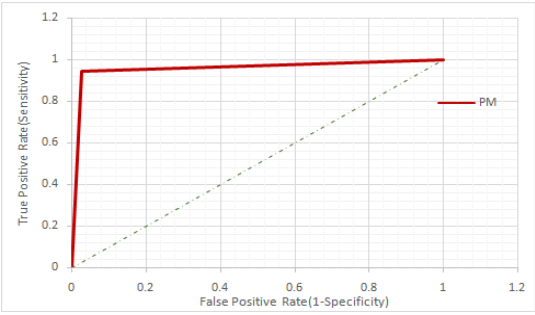

Figure 2.20 : Pictorial representation of ROC graph

The performance of classification of skin lesion is extensively measured by metrics such as Precision (Pr), False Positive Rate (FPr), False Negative Rate(FNr), True Positive Rate (TPr) and True Negative Rate (TNr), these are the measure of accurate detection of malignant lesion as melanoma. Pr is considered to be accuracy of classification method to generate only valuable data, that is, it determines the rate of accurate detection. Equation 2.20 represents the mathematical structure of Pr. On the other hand, recall is the ability of the classifier to detect true values as true, it is also termed as Sensitivity or TPr. Equation 2.21 shows the mathematical representation of the recall.

$$Pr = \frac{TP}{TP+FP} \tag{2.20}$$

$$TPr = \frac{TP}{TP+FN} \tag{2.21}$$

False Positive Rate (FPr):

FPr, represents the inability of the classifier to detect true values as false entities. Equation 2.22 depicts the formula of FPr.

$$FPr = \frac{FP}{FP+TN} \tag{2.22}$$

False Negative Rate (FNr):

It is ratio of True value which are wrongly detected as False value. It is also known as miss rate. Mathematical representation it shown in Equation 2.23.

$$FNr = \frac{FN}{FN+TP} \quad (2.23)$$

True Negative Rate (TNr):

Rate of prediction of false value to be false, is classified in TNR. It is also known as Specificity. Equation 2.24 have represented its mathematical term.

$$TNr = \frac{TN}{TN+FP} \quad (2.24)$$

F1-score:

The weighted mean of recall and precision is termed as F1 score or harmonic mean. F1 is used to measure accuracy of machine learning architecture in a single score metric by evaluating both recall and precision together.

$$F1 - Score = 2 * \frac{Precision * Recall}{Precision + Recall} \quad (2.25)$$

2.5 Conclusion:

The literature so far have tried to perform different methods for accurate classification of skin lesion, however they have always failed to achieve the desired outcome which would be accepted by medical practitioners. One of the major reason for poor classification is lack of pre-processing technique in the literature of numerous articles, however few articles have performed pre-processing and have achieved fairly reasonable classification result. Thus, execution of an enhanced pre-processing technique before classification of lesion might boost the classification outcome. Some of the articles in literature employs orthodox and old methods for segmentation of skin lesion which results in irregular selection of ROI. Otsu's method, K-Mean clustering method and few of the quantisation methods fails to fetch desired segmentation results. Additionally these methods might

eliminate important features while segmenting the lesion. Therefore a modified mathematical model should be proposed which will segmented the skin lesion accurately without eliminating key features of the dermoscopic image. Various conventional and deep learning based classification methods are mentioned in the literature which tries to yield high score of sensitivity and specificity, however most of the articles are still convinced to employ conventional methods such as genetic algorithm which is not capable of correctly classifying dermoscopic image. Thus, modern methods of deep learning such as YOLO, should be employed to fetch enhanced result of classification. The dense and complex architecture of neural network of these classifiers are capable of fetching high scores for sensitivity and specificity. Additionally these classifiers are computationally viable and executes classification much faster than other deep learning models. Therefore an enhanced method of CAD is proposed in forthcoming chapters which have overcome these difficulties and have successfully achieved enhanced results.

Chapter 3: Proposed method for diagnosis of melanoma using L-R fuzzy logic and YOLO

3.1 Introduction

This dissertation employs a computer-vision based diagnosis method for detection of malignant lesion. It can be sequentially framed as pre-processing of lesion, segmentation of pre-processed lesion image, followed by classification of the lesion. Figure 3.1 pictorially represents the flow of the proposed algorithm where each step is represented in the flow chart. The first step of pre-processing includes removal of hair and other artifacts from the image using dull razor method followed by histogram equalization, which enhances the input image quality. Then, segmentation of lesion is performed by a novel algorithm using dynamic threshold calculation by standard deviation techniques and L-R fuzzy logic that is proposed in the paper. Deep convolutional neural network named YOLO [99] is employed for classification, which is capable of vanquishing other CNN models [17]. The classifier is trained on ISIC 2017 and ISIC 2018 dataset. Though the proposed work depends on conventional methods of CAD system for melanoma lesion identification, its originality lies in blending of modern aspects with highly accepted existing algorithms on malignant diagnosis. The primary advantages of the proposed work are: i) the selection of publicly sourced deep learning based neural network- YOLO, which speeds up classification process and lowers the error rate of false detection; and ii) the proposed segmentation method which works based on standard deviation, and dissects the affected region roughly from the skin. This algorithm works separately for all the three colour channels and an ensemble logic is used to ensemble the segmented marks. In order to further improve the segmentation results, we ventured L-Function fuzzy number for a second iterative procedure to further enhance the segmentation results. In this consequence, we have applied the impression of fuzzy theory and set the threshold series more significantly such that it will provide us improved effect rather than first iteration. Here we consider the L-Function fuzzy number to deal with the indistinctness section and also improvised defuzzification technique of L-Function fuzzy number. Additionally, we utilized improved consequence for the adapted threshold assessment rate.

Incorporation of such worthy algorithms within this paper has considerably supported the process of detection of melanoma lesion [100]. In the next section, preliminaries are given which gives a brief introduction to fuzzy logic. In subsequent sections, description of dataset and implementation of YOLO is being mentioned. Then the proposed method is highlighted which is supported by Result and Analysis section.

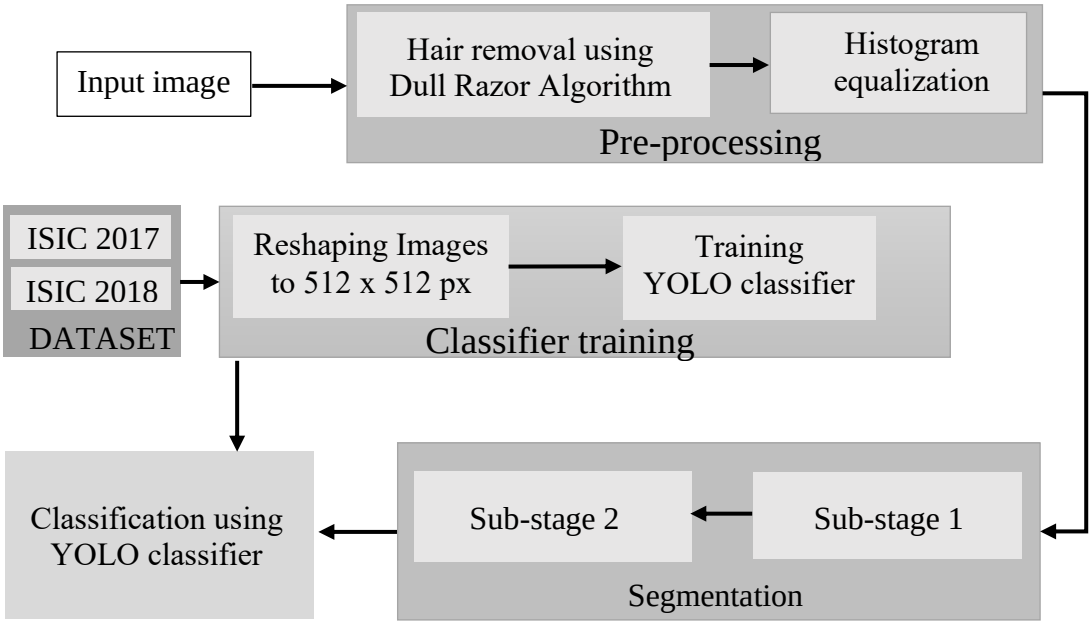

Figure 3.1: Flowchart of proposed algorithm

3.2 Preliminaries of fuzzy logic

This section deals with the introduction to fuzzy logic, where fuzzy set, fuzzy number and triangular fuzzy number are explained. The section gives a brief summary about fuzzy logic, both mathematically and graphically.

Definition. Interval number: An interval number U is designated by $[U_L, U_R]$ and named as $U = [U_L, U_R] = \{x: U_L \leq x \leq U_R, x \in R\}$, where R is the set of real number. The right and left range of the interval is denoted by U_R and U_L respectively.

Definition. Fuzzy set: Let $\tilde{S}$ be a set such that $\tilde{S} = \{(x, \alpha_{\tilde{S}}(x)): x \epsilon S, \alpha_{\tilde{S}}(x) \epsilon [0,1]\}$ which is often represented as $(x, \alpha_{\tilde{S}}(x))$ which is an ordered pair, here x is an element of the set S and $0 \leq \alpha_{\tilde{s}}(x) \leq 1$, then set $\tilde{S}$ is called a fuzzy set.

Definition. Fuzzy number: Fuzzy number is represented as $\tilde{S} \in F(R)$, where the set of real number is denoted by R if

i) $\tilde{S}$ is normal. that is, $x_0 \in R$ exists such that $\alpha_{\tilde{S}}(x_0) = 1$.

ii) For all $\alpha \in (0,1]$, A_α is a closed interval.

Definition. Triangular fuzzy number: $\tilde{P} = (p_1, p_2, p_3)$ should gratify the following situations:

(1) In the interval [0,1], $\alpha_{\tilde{S}}(x)$ is a continuous function.

(2) In the intervals $[p_1, p_2]$, $\alpha_{\tilde{S}}(x)$ is a continuous function and strictly increasing.

(3) In the intervals $[p_2, p_3]$, $\alpha_{\tilde{S}}(x)$ is a continuous function and strictly decreasing.

Definition. Linear Triangular Fuzzy Number (LTFN): It can be presented as $\tilde{P}_{TFN} = (p_1, p_2, p_3)$ whose membership function is defined below:

$$\mu_{\tilde{p}_{TFN}}(x) = \begin{cases} \frac{x-p_1}{p_2-p_1} if p_1 \le x \le p_2 \\ 1 \quad if x = p_2 \\ \frac{p_3-x}{p_3-p_2} if p_2 \le x \le p_3 \\ 0 \quad Elsewhere \end{cases} \tag{3.1}$$

Figure 3.2 shows graphical representation of linear TFN, where points p1, p2, and p3 represent different intervals of fuzzy number which ranges between 0 and 1.

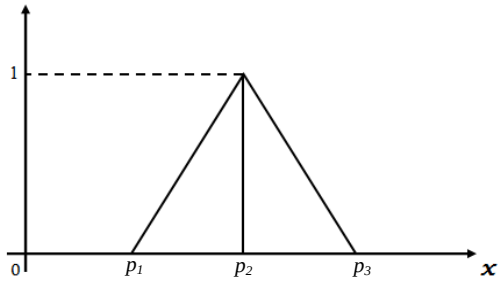

Figure 3.2: Illustration of Linear triangular fuzzy number

Definition. α-cut form of linear TFN: α-cut, which is also known as parametric form of TFN is defined as $A_\alpha = \left\{x \in X | \alpha_{\tilde{S}_{TFN}}(x) \geq \alpha\right\} = \begin{cases} S_L(\alpha) = p_1 + \alpha(p_2 - p_1) & for \alpha \in [0,1] \\ S_R(\alpha) = p_3 - \alpha(p_3 - p_2) & for \alpha \in [0,1] \end{cases}$ (3.2)

Where, right segment $(S_R(\alpha))$ is the decreasing function with respect to α, and left segment $(S_L(\alpha))$ is the increasing function with respect to α.

3.3 Proposed method

3.3.1 Pre-processing

Pre-processing of lesion image is the preliminary step of CAD system, which includes removal of noise and other artefacts. This section proposes three remarkable steps for preprocessing of dermoscopic images. For the first step, Dullrazor algorithm [31] is applied for digital hair removal over the lesion image. A grey-morphological operation is used to identify the location of hair in the dermoscopic image. The location is then verified by eliminating the concurrent pixels based on thickness and length of the hair follicle. Bilinear interpolation algorithm and adaptive-median filter are operated to replace and smoothened these pixels respectively. In the second step, histogram equalization is employed to adjust the contrast and brightness of the image, thereby enhancing the dermoscopic image. The above sequential outputs have been illustrated in Figure 3.3. Figure 3.3(a) represents an input dermoscopic image where hair removal algorithm is applied to produce Figure 3.3(b). Further, the image undergoes histogram equalization to enhance the quality of image such that lesion features are well described, this enhancement is portraited in Figure 3.3(c).

(a) (b) (c)

Figure 3.3: Pre-processing of skin lesion (a) Raw dermoscopic image (b) Removal of hair using Dull Razor algorithm (c) Image enhancement by histogram equalization

3.3.2 Segmentation

Segmentation is the procedure of identification of lesion boundary from the pre-processed dermoscopic image. It is performed for digital dissection of affected area from the regular skin with high-correlation and Region-of-Interest (RoI). Threshold, clustering, Active contours, quantization, pattern clustering, merging threshold and fuzzy methods are seven categories of segmentation methods. According to the literature, conventional segmentation methods like region enhancing, thresholding and clustering were unable to process complex lesion images and the algorithms fail owing their computational and time complexity. To resolve this drawback many researchers, prefer to use segmentation methods based on deconvolutional networks, fuzzy method, saliency and k-mean algorithm. The proposed method here describes segmentation into two stages. Sub-matrix window of size 5x5 is considered for processing, thereby reducing the computational burden.

3.3.2.1 Substage-1 of segmentation using dynamic thresholding

Step 1: The input image is represented as a (M×N) matrix where the location of each pixel can be established as:

$$(\mathrm{m},\mathrm{n}) \in \mathrm{X} \equiv \{(1,2,\dots,\mathrm{M}) \times (1,2,\dots,\mathrm{N})\} \qquad (3.3)$$

Step 2: The operation is executed on the all three colour channels and the instance of the red plane $\mathrm{red}_{m,n}$ is considered to be the value of intensity for the pixel (m,n). Concurrently, (M×N) binary mask is considered by all the pixels $f_{red}(m,n)$ to be zero.

Step 3: A 3×3 FOV is considered, with (m,n) being its centre pixel, where $\mathrm{m} = (3,4,\dots,\mathrm{A}-3) \& n = (3,4,\dots,\mathrm{B}-3)$

Step 4: For a specific window having centre (p,q) the pixel values are $r_{p-3,q-3};\dots;r_{p,l};\dots r_{p+3,q+3};$

Step 5: If($|r_{p-3,q-3}-r_{p,q}| \geq X$) where X=σ then $f_{red(p-3,q-3)}=1$ else $f_{red(p-3,q-3)}=0$, where σ is the standard deviation of that particular region.

Step 6: Moving forward we can check, If($|red_{p+3,q+3}-red_{p,q}| \geq X$) then $f_{red(p+3,q+3)}=1$ else $f_{red(p+3,q+3)}=0$

Step 7: An updated binary flag image will be created. Proceeding in this way, new binary flag images will be generated from Green (f_{green}) and Blue (f_{blue}) planes. From all the flag images final binary mask image (f_{mask}) is generated by executing the following operation.

Step 8: If ($f_{red}(m,n)$ && $f_{green}(m,n)$ && $f_{blue}(m,n)$) equals 1) then $f_{mask}(m,n)=1$ and the segmented region is identified from the pre-processed (A×B) image through border line using the following operation. If $f_{mask}(m,n) = 0$ then marked else continue, where $m = (1,2,\dots,M) \& n = (1,2,\dots,N)$.

A pictorial representation of the first substage of segmentation is shown in an example image in Figure 3.4. The pre-processed image is segmented by dynamic threshold calculation using standard deviation methods and ensemble logic. A binary mask is formed (as represented in Figure 3.4(b)) along with the segmented lesion region (as represented in Figure 3.4(a)) by employing the above-mentioned algorithm.

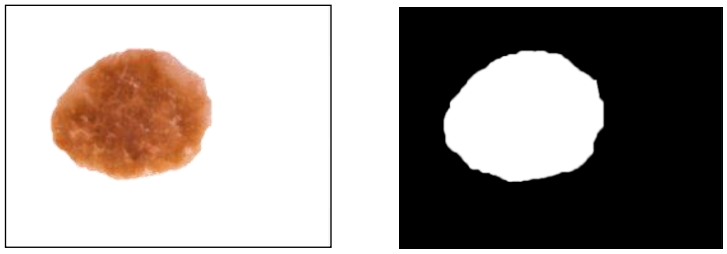

Figure 3.4: Segmentation result after first Iteration (a) Segmented output of lesion (b) Segmented mask of the lesion

3.3.2.2 Substage-2 of segmentation using L-R fuzzy logic

After judging the affected region generally we progress to supplementary authentic image segmentation. The substage-1 threshold assessment is elected according to the hypothetical ground, but we scrutinize that a number of non-affected regions are still integrated in the image segmentation branch. To lessen it we place one more threshold assessment rate less than T which specifies the entirely affected region. As we are employing standard deviation method for segmentation of lesion in first substage, we might encounter extra pixels, to eliminate those unnecessary clusters of pixel we will perform substage-2. Most of the threshold based segmentation models work on definite threshold values, such that they validate the region within the threshold and anything another side the range is

considered to be void even if it is just a mark more than acceptable threshold value. Due the occurrence of imprecision of uncertainty we presented L-Function fuzzy number in second iterative step such that the image segmentation technique will provide us an outstanding consequence in comparison with the first iteration. We ventured the notion of L-Function fuzzy number at this time to attempt the hesitation and also erected a defuzzification scheme of L-Function fuzzy number for crispification. This defuzzified product in fact specifies the threshold assessment rate of Substage 2.

L-R Type Fuzzy Number (LR-FN): ($\tilde{P}$)is LR-FN when

$$\mu_{\tilde{P}}(x) = \begin{cases} L\frac{(h-x)}{\gamma}, \text{for } x \leq h, \gamma > 0 \\ R\frac{(x-h)}{\delta}, \text{for } x \geq h, \delta > 0 \end{cases} \quad (3.4)$$

Here, the reference functions are represented as R for right and L is for left. δ, γ are called right and left spreads respectively, and x is any point less than γ which is equivalent to 1 on y-axis.

L- Function Fuzzy Number (L-FN): $\tilde{P}$ is L-FN when

$$L(x; \gamma, \delta) = \begin{cases} 1, & x < \gamma \\ \frac{(x-\gamma)}{\delta-\gamma}, & \gamma \leq x < \delta \\ 0, & x \geq \delta \end{cases} \quad (3.5)$$

L-function fuzzy number is represented in Figure 3.5. Whereas left and right region on defuzzification is represented in Figure 3.6(a) and (b) respectively.

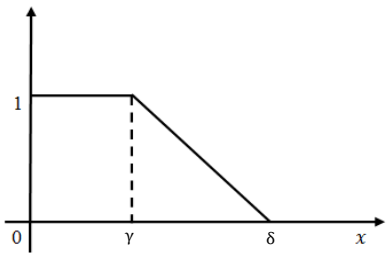

Figure 3.5: Graphical Representation of L–Function fuzzy number

Method for Approximation of Area: L-Typed fuzzy number is defuzzied to form a crisp number that can be generated by employing area approximation system on a linear L-Type fuzzy number $\tilde{p}_{FN}$. It can be mathematically expressed as:

$$\emptyset = \mathbf{X_L}(\boldsymbol{\partial}) + \mathbf{X_R}(\partial) \qquad (3.6)$$

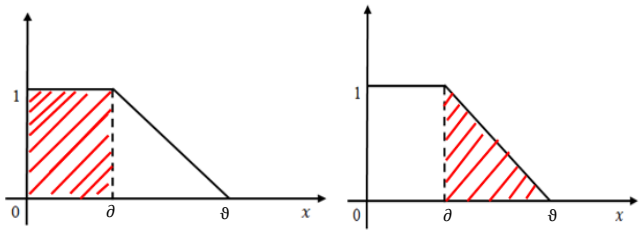

Figure 3.6 (a): First quadrant(rectangle) Figure 3.6 (b): Second quadrant(triangle)

Where, $X_L(\partial) = \text{Area of first quadrant } = 1.\partial = \partial$

$X_R(\partial) = \text{Area of second quadrant } = \frac{1}{2}(\vartheta - \partial).1 = \frac{(\vartheta - \partial)}{2}$

Therefore, Defuzzification value:

$$\emptyset = X_L(\partial) + X_R(\partial) = \frac{(\vartheta+\partial)}{2} \qquad (3.7)$$

The defuzzification value is used to calculate the threshold mark for segmentation of lesion between a small pixel range of ϑ and ∂. The pixel value of the lesion beyond the threshold mark is discarded, thereby forming a mask around the lesion. Result of second sub-stage of segmentation along with its mask is represented in Figure 3.7. Figure 3.7 marks more appropriate and specific mask as compared to output of first sub-stage of segmentation which is further illustrated in forthcoming sections.

(a) (b)

Figure 3.7: Segmentation result after second substage (a) Segmented output of lesion (b) Segmented mask of lesion

3.4 Classification

3.4.1 Overview of YOLO classifier

In this technical era of ever changing and growing technology, there had been significant growth in the medical vision field which had resulted in admirable and capable strategies that could handle various complications. The algorithms for object detection in the vision sphere circumscribe many innovative ideas on evidencing target and locating those multiple targets inside a described image [99]. On contrary, the algorithms involving classification technique signifies the subject of the stipulated image on checking its existence in the specified image. Classification algorithms trade in with CNN classifiers being passed in the formerly deputed boxes, in other words those boxes which were to be created at inception of the procedure which is followed by removal of peculiarity of the processes, concerning to the retardation of the function in addition to arduous increase of discrete component of the asserted image. Contrarily, the algorithms involving object detection divulge regressive technique that includes deep learning which finishes to a single step process of conceiving those boxes in the entire image, thus avoiding the focusing of its individual enticing portions. Hence this algorithm processes the result faster than the previous one. YOLO is a path breaking and genius approach in field of computer vision with application focusing on detection of object in actual time. The focus of the researchers for this algorithm is on passing the classifiers on the entire image, instead of its discrete fragments, conventionally the algorithm is performed in 45 video frames in one second, which defines it ability to process data faster than most of the classifiers. CNN including crumpling and amalgamating layers comprises in a YOLO with the collaboration of two thoroughly comparable CNN layers. As far as object detection in real time is concerned, YOLO is indisputably the fastest algorithm. This is because of the fact that in the initial step of learning it uses regression and thus using neural network in its technique. With the knowledge of diagnosis tensor in YOLO, its algorithm increases which could be explained by an equation:

$$(T \times T) * P * (5 + Z) \tag{3.8}$$

Here $(T \times T)$ symbolize the non-intersecting grid cells after splitting the particular image. P represents bounding boxes whose predictions and confidence score calculations depends fully on the

grid cells. Whereas Z is the representation of confidence score. The pre-existence of an object within the bounding box could be found by using Confidence score. If prior existence of the object is NULL, then the confidence score will return zero. It could be represented as:

$$\text{Confidence Score} = \Pr(\text{Object}) * \text{IoU}^{\text{groundtruth}}_{\text{predicted}} \quad (3.9)$$

As per Google-Net, YOLO architecture possesses convolution layer of count 24, which eventually provides a tensors (7, 7, 1024) to the researchers along with the shape as the final product. This is followed by a totally connected layer of 2 which provides 7x7x30 parameters which eventually moulds it as (7,7,30). It means that for every location there is 2 boundary boxes. Brief workflow of YOLO is explained in Figure 3.8 where $T \times T$ size image is taken as input image in Figure 3.8(a), bounding-boxes are generated in Figure 3.8 (b), Figure 3.8(c) shows probabilistic mapping of classes and final detection of lesion is shown in Figure 3.8(d).

For calculating the sequestration of the countless bounding boxes comprising every grid cell, YOLO provides the highest Intersection Over Union (IoU) value. The sum squared error technique for listing the loss function comprised of classification loss, localization loss and the confidence loss. Moreover, YOLO ensures spatial diversity for envisions and interprets lesser false positives in its proceedings. The YOLO algorithm is available in terms of various versions like YOLO v1, YOLO v2 and YOLO v3 indicating fruitful solutions to the versatile setbacks found in the previous versions. Numerous conclusions have been generated and finally it came out that envisions of class and object confidence must be inferred from logistic regression which is a necessary invention in YOLO v3 which were absent in the previous versions. Moreover, taking up the group of Melanoma (classes) with the highest-class scores was an essential step which is also forbidden in the YOLO v3 version and replaced it with multilabel classifications. Finally, the latest version of YOLO i.e.; YOLO v3 performs at a very high pace at a benchmark of COCO mAP 50, which was never been found at the previous versions [101].

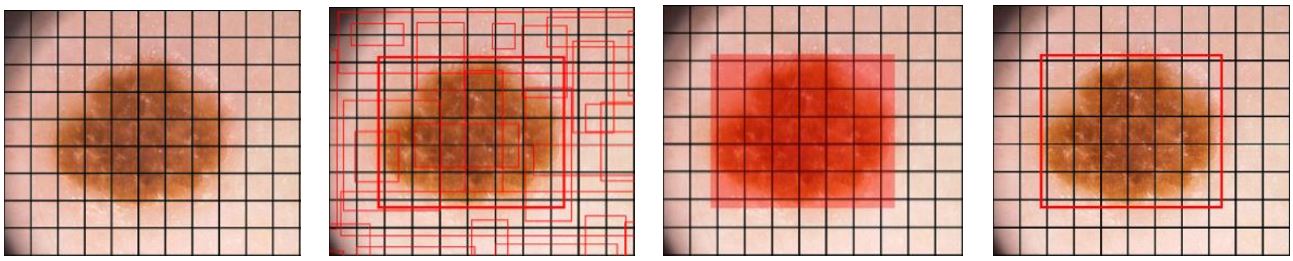

Figure 3.8: Classification process by YOLO is illustrated on a skin lesion image (a) TxT sized grid input (b)Generation of bounding-boxes on the basis of confidence score (c) Mapping of class probability (d) Detection of lesion

3.4.2 Implementation and training of classifier

For the proposed algorithm, all the dermoscopic images of varied resolutions are resized into 512×512 pixels, before undergoing training process. Images are resized to decrease computational usage. Yolo classifier was trained with the reshaped dataset under following parameters: batch size of 64, subdivision of 16, decay rate of 0.0005, momentum of 0.9, through 40,000 epochs and learning rate of 0.001. Weight was saved after every 5000th epoch for efficient detection of dermoscopic lesion. The trained classifier is then used for testing the proposed algorithm where the output from last sub-stage of segmentation is used as input for the classifier to detect the lesion. Figure 3.9 illustrates the detection process of the classifier, where it detects the malignant lesion and form a box around the lesion, thereby enabling location detection of melanoma lesion.

While testing the accuracy of the classifier, the dermoscopic image undergoes a series of pre-processing and segmentation steps which enhances the accuracy performance of the classifier, which is further illustrated in result and analysis section. Whereas the classifier is being trained by just resizing the image to 512 x 512 pixels with modified last layer of yolo classifier.

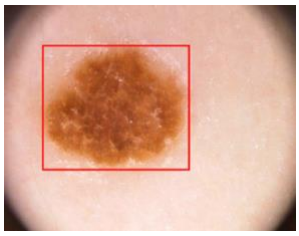

Figure 3.9: Classification by YOLO classifier

3.5 Result analysis

The section deals with the performance analysis of the proposed algorithm in this section. The system configuration for the entire operations and computations is as follows: Core-i7 PROCESSOR, 16 GB RAM and Ubuntu 18.10 operating system. Python and OpenCV framework for image processing were being employed to develop entire system. The performance analysis of the algorithm is noted on the premise of four significant parameters namely, Competency of Lesion Location Detection, Segmentation Performance, Accurateness of classification and Computational Time. Three publicly available dataset are used in the detection and segmentation process. The datasets are namely-PH2, ISIC 2017 AND ISIC 2018.

3.5.1 Performance analysis for localisation of lesion

Sensitivity, specificity and IoU are three parameters, considered for determining the extent of location detection. While the sensitivity and specificity score for PH2 dataset results to be 95% and 96.25% respectively, with 94% of IoU value. ISIC2017 and ISIC2018 datasets produce significantly high sensitivity and specificity score. Table 3.1 illustrates analysis of location detection using YOLOv3. High score value for IoU specifies the accurate location detection of lesion. Whereas high rated values for Sensitivity and Specificity resembles precise identification of melanoma and non-melanoma lesion respectively.

Table 3.1 : Performance analysis for localisation of lesion using YOLO

Dataset	Sensitivity (%)	IoU (%)	Specificity (%)
PH2	95	94	96.25
ISIC 2017	95.43	91	95.78
ISIC 2018	95.51	90	95.54

3.5.2 Performance analysis for segmentation of lesion

Followed by pre-processing of dermoscopic images, segmentation process is executed on each dataset. Segmentation performance is evaluated on aforementioned metrices i.e. Accuracy, Specificity, Sensitivity, Jaccard score and Dice index score. Recall that we have demonstrated two

substages for segmentation; First step intends to selection of substantial area of lesion mask, to ensure no features of melanoma is lost in this process. Thereafter in second step, fuzzy based probabilistic thresholding method is used to form an accurate segmented mask, thereby producing better segmentation outcome. Table 3.2 outlines the results of first sub-stage of the proposed segmentation method, whereas Table 3.3 depicts outcomes of second sub-stage. Evaluation metric score tends to set higher marks for second substage as the LR based fuzzy logic segments the lesion more precisely and effectively. Average accuracy mark after first sub-stage of segmentation lies around 95% which jumps a step forward with an average figure of around 96% after second sub-stage, which is a clear demarcation of importance of L-R fuzzy logic and fuzzy thresholding in segmentation process.

Table 3.2 : Segmentation results of first substage

Dataset	Acc (%)	Sen (%)	Spe (%)	Jac (%)	Dic (%)
PH2	95.00	92.50	95.63	78.72	88.10
ISIC 2017	95.16	90.86	97.27	86.06	92.51
ISIC 2018	95.08	90.12	96.75	82.24	90.25

Table 3.3: Segmentation results of second substage

Dataset	Acc (%)	Sen (%)	Spe (%)	Jac (%)	Dic (%)
PH2	96.50	97.50	96.25	84.78	91.76
ISIC 2017	96.16	91.88	98.26	88.73	94.03
ISIC 2018	95.91	91.62	97.36	85.00	91.89

Proper collection of datasets, pre-processing steps and two substages of segmentation methods have fetched edge-cutting results over pre-existing models. Here, the proposed algorithm is compared with available works for the similar dataset and it proves to produce superior results. Detailed comparison of projected algorithm based on Acc, Sen, Spe, Jac and Dic for PH2, ISIC 2017 and ISIC 2018 is encapsulated in Table 3.4, Table 3.5 and Table 3.6 respectively.

Our proposed method marks the highest accuracy score in comparison with few well know recently published works. Segmentation result for PH2, ISIC 2017 and ISIC 2018 produces better accuracy value than existing works. Moreover, the highly specified pre-processing step and novel segmentation methods using dynamic threshold calculation by fuzzy logic, helps in producing such higher values of evaluation metrics. Proposed work is compared with few of the most inspiring and successful segmentation methods for PH2 datasets which employs multi-staged FCN with parallel integration (mFCN-PI) [102], semi-automated grab cut algorithms [103], semantic segmentation techniques [104] and synchronized segmentation with classification methods using bootstrapping convolutional neural network model[105]. However, the proposed method yields an accuracy score of 98.50% which is significantly higher than most of the well-known works. Moreover, for all the remaining four evaluating parameters the proposed method yields highest score with 97.50%, 98.75%, 92.75% and 96.30% for sensitivity, specificity, Jac score and Dic score respectively.

For ISIC 2017 the proposed algorithm is compared with deep convolutional deconvolution neural network (CDNN) [106], fully convolutional-network (FCN) [107], FrCN model for simultaneous segmentation and classification [108], segmentation by the mean of assembling crowdsourced results of ISIC 2017 challenge [110] and a fully convolutional-residual network (FCRN). The accuracy performance of [104] is second best in table with the mark of 95.3%, whereas the proposed method achieves the mark of 96.17% for accuracy. Parameter like accuracy which resembles degree of accurate detection of malignant melanoma, marks the highest of 95.90% by [111], whereas our method scores 96.17%. Similarly, towering results have been noticed for all the evaluating parameters over existing published work.

Proposed method for ISIC 2018 dataset is compared with Encoder-Decoder based ResNet34 and DCNN [113], encoder-decoder network with CRF [114], Encoder-decoder algorithm with Deeplab and PSPNet [115]. The comparative study depicts highest score for accuracy, Jaccard index and dice coefficient, which is 95.9%, 85.00%, 91.9% respectively for proposed algorithm. Score for

specificity for ISIC 2018 dataset is 97.4% which is alike with [113]. A receiver operating characteristic(ROC) curve is use to plot false positive rate against true positive rate. It illustrates the accuracy of proposed method for all the three datasets over other published works. Effectiveness of the algorithm is directly proportional to area under the curve. Figure 3.10(A) graphically represents the ROC curve for PH2 dataset, where the plotted curve for proposed method(PM) tends to be more towards y-axis then other published works, which clearly indicates the supremacy of accuracy for melanoma detection. Comparative ROC curves for segmentation of melanoma lesion for ISIC 2017 and ISIC 2018 dataset are plotted in Figure 3.10(B) and Figure 3.10(C) respectively, both the plotted graphs depicts the larger area under curve and higher accuracy of diagnosis for proposed method over pre-existing algorithms.

Table 3.4 : Comparative study of proposed segmentation result with recent work for PH2 dataset

References	Year	Acc (%)	Sen (%)	Spe (%)	Jac (%)	Dic (%)
Bi et al. [102]	2019	95.03	96.23	94.52	85.90	92.10
Unver et. al. [103]	2019	92.99	83.63	94.02	79.40	88.13
Hasan et. al. [104]	2020	98.70	92.90	96.90	-----	-----
Xie et. al. [105]	2020	96.50	96.70	94.60	89.40	94.20
Proposed method	2021	98.50	97.50	98.75	92.86	96.30

Table 3.5: Comparative study of proposed segmentation result with recent work for ISIC 2017 dataset

References	Year	Acc (%)	Sen (%)	Spe (%)	Jac (%)	Dic (%)
Yuan et al. [106]	2017	93.4	82.5	97.5	76.5	84.9
Bi et al.[107]	2017	93.4	80.2	98.5	76	84.4
Li et al.[108]	2018	93.2	82	97.8	76.2	84.7

Sarker et al. [109]	2018	93.6	81.6	98.3	78.2	87.8
Soudani et al. [110]	2019	94.95	85.87	95.66	78.92	88.12
Akram et.al. [111]	2020	95.90	----	----	----	----
Hasan et al. [104]	2020	95.3	87.5	85.5	----	----
Al-Masni et al. [112]	2020	81.57	75.67	80.62	----	----
Proposed method	2021	96.17	91.88	98.26	88.73	94.03

Table 3.6: Comparative study of proposed segmentation result with recent work for ISIC 2018 dataset

References	Year	Acc (%)	Sen (%)	Spe (%)	Jac (%)	Dic (%)
Shahin A.H et al. [113]	2019	----	90.2	97.4	83.7	90.3
Ji Y et al. [114]	2018	94.3	91.8	96.4	83.4	90.0
Koohbanan NA et al [115]	2018	94.5	94.0	94.2	87.7	90.3
Qian C et al. [116]	2018	94.2	90.6	96.3	83.8	89.8
Proposed method	2021	95.9	91.6	97.4	85.0	91.9

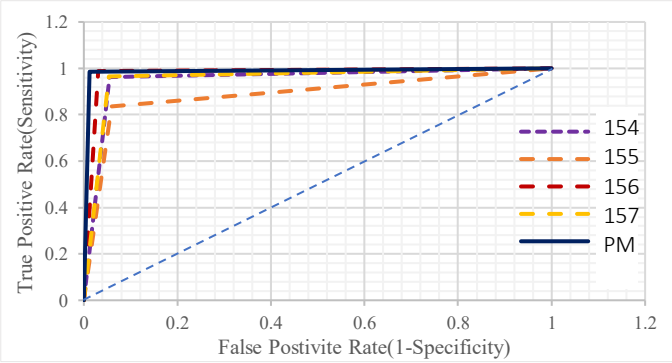

Figure 3.10(A): ROC curve for comparison of segmentation results for PH2 dataset

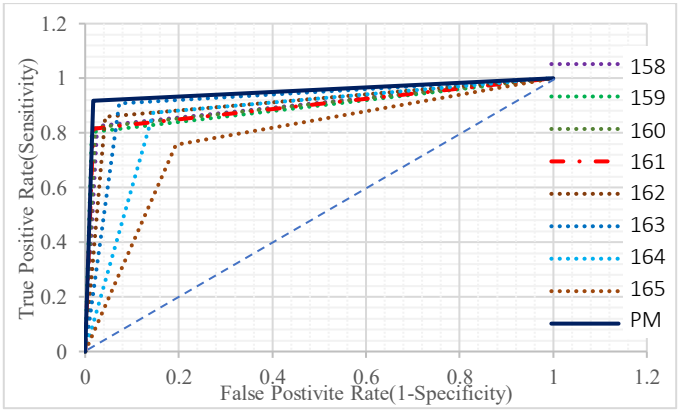

Figure 3.10(B): ROC curve for comparison of segmentation results for ISIC 2017 dataset

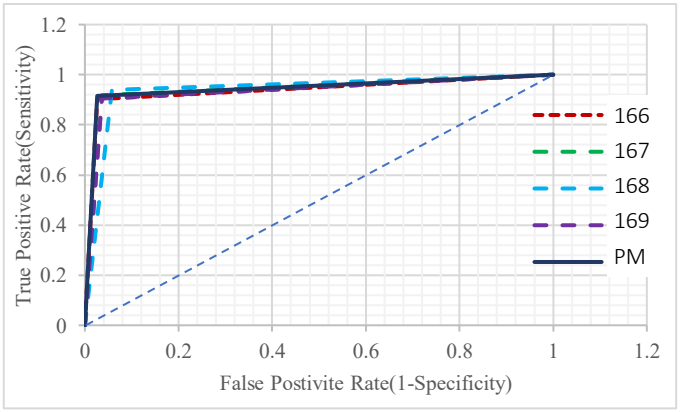

Figure 3.10(C): ROC curve for comparison of segmentation results for ISIC 2017 dataset

3.5.3 Performance analysis for classification of lesion

The classifiers taken for comparison with our proposed recognition algorithm are KNN, SVM, decision tree, and Yolov3. Comparison between our proposed method using YOLO and the well-established classifiers was drawn taking in account of different metrics. Time (in second) is also used as a comparison metrics to validate the speed of our method. Additional parameters for comparison include – Sensitivity, Specificity, Precision, Accuracy and Area under curve (AUC). Different method of SVM- namely Lagrangian support vector machine (LSVM), Consensus support vector machine (CSVM), Quantum support vector machine (QSVM), Medium Gaussian support vector machine(MGSVM) are used to classify malignant lesion for the same set of datasets. Various methods of KNN are also employed for the same task, those methods are- Fuzzy K-nearest neighbour (FKNN), Modified K-nearest neighbour (MKNN), Weighted K-nearest neighbour (WKNN), Cosine and Cubic

KNN. Notwithstanding the fact that the classification of melanoma lesion by different classifiers are performed over similar dataset, YOLO classifier not only score highest in terms of accuracy and AUC value but also performs the classification task in 7.01 seconds. Tabular representation of different classifier along with various methods and evaluating parameters are encapsulated in Table 3.7.

Table 3.7: Comparison between YOLO classifier (proposed) and other well-known classifiers

Classifier	**Method**	**Acc (%)**	**Sen(%)**	**Spec(%)**	**Prec (%)**	**AUC(%)**	**Time**
YOLO	Proposed Method	98.16	95.43	99.50	98.95	0.99	7.01
TREE	CT	91.5	87.82	93.30	86.5	0.95	8.79
	ST	88	88.33	87.84	78.03	0.92	12.65
SVM	LSVM	96.5	93.91	97.77	95.36	0.96	11.21
	CSVM	86.5	85.28	87.10	76.36	0.91	142.76
	QSVM	97	94.42	98.26	96.37	0.97	21.41
	MGSVM	96.33	94.92	97.02	93.97	0.98	14.64
KNN	FKNN	93.83	92.39	94.54	89.22	0.91	10.45
	MKNN	97.33	94.42	98.76	97.38	0.97	10.1
	Cosine	97	93.91	98.51	96.86	0.98	11.02
	Cubic	96.66	93.40	98.26	96.34	0.97	101.42
	WKNN	98.16	96.45	99.01	97.94	0.98	12.94

The comparison between different classifiers and the suggested method had clearly depicted the increase in accuracy and decrease in detection time. As mentioned in Table 3.8 accuracy of the proposed method is 98.17% with sensitivity and specificity as 95.43% as 99.50% respectively. The detection time of the melanoma using the presented method is 7.01 s which are compatibly lower than most of the classifiers. Additionally, automatic hair removal and image enhancement using the pre-processing models had contributed to enhanced accuracy of the proposed method. YOLO as a classifier have been proved to be much efficient and reliable than most of the renowned classifiers.

Table 3.8: Performance analysis of detection of lesion using YOLO without proposed segmentation

Dataset	Sensitivity (%)	Accuracy (%)	Specificity (%)
PH2	90.00	93.00	93.75
ISIC 2017	91.00	91.00	90.32
ISIC 2018	92.00	91.29	90.97

Table 3.9: Performance analysis of detection of lesion using YOLO with proposed segmentation

Dataset	Sensitivity (%)	Accuracy (%)	Specificity (%)
PH2	95.00	96.83	96.25
ISIC 2017	95.43	95.58	95.78
ISIC 2018	95.51	95.19	95.54

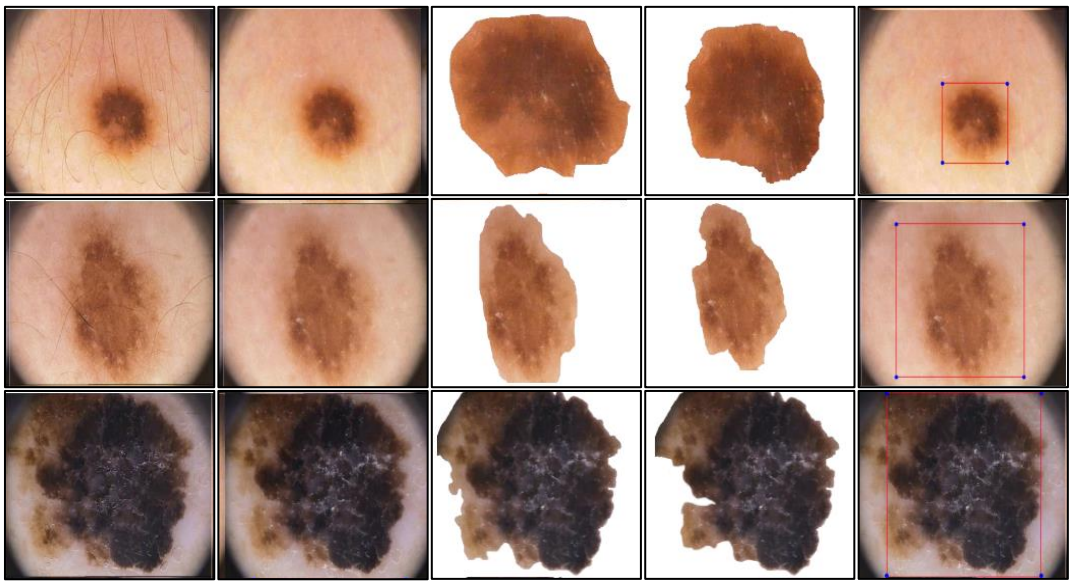

(a) (b) (c) (d) (e)

Figure 3.11: (a) Input image (b) Pre-processed lesion- after hair removal and image enhancement (c) Segmentation outcome after first substage (d) Segmentation outcome after second substage (e) Detection of melanoma lesion and bounding box formation by YOLO classifier

Significance of segmentation is exemplified in Table 3.9 and Table 3.10 where the value of Accuracy, Sensitivity and Specificity is higher when proposed segmentation is applied before classification of lesion. This shows the importance and benefit of proposed pre-processing and segmentation steps. Significantly high value of performance metric is achieved for YOLO classification when segmentation and pre-processing techniques are used prior to classification because the image quality of lesion is enhanced, and its features are exposed for appropriate detection.

3.6 Discussion

The progressive rise in melanoma incidence is evident since last few decades and it is projected to grow more in coming future all over the world. The impermanence drifts for melanoma are random and gets influenced by age, sex, ethnicity and geography. The accuracy for diagnosis of melanoma always had a room for improvement, though with the rise in field of deep learning and computer vision this problem is been addressed. Diagnosis and treatment of melanoma had marked an significant advancement due to innovative ideas and modern that are employed in recent research works. This dissertation attempts to make a major contribution towards accurate and fast detection by employing a novel self-designed algorithm for segmentation. Two sub-stages of segmentation along with appropriate pre-processing techniques on the dermoscopic images, enables the classifier to produce better and enriched output for accuracy. The use of YOLO classifier fetches an instant classification outcome without hampering the accuracy. Moreover, modified YOLO classifier produces best fit results with accelerated detection time. PH2, ISIC 2017 and ISIC 2018 dataset are three publicly available datasets that are used for training and testing. The proposed work is evaluated against distinguished research works in today’s time and performs moderately better on evaluating

parameters. Though we have seen reducing mortality rate amongst melanoma victims, more advanced research is still the need of the hour for the benefit of all patients irrespective of the lesion. Therefore, advance and novel methods of pre-processing, segmentation and classification is proposed in chapter 4. Digital artefacts and noise are removed from the acquired image using proposed pre-processing method. Henceforth neutrosophic based segmentation is proposed for accurate segmentation of diseased lesions. A deep learning based model is employed for classification of lesion which increased the accuracy of classification.

Chapter 4: Proposed method for detection of the malignant lesion using neutrosophic analysis

4.1 Introduction

In this section, a novel computed aided diagnosis system (CADs) is proposed for digital diagnoses the suspected lesion. A novel and effective pre-processing phase is introduced in the article which not only removes the artefacts (such as hair follicles, blood vessels, dermoscopic ruler and frames) and reflections from the acquired images but also enhances the image but automatically adjusting contrast and brightness of the image. We have tried to answer few of the most generic but challenging questions like can we segment a lesion from FOV using definite mathematical equation using pixel values? How could we relate matrix representation of an image with different pixel values of the original image and perform the iteration such that we may extract the maximal affected region? To answer these question we have deployed a determinant based segmentation method in our proposed work, which can find absolute region of the affected area from the total image using a computational algorithm. This algorithm is based on construction of 3×3 determinant in order to segment the image and compute the minimal pixel weight for the complete image. Additionally, we have logically selected a threshold value which is compared with the minimal weight of the matrix to select the affected area from the acquired image. Here, we have introduced a neutroscophic number for second phase of segmentation in order to evaluate the exact threshold value such that the image segmentation method can be performed accurately, such that we get more accurate approximation. To tackle the ambiguous portion we have considered a triangular neutroscophic number to calculate the dynamic threshold value. Then the proposed method utilizes the segmented region for classification of lesion using proposed classifiers which is trained over ISIC 2017, ISIC 2018 and ISIC 2019 dataset of dermoscopic images. Huge set of dermoscopic data along with modified layers of classifier help the classifier fetch effective score of sensitivity and specificity.

Moreover, various data tuning methods are being employed in this proposed work, such as augmentation and balancing of data. Our proposed work also evaluates the effect of lesion

segmentation prior to classification and the results portray that data rebalancing, augmentation, and pre-segmentation phase critically increases the classification score. Addition of extra artefact or using weighted classes while training the classifier is termed as data balancing, this method is not adequately addressed in the field of skin lesion diagnostic. The experimental results illustrates that accurate rebalancing of training data could, not only avoid biases for most of its class but also significantly increase the diagnostic performance. The phase of pre-segmentation of dermoscopic image is a critical pre-requisite of CAD, as it assists the classifier to learn relevant features about the lesion and avoid any unreliable features that might be present in FOV of the image, thereby increasing the diagnostic performance. Finally, selection of classifier is also a challenging task as the classification of lesion is mostly dependent on the algorithm and architecture of classifier, thus we have employed classifier which seems to perform significantly well for skin lesion diagnosis. Performance evaluation of proposed method represents the high score of classification accuracy, therefore concluding the effectiveness of proposed method. In the forthcoming sections, preliminaries to neutrosophic number is given which helps the reader know bit about neutrosophic, which is used for segmentation. Thereafter, the proposed method is illustrated in section 4.3, which is followed be performance analysis and discussion in section 4.4 and 4.5 respectively.

4.2 Preliminaries to neutrosophic number

Neutrosophic number is employed for segmentation of skin lesion in this chapter, thus a brief introduction to neutrosophy is mentioned in this section.

Neutrosophic set

$\widetilde{A_{Nue}}$ is considered to be a set in the universal discourse A which is most commonly designated by $'a'$ is termed as a neutrosophic set if $\widetilde{A_{Nue}} = \{(a; [\omega_{\widetilde{A_{Nue}}}(a), \sigma_{\widetilde{A_{Nue}}}(a), \eta_{\widetilde{A_{Nue}}}(a)]) : a \in A\}$, where $\omega_{\widetilde{A_{Nue}}}(a): A \rightarrow]0^-, 1^+[$ is termed as the truth membership method which represents the index of truthiness, $\sigma_{\widetilde{A_{Nue}}}(a): A \rightarrow]0^-, 1^+[$ is called the hesitant membership method which depicts the degree

of uncertainty and $\eta_{\widetilde{A_{Nue}}}(a): A \rightarrow]0^-, 1^+[$ is termed as the inaccuracy membership method which depicts the falsity in the procedure of decision making.

Where, $\omega_{\widetilde{A_{Nue}}}(a), \sigma_{\widetilde{A_{Nue}}}(a)$ & $\eta_{\widetilde{A_{Nue}}}(a)$ Satisfy the following the relation,

$$0^- \leq Sup\{\omega_{\widetilde{A_{Nue}}}(a)\} + Sup\{\sigma_{\widetilde{A_{Nue}}}(a)\} + Sup\{\eta_{\widetilde{A_{Nue}}}(a)\} \leq 3^+ \quad (4.1)$$

Triangular neutrosophic number (TNN)

TNN is employed for calculation of threshold value of each window of 5×5 in a dermoscopic image, thereafter the threshold is employed to segment the lesion and indicate the ROI of the image. A triangular neutrosophic number of is defined as: $\widetilde{\mathrm{A_{Nue}}} = (\mathrm{x1, x2, x3;\ y1, y2, y3; z1, z2, z3})$, whose truth ($T_{\widetilde{A_{Nue}}}$), indeterminacy($I_{\widetilde{A_{Nue}}}$) and falsity($F_{\widetilde{A_{Nue}}}$) membership methods are termed as follows:

$$T_{\widetilde{A_{Nue}}}(a) = \begin{cases} \frac{a - x_1}{x_2 - x_1} \ when\ x_1 \leq a < x_2 \\ 1\ when\ a = x_2 \\ \frac{x_3 - a}{x_3 - x_2} \ when\ x_2 < a \leq x_3 \\ 0\ otherwise \end{cases} \quad (4.2)$$

$$I_{\widetilde{A_{Nue}}}(a) = \begin{cases} \frac{y_2 - a}{y_2 - y_1} \ when\ y_1 \leq a < y_2 \\ 0\ when\ a = y_2 \\ \frac{a - y_2}{y_3 - y_2} \ when\ y_2 < a \leq y_3 \\ 0\ otherwise \end{cases} \quad (4.3)$$

$$F_{\widetilde{A_{Nue}}}(a) = \begin{cases} \frac{z_2 - a}{z_2 - z_1} \ when\ z_1 \leq a < z_2 \\ 1\ when\ a = z_2 \\ \frac{a - z_2}{z_3 - z_2} \ when\ z_2 < a \leq z_3 \\ 0\ otherwise \end{cases} \quad (4.4)$$

Where, $-0 \leq T_{\widetilde{A_{Nue}}}(a) + I_{\widetilde{A_{Nue}}}(a) + F_{\widetilde{A_{Nue}}}(a) \leq 3+, a \in \widetilde{A_{Nue}}$

4.3 Proposed method

This section explains the proposed method in detail which uses different stages of computer aided diagnosis, namely: pre-processing, segmentation, lesion localization and classification. Novel method of pre-processing is introduced in this chapter, which not only enhances the image quality but also digitally removes the artifacts present in it. Unique segmentation phase is proposed in the chapter using neutroscophy and determinant to calculate threshold value for segmentation of lesion.

Thereafter, proposed classifier is employed for classification of skin lesion into malignant and non-malignant class.

4.3.1 Pre-processing

In order to remove noise over acquired input image f[x, y], we have applied a filter n_{σ_s} over the image f[x, y] for such that noise at pixel (i, j) is flattened.

$$Filter = n_{\sigma_s}[i - x, j - y]$$

$$where, n_{\sigma_s}[x, y] = \frac{1}{2\pi\sigma_s^2} e^{-\frac{1}{2}\left(\frac{x^2+y^2}{\sigma_s^2}\right)} \quad (4.5)$$

Thus we get a modified image m[i, j] by applying the filter over the image which is:

$$m[i, j] = \frac{1}{W_b} \sum_x \sum_y f[x, y] n_{\sigma_s}[i - x, j - y] \quad (4.6)$$

In order to maintain the energy in the filter = 1, W_b (Weighting function) is made as adding the product of spatial filter and brightness filter.

$$W_b = \sum_x \sum_y n_{\sigma_s}[i - x, j - y] n_{\sigma_s}(f[x, y] - f[i, j]) \quad (4.7)$$

Although, due to variation in the intensity of image, a global filter alone cannot be employed to reduce digital image noise. Moreover, the image is smoothened to a great extent with increase value of σ_s which might lose few important features of the image and a low value of σ_s might not be effective in the process of noise removal. Thus a dynamic filter is required for enhanced noise filtering. The proposed filter works on the intensity value of the image and the filter is modified for each pixel. If the modular difference between the centre [m, n] and [i, j] is more than $L + s\frac{(f_m - f_p)}{(f_m - f_p) + (f_m - f_s)} - \frac{\sum f_i}{s}$ then the [i, j] is modified to 0 to avoid obsoletion of features. The modified brightness filter can be shown as :

$$n_{\sigma_b}[a] = \frac{1}{\sqrt{2\pi\sigma_b}} e^{-\frac{1}{2}\left(\frac{k^2}{\sigma_b^2}\right)} \quad (4.8)$$

Thus, our modified equation for removal of extra unwanted noise is:

$$m[i,j] = \frac{1}{W_b}\sum_x \sum_y f[x,y] n_{\sigma_s}[i-x, j-y] n_{\sigma_b}(f[x,y] - f[i,j]) \qquad (4.9)$$

As mentioned in equation 4.9, digital noise is removed and the image is smoothen without losing the key features which might be lost if we have only employed Gaussian filter. Artefacts such as the presence of hair follicles (both thin and thick), the presence of blood vessels, a reflection of dermoscopic gel and dermoscopic frames are digitally removed by proposed method. Where the noise free image $m[i,j]_3$ is converted into $m[i,j]_1$, which is a monochromatic image.

Henceforth, m[i, j] is binarize and checked if the selected pixels are continuous or discrete. Continuous and regular block of mask is not considered to be hairs follicles and it is set as background of mask. Thereafter the binarize mask is alternatively diluted and convolved to form prominent lines of hair, which could be masked out from the original image f[x, y]. This method of hair removal also enables to remove marks of dermoscopic ruler and frames.

Finally, the pre-processed image undergoes the process of image enhancement by histogram equalisation to adjust the brightness and contrast of each pixel. The enhances image is further used for lesion localisation and segmentation. Additionally, the accuracy of the proposed method, is illustrated in result and analysis section, which clearly depicts the effectiveness of proposed pre-processing method. Figure 4.1 represented the pre-processing of dermoscopic lesion at different proposed stages.

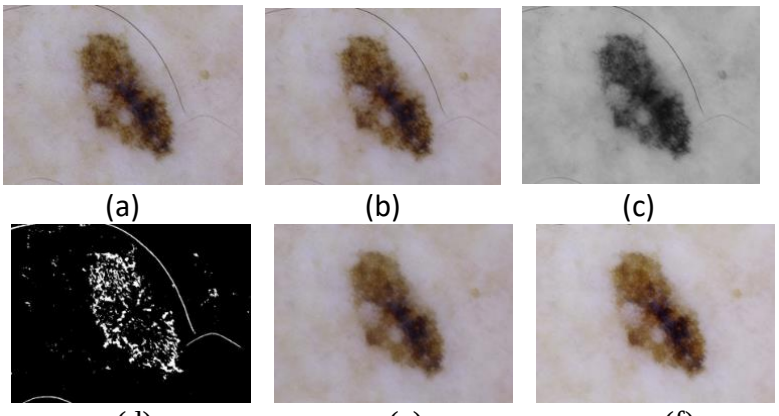

Figure 4.1: Pictorial representation of proposed pre-processing phase (a) Image Acquisition (b) Removal of digital noise (c) Gray scaling of image (d) Binarization of image (e) Removal of artefacts (f) Digitally enhanced images

4.3.2 Segmentation

Initially, an image is acquired and its pixel values is measured in all directions. Henceforth, the image is sliced into finite set of 3×3 order matrices such that the total image can be captured by the sum of all matrices. Thereafter, the determinant value of each 3×3 sized matrix is computed to calculate the absolute values of each sub matrices of the total image. Further, a threshold value ν is selected among the computed determinant value and few of the matrices are selected in the 2nd iteration process according to the threshold value. Lastly the idea of triangular neutrosophic number is incorporated here in order to adjust the proper threshold value.

Case-1: If$|X_i| < \nu$, where$|X_i|$ is the determinant value of the ith matrix of the segmented image, then the matrix is discarded.

Case-2: If$|X_i| \geq \nu$, where $|X_i|$is the determinant value of the ith matrix of the segmented image, then the matrix is accepted for the next round.

The uncertainty set of calculating threshold value ν is tackled by the idea of neutrosophic. A neutrosophic number is capable to define all three components of an uncertain parameter that is : i) true (T) ii) false (F) or iii) hesitation (I) , so in this circumstances Triangular Neutrosophic Number (TNN) is proposed to tackle the threshold value computation. The value of T is 1 and F is 0 and any value in between [0,1] is considered to be I. Therefore, TNN is employed to set the threshold value θ, which yields high score for segmentation. The value of θ is depented on all the three triplets and the values of T, F and I which makes the threshold calculation more generalised for segmentation of all the lesion.

Thus, $\theta = \frac{1}{8}[(\text{a} + \text{b} + \text{c}) \text{ x } (2 + \text{T} - \text{I} - \text{F})]$ such that $T, F, I \in [0,1]$ where (a, b, c) is the triplet represents the triangular neutrosophic number and T denotes the truth; I denotes the indeterminacy; F denotes the falsity part of the membership function. The asymmetrical TNN is also considered, as in real-time situations the threshold value may not always be symmetrical TNN. Thus, the position of b is further fluctuating and can check the dynamic threshold value. This is the biggest

advantage of this computation. Figure 4.2 represented the segmentation performance of the proposed method.

(a) (b) (c)

Figure 4.2: Segmentation of dermoscopic image by proposed method (a) Acquired image (b) Segmentation mask (c) Segmented portion of skin lesion

4.3.3 Classification

Classification is the fundamental phase of computer-aided diagnosis, where the acquired skin lesion image is classified to be malignant or non-malicious by using a recently developed and efficient deep learning model. It is trained over a publicly available and standard dataset of ISIC. The forthcoming subsections deal with a detailed description of datasets that are employed for training and the training parameters used to fetch the best fit results of classification.

4.3.3.1 Augmentation of dataset

Efficient processing of dermoscopic images and accurate classification of skin lesions has emerged as a vital field of research. Accumulation of relevant datasets and accurate training of the classifier under specific parameters has always been a perplexing job. The proposed method is trained over publicly accessible dataset of ISIC 2017, ISIC 2018, and ISIC 2019. These datasets are reliable and easily available, ground truth images are drawn by a panel of expert dermatologists which enable the researchers to compare and evaluate the proposed methodology. A huge set of dermoscopic data not only helps the classifiers to train under rigorous conditions but also increases the test size, thereby producing an enhanced report of classification. Table 4.1 gives a summarized figure of the total number of dermoscopic images for each dataset for training, testing and validation respectively. The sum of each training dataset is three times the original count, as each dermoscopic image is replicated

thrice at an angle of 65^0, 135^0, and 215^0. Additionally, extra artefacts such as thick and thin hair, ruler marks and unwanted reflections are added to these replicated images, such that it can train the classifier to fetch enhanced results under any condition. The augmentation of dataset at various angles is performed to produce modified classification outcome, even for an image acquired at a different angle. The total count of dermoscopic images for training the classifier was 30,946 which is increased to 92,838 after replication of training dataset. Therefore, a total of 100,168 dermoscopic images are used for training, testing and validation in this proposed method.

Table 4.1: Dataset distribution of different datasets that are employed in this section

Dataset	Training	Modified training images	Testing	Validation	Total
PH2	0	0	0	200	200
ISIC17	2000	6000	600	150	6750
ISIC18	8695	26085	1320	0	27405
ISIC19	20251	60753	2530	2530	65813

4.3.3.2 Implementation and training

With the advancement in medical vision and computer-aided diagnostics system, classification of malignant lesion have significantly improved. However, training a classifier to detect a particular class is a strenuous task. Our proposed system is trained with series of inception and residual blocks with softmax layer at each residual unit, which is proved to work most efficiently for skin lesion diagnosis as it can distinguish minute change on skin pigment. Our model is inspired from Inception-Resnet but it has additional softmax at each residual unit which make it more wide and less deep in architecture, therefore enabling it to train faster than inception net, without losing any important features. ISIC 2017, ISIC 2018, and ISIC 2019 datasets are used for training the classifier, with a total of 92,838 images, out of which 14,325 are melanoma images while 78,513 belong to a non-malignant class. Augmentation of training data have increased the accuracy of classification. In order to unify the dataset to overcome the problem of classification for various images of multiple dimensions, the

training images are resized to 480×480 pixels. Additionally, resizing of the dataset also decreases the computational processing of skin lesion classification, thereby increasing training speed. Moreover, the hyperparameters are tuned to achieve high score of accuracy, sensitivity and specificity, and the modifications are as follows: batch size = 32, subdivision = 16, learning rate = 0.0001, decay rate = 0.0005 and momentum = 0.7. The classification result is generated for 50,000 epochs while saving results after each 5,000th epoch. This criterion is evaluated to fetch enhanced classification results as the learning rate is increased by saving epochs after the 5000th phase. The classifier is tested after each 5000th epoch to check the enhanced accuracy of lesion detection, figure 4.3 graphically represents the modified accuracy of classification after each phase. The configuration file generated after training over a huge dataset of ISIC is used to classify skin lesion images of the test dataset.

Localization of lesion is performed by the proposed classifier to form a bounding box across the lesion which will help the system to locate the lesion easily, thereafter, focusing on only the region of interest (inside the bounding box) instead of a field of view (complete image). The performance of the classifier is tested by pre-processing the acquired image, followed by a segmentation phase, henceforth the trained file is used for localization and classification of dermoscopic images.

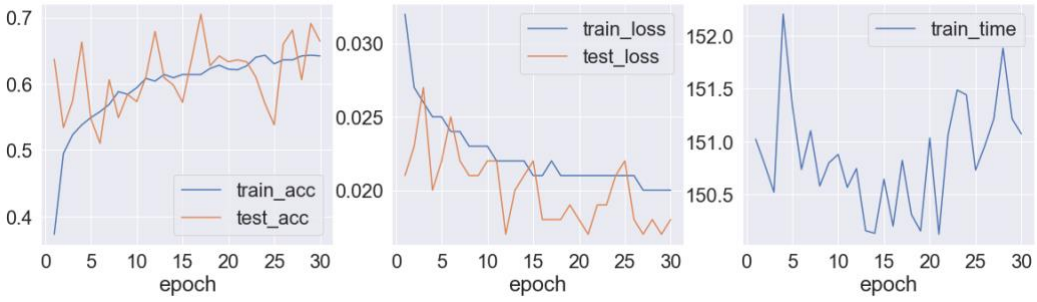

Figure 4.3: Graphical representation of training of proposed classifier (a) Accuracy of classification overtraining and test dataset after every 5,000 epochs (b) Loss of classification score overtraining and test dataset after every 5,000 epochs (c) Training time in milliseconds after every 5,000 epochs

4.4 Performance analysis

This section comprises of a detailed performance analysis of the proposed method. Complete computation and processing of proposed system is computed on Core-i7 processor with 32GB of RAM and 512 GB of SSD. OpenCV framework is used for processing and classification of acquired image on python programming language. Different parameters are used for analysis of performance at various stages of classification, namely: Evaluation of skin refinement, performance analysis of lesion localization, segmentation analysis and evaluation of classification model. Accuracy of the proposed method is evaluated over five publicly accessible dataset: PH2, ISIC 2017, ISIC 2018, and ISIC 2019.

4.4.1 Performance analysis for pre-processing of lesion

Pre-processing of skin lesion is considered to be one of the most important and vital stages in lesion classification. Efficient refinement of skin lesion enhances the classification results, as the pre-processing phase not only modifies the contrast and brightness of dermoscopic image, but also digitally removes the artifacts which might end up misleading the classification result. Table 4.2, 4.3, 4.4 and 4.5 illustrates the performance of removal of artefacts digitally using proposed method for PH2, ISIC 2017, ISIC 2018, and ISIC 2019 datasets respectively. Evaluation metrics like PSNR, MSE, RMSE and UIQI are used to evaluate the accuracy of pre-processing. A low value of MSE and RMSE signifies to robust image enhancement. The loss of energy in pre-processed image is depicted by value of RMSE. It evaluates the difference in intensity of pre-processed and acquired image. Low value of RMSE portrays less distortion of processed image. If the empirical score of PSNR is higher than 20 dB it is considered to be a well-enhancement image. The quality of information sustained in the pre-processed image is portrayed by PSNR, higher values of PSNR depicts more sustained valuable details after removal of artefacts in pre-processed image. The value of UIQI ranges from -1 to 1, which is used to ensure the image quality after enhancing the image. This matrix is used to express the evident change of removal of digital artifacts such as hair and thereafter refining the image

from natural and clinical artifacts like clinical colour swatches, clinical ruler marks, black frame, etc. Image quality is measured by UIQI with respect to human vision by employing parameters like structural information, contrast, and luminance. Thus, it is used to measure the capacity of pre-processing method to remove the artifacts of images along with enhancing the image by modifying its contrast and sharpness, without lowering the image quality.

Table 4.1, 4.2, 4.3 and 4.4 shows highly acceptable range of PSNR and UIQI which represent the high-quality enhancement of images in pre-processing phase. Figure 4.4 pictorially represents the pre-processing phase where artefacts like thick and thin hair, black frame, ruler mark and unwanted reflections are removed digitally by the proposed method of pre-processing. Table 4.5 and 4.6 shows classification of skin lesion with and without undergoing pre-processing phase, the accuracy mark illustrated in the tables for each dataset clearly concludes and supports the importance of pre-processing phase in computer aided diagnostic system. The above mentioned tables shows an enhanced accuracy score of about 8% to 9% when the acquired image is pre-processed. The above-mentioned experimental results and pictorial representation illustrates the need and importance of pre-processing of image before classification.

Table 4.1: Evaluation of performance of pre-processing of PH2 dataset

ARTEFACTS	PSNR	MSE	RMSE	UIQI
THICK HAIR	39.37	34.69	5.89	0.64
THIN HAIR	40.53	12.75	3.57	0.67
RULAR MARKS	37.76	83.54	9.14	0.68
BLACK FRAME	39.64	58.98	7.68	0.65
COLOUR PATCH	38.99	46.51	6.82	0.70

Table 4.2: Evaluation of performance of pre-processing of ISIC 2017 dataset

ARTEFACTS	PSNR	MSE	RMSE	UIQI
THICK HAIR	35.70	37.58	6.13	0.59
THIN HAIR	37.58	32.38	5.69	0.62
RULAR MARKS	32.67	115.99	10.77	0.60
BLACK FRAME	36.00	98.61	9.93	0.61
COLOUR PATCH	35.79	55.80	7.47	0.63

Table 4.3: Evaluation of performance of pre-processing of ISIC 2018 dataset

ARTEFACTS	PSNR	MSE	RMSE	UIQI
THICK HAIR	31.75	62.41	7.90	0.55
THIN HAIR	34.56	62.25	7.89	0.59
RULAR MARKS	32.56	113.42	10.65	0.57
BLACK FRAME	34.67	129.28	11.37	0.60
COLOUR PATCH	33.13	92.54	9.62	0.58

Table 4.4: Evaluation of performance of pre-processing of ISIC 2019 dataset

ARTEFACTS	PSNR	MSE	RMSE	UIQI
THICK HAIR	30.78	110.67	10.52	0.50
THIN HAIR	33.24	71.91	8.48	0.55
RULAR MARKS	29.45	180.37	13.43	0.55
BLACK FRAME	33.45	218.45	14.78	0.50
COLOUR PATCH	32.09	104.45	10.22	0.57

Table 4.5: Classification result without undergoing pre-processing phase

Dataset	Accuracy	Sensitivity	Specificity
PH2	91.00	87.50	91.88
ISIC 2017	91.50	89.34	92.56
ISIC 2018	90.53	89.22	90.97
ISIC 2019	90.35	88.67	90.94

Table 4.6: Classification result after undergoing pre-processing phase

Dataset	Accuracy	Sensitivity	Specificity
PH2	99.50	100	99.38
ISIC 2017	99.33	98.48	99.75
ISIC 2018	98.56	97.61	98.88
ISIC 2019	98.04	96.67	98.52

4.4.2 Performance analysis for localisation of lesion

Localization of suspected lesion is performed using proposed classifier, which forms bounding box around the lesion and marks it to be ROI. Accuracy of localization is measured by metrics such as: mAP and IOU. The acceptable range of IOU for accurate area localization lies from 0.5 to 1. This matric is used to compare the predicted area with the ground truth which are generated by expert dermatologist, in order to calculate the accuracy of localization. Table 4.7 represents performance analysis of lesion localization by proposed classifier on various dermoscopic datasets. The classifier successfully fetches an accuracy of 100% for PH2 and ISIC 2017 for skin lesion localisation which

symbolises the effectiveness of modified layers of classifier along with enhances and enriches pre-processing step. Furthermore, the ISIC 2018 and ISIC 2019 dataset yields an accuracy of 99.40 % and 99.56% respectively which is nearly 100% score, this enhanced tabulated result shows the effectiveness of the classifier and it provides an clear indication of that the modified classifier is capable to fetching improved results of classification of dermoscopic images. Figure 4.5 shows the lesion localization phase using proposed classifier.

Table 4.7: Performance of lesion localization is evaluated for PH2, ISIC 2017, ISIC 2018, and ISIC 2019 dataset.

Datasets	Sen	Spe	mAP	IOU
PH2	100	100	0.94	100
ISIC 2017	100	99.75	0.98	98.99
ISIC 2018	99.40	99.90	0.98	98.21
ISIC 2019	99.56	99.77	0.97	97.79

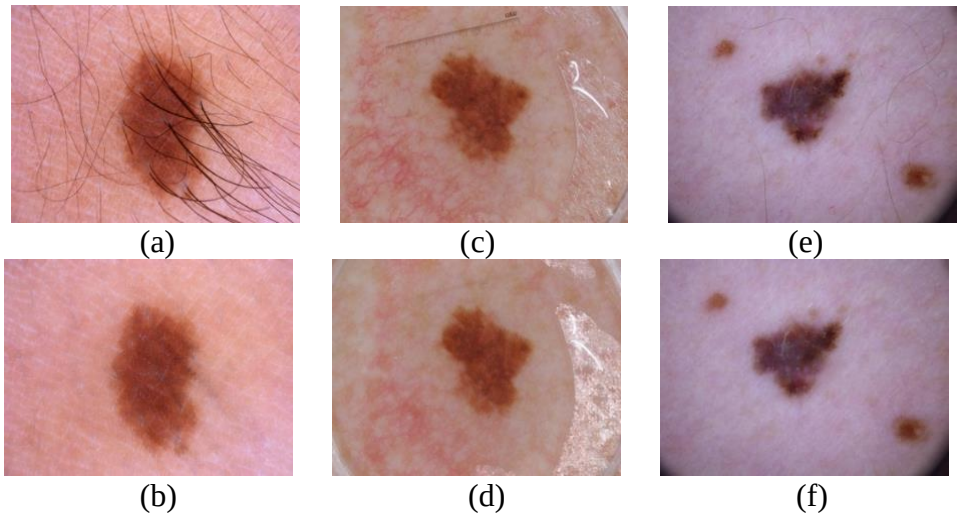

Figure 4.4: Illustration of proposed pre-processing for various artefacts (a) ISIC_0000115 image with thick hair follicle (b) Pre-processed output (c) ISIC_0012395 image with ruler mark (d) Pre-processed output (e) ISIC_0024315 image with thin hair follicles (f) Pre-processed output

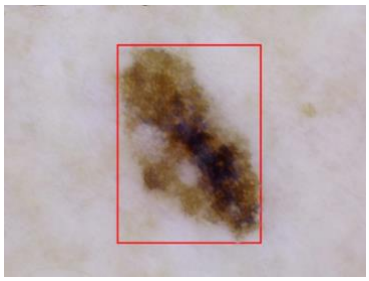

Figure 4.5: Lesion localization using proposed classifier

4.4.3 Performance analysis for segmentation of lesion

Pre-processing phase is followed by segmentation phase, whose accuracy is calculated and compared over parameters such as: Sensitivity, Specificity, Dice score, Jaccard index and Accuracy. Analysis of performance, based on these parameters was proposed by ISIC, who is official organization for publishing free accessible dermoscopic images for research and analysis on skin cancer. Table 4.8 encapsulates the analysis of segmentation performance over different dataset by the proposed method using neutrosophy and determinant method. The novel proposed system seems to fetch an accuracy mark of 99.00% for PH2 dataset, 98.83% for ISIC 2017, 98.56% for ISIC 2018, an 97.86% for ISIC. The system successfully fetches the sensitivity score (Rate of accurate segmentation of True positives) of 97.56% for ISIC 2019, which have visually challenging melanoma image. Similarly, the effectiveness of proposed method is reflected when it attains a mark of 97.97% of specificity (Rate of accurate segmentation of false negatives) for ISIC 2019, which have maximum number of different skin lesion classes which makes it most challenging dataset for even an expert dermatologist to perform accurate segmentation. Figure 4.6 illustrates the value of TP, TN, FP and FN for each dataset along with total count of melanoma and non-melanoma dermoscopic images.

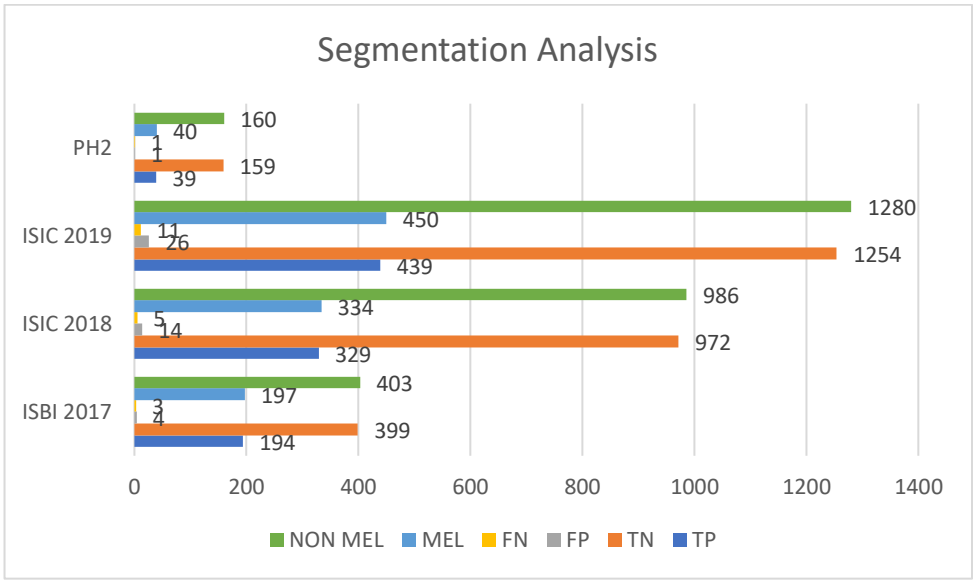

Figure 4.6: Graphical representation of TP, TN, FP and FN values of each dataset.

Table 4.8: Performance analysis of segmentation of each dataset.

Datasets	Acc (%)	Sen (%)	Spe (%)	Jac (%)	Dic (%)
ISBI 2017	98.83	98.48	99.01	96.52	98.23
ISIC 2018	98.56	98.50	98.58	94.54	97.19
ISIC 2019	97.86	97.56	97.97	92.23	95.97
PH2	99.00	97.50	99.38	95.12	97.50

Efficient mathematical logic of uncertainty principle by neutroscopy assists the proposed system to fetch accurate and out-topping score for segmentation of lesion over state-of-art methods. Table 4.10 illustrates comparison between proposed segmentation method and well-established state-of-the-art techniques. Segmentation performance of the proposed work is compared with most inspiring methods for segmentation of dermoscopic images from PH2 dataset. [119] uses two stage segmentation model by employing L-R fuzzy logic and graph theory to yield efficient segmentation results, [104] employs a framework which works on the principal of semantic segmentation model for automatic segmentation. [105] uses alternate segmentation and classification by bootstrapping DCNN model. Grab cut algorithm which is semi-automatic in nature is used by [103] where as a deep convolutional neural network is employed for segmentation by [1]. We have also drawn inspiration for efficient segmentation models which are proposed by [102,107], where FCN networks and multi stage fully convolution network (FCN) with parallel integration (mFCN-PI) is used for segmentation of dermoscopic lesion. However, our proposed method yields 99%, 97.50%,99.36%, 95.12% and 97.50% for accuracy, sensitivity, specificity, Jaccard score and dice index respectively, which is highest score for all the evaluation parameters when compared with state-of-art methods.

Table 4.10: Evaluation of proposed segmentation method against state-of-art methods for PH2 dataset

References	Year	Acc	Sen	Spe	Jac	Dic
Proposed method	**2021**	**99.00**	**97.50**	**99.38**	**95.12**	**97.50**
Banerjee et al. [119]	2020	97.50	97.50	95.50	88.64	93.97
Hasan et al. [104]	2020	98.70	92.90	96.90	----	----
Xie et al. [105]	2020	96.50	96.70	94.60	89.40	94.20
Unven et al. [103]	2019	92.99	83.63	94.02	79.54	88.13
Saba et al. [1]	2019	95.41	----	----	----	----
Bi et al. [102]	2019	95.03	96.23	94.52	85.90	92.10
Bi et al. [107]	2017	94.24	94.89	93.98	83.99	90.66

Comparison of proposed method against recently published and well known segmentation methods for ISIC 2017 dataset is tabulated in Table 4.11. Proposed method is contrasted against state-of-art methods for segmentation such as [112], which utilizes an extension and amendment of FCN architecture, i.e. a fully-convolutional residual networks (FCRN). A robust deep learning SLS model of encoder-decoder network is present by [109] where the dilated residual layers form the encoder network and decoder layer is constructed by a pyramidal pooling network which is followed by three layers of convolution. [108] proposes a simultaneous segmentation and classification model using FrCN to yield high score of specificity for ISIC 2017 dataset. When the proposed segmentation method is computed for ISIC 2017 dataset it yields an accuracy mark of 98.83% while other well-known and published works manages to fetch 97.33%, 95.30%, 81.57%, 95.06%, 93.39%, and 93.60% mark respectively for [119], [104], [112], [102], [103] and [109].

Table 4.11: Evaluation of proposed segmentation method against state-of-art methods for ISIC 2017 dataset

References	Year	Acc	Sen	Spe	Jac	Dic
Proposed method	2021	**98.83**	**98.48**	**99.01**	**96.52**	**98.23**
Banerjee et al. [119]	2020	97.33	91.45	98.76	86.99	93.04
Hasan et al. [104]	2020	95.30	87.5	85.5	----	----
Al-Masni et al. [112]	2020	81.57	75.67	80.62	----	----
Bi et al. [102]	2019	95.06	86.05	95.95	79.15	88.95
Unver et al. [103]	2019	93.39	90.82	92.68	74.81	84.26
Sarker et al. [109]	2018	93.60	81.6	98.3	78.2	87.8
Li et al. [108]	2018	93.20	82.00	97.80	76.20	84.70

Segmentation performance of our method is contrasted against recently published segmentation methods where [120] uses a Difficulty-Guided Curriculum Learning (DGCL), [121] employs a Deep Saliency Segmentation method which employs a custom CNN of 10 convolutions, [122] uses AlexNet along with transfer learning for segmentation. Additionally, few of the most successful segmentation models are proposed by [123] where the performance of U-Net is enhanced by BCDU-Net with convLSTM. [116] designs an architecture based on network of encoder and decoder for segmentation of skin lesion by Deep-Lab and PSP-Net, additionally, extraction of key features are

performed by ResNet101. Notwithstanding the fact that the proposed system yields the accuracy mark of 98.56%, which is better than other well know literature that are mentioned in this dissertation. Our system not only fetches higher score for sensitivity (98.50%) but also shows its effectiveness by yielding highest specificity score of 98.58%. Table 4.12 represents a detailed comparison of proposed segmentation method against state-of-art technology for ISIC 2018 dataset.

Table 4.12: Evaluation of proposed segmentation method against state-of-art methods for ISIC 2018 dataset

References	Year	Acc	Sen	Spe	Jac	Dic
Proposed method	**2021**	**98.56**	**98.50**	**98.58**	**94.54**	**97.19**
Tang et.al [120]	2021	94.80	89.10	96.40	80.70	88.10
Khan et al. [121]	2021	92.69	----	----	----	----
Al mansi et al. [112]	2020	81.79	81.8	71.4	----	----
Hosny et al. [122]	2020	98.70	95.60	99.27	----	----
Azad et al. [123]	2019	93.70	78.50	98.20	93.70	----
Qian et al. [116]	2018	94.20	90.60	96.30	83.80	89.80

Segmentation performance for ISIC 19 dataset is evaluated and compared against [119] which fetches 93.98% score for accuracy, while our method yields 97.86%. Dynamic thresholding using neutrosophic and determinant method, proofs to work efficiently for all the datasets. Thus an enhanced and modified pre-processing along with advance segmentation method will yield a better performance for classification of lesion, which is fundamental aim of this research work. Tabular representation of performance evaluation metrics is illustrated in Table 4.13.

Table 4.13: Evaluation of proposed segmentation method against state-of-art methods for ISIC 2019 dataset

References	Year	Acc	Sen	Spe	Jac	Dic
Proposed method	2021	**97.86**	**97.56**	**97.97**	**92.23**	**95.96**
Banerjee et al. [119]	2020	93.98	91.55	94.84	79.84	88.79

Receiver operating characteristic (ROC) graphs are plotted using True positive rate and false positive rate in Y and X axis respectively. ROC curve is used to analyse the performance of proposed method. Area under curve (AUC) metric is used for assessing performance by calculating the area of ROC curve for each state-of-art method, where area of curve is directly proportional to segmentation performance. The probabilistic curve of ROC and AUC depicts the measure or degree of separation.

It indicates the capacity of classifier to differentiate different classes. High value of AUC represents better classification architecture for prediction of true values as true and false entities as false. Figure 4.7 shows the pictorial representation of ROC curve for different segmentation methods of each dataset. Proposed method seems to cover most of the area of the graph for all the four graphs, thus this represents enhanced performance of segmentation.

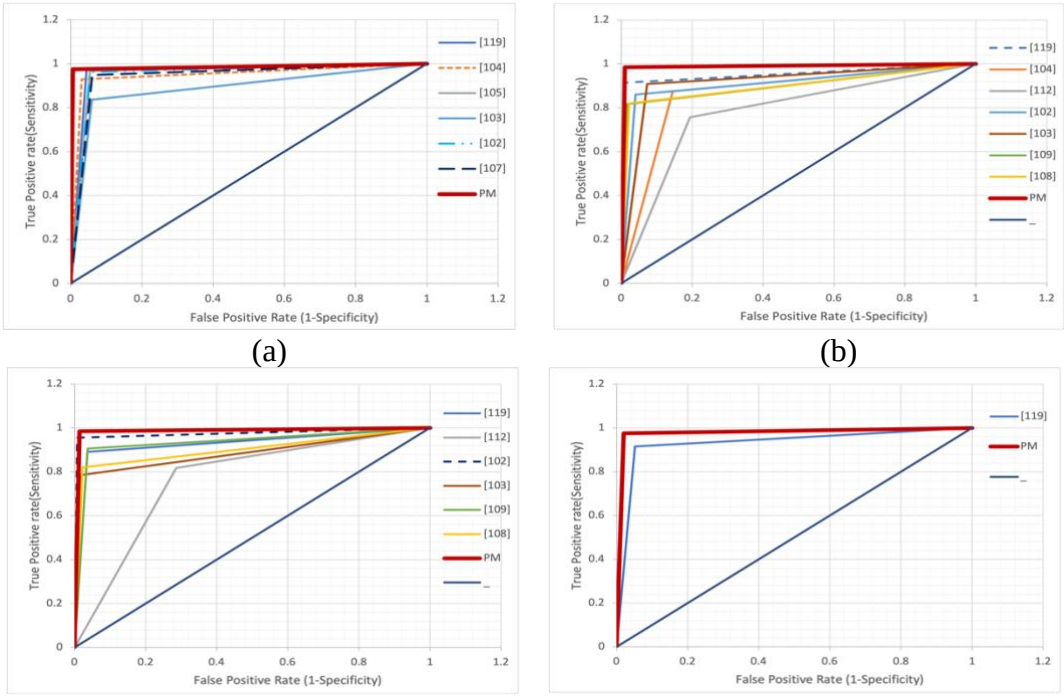

Figure 4.7: ROC curve for (a)PH2, (b)ISIC 2017, (c)ISIC 2018, and (d)ISIC 2019 dataset

4.4.4 Performance analysis for classification of lesion

Classification performance is evaluated for proposed classifier and compared with other well-known classifiers such as YOLO, Decision Tree (DT), Random forest (RF), Multilayer perceptron (MLP), SVM, KNN, Bayesian network (BN), logistic and naïve bayes (NB) algorithm. The performance is evaluated over Accuracy, Sensitivity, Specificity, Precision and F1-Score to determine the accuracy of classification by different classifiers. The performance analysis is tabulated in Table 4.14, 4.15, 4.16 and 4.17 for PH2, ISIC 2017, ISIC 2018 and ISIC 2019 datasets respectively. Proposed classifier proves to perform extremely well for all the four dataset and the statistical figures proved proposed classifier to be much more efficient than any other classifiers that are present in

state-of-art. Proposed classifiers seems to score 99.50%, 99.33%, 98.56%, and 98.04% for classification of dermoscopic lesion from PH2, ISIC 2017, ISIC 2018 and ISIC 2019 datasets respectively. Although the sensitivity score of YOLO classifier for ISIC 2019 dataset is best out of other classifiers(with those which are compared), it scores 97.11% as its sensitivity score whereas proposed classifier is. With such high scoring accuracy marks the modified classifier proves itself to be eligible for execution of the application in real life scenario by dermatologist for diagnosis of skin lesion. Graphical representation of accuracy score for classification of skin lesion by different classifiers on PH2, ISIC 2017, ISIC 2018 and ISIC 2019 dataset is illustrated in Figure 4.8, which clearly indicated the supremacy of proposed classifier over other classifiers for skin lesion identification. It clearly indicates the need to selecting inception and residual block as an ideal classifier for classification of malignant melanoma.

Table 4.14 : Evaluation of classification performance of different classifiers for PH2 dataset

CLASSIFIER	Acc	Sen	Spec	Prec	F1
PROPOSED	**99.50**	**100**	**99.38**	**97.56**	**98.77**
YOLO	97.50	97.5	97.50	90.70	93.98
KNN	94.00	95.0	93.75	79.17	86.36
MLP	95.00	95.0	95.00	82.61	88.37
MG SVM	93.50	90.0	94.38	80.00	84.71
RF	90.00	82.5	91.88	71.74	76.74
NB	90.00	92.5	89.38	68.52	78.72
LINEAR SVM	92.50	90.0	93.13	76.60	82.76
LOGISTIC	90.50	87.5	91.25	71.43	78.65
DT	87.00	82.5	88.13	63.46	71.74
BN	89.50	85.0	90.63	69.39	76.41

Table 4.15 : Evaluation of classification performance of different classifiers for ISIC 2017 dataset

CLASSIFIER	Acc	Sen	Spec	Prec	F1
PROPOSED	**99.33**	**98.48**	**99.75**	**99.49**	**98.98**
YOLO	98.33	96.95	99.01	97.95	97.45
KNN	97.00	94.92	98.02	95.90	95.41
MLP	95.67	92.39	97.27	94.30	93.33
MG SVM	93.67	89.85	95.53	90.77	90.31

RF	93.67	88.33	96.28	92.06	90.16
NB	90.67	86.29	92.80	85.43	85.86
LINEAR SVM	88.17	85.28	89.58	80.00	82.56
LOGISTIC	90.83	86.29	93.05	85.86	86.08
DT	88.50	81.22	92.06	83.33	82.26
BN	85.17	80.20	87.59	75.96	78.03

Table 4.16 : Evaluation of classification performance of different classifiers for ISIC 2018 dataset

CLASSIFIER	Acc	Sen	Spec	Prec	F1
PROPOSED	**98.56**	**97.61**	**98.88**	**96.74**	**97.17**
YOLO	97.50	96.11	97.97	94.14	95.11
KNN	96.36	93.11	97.47	92.56	92.84
MLP	95.08	89.82	96.86	90.63	90.23
MG SVM	93.64	86.53	96.05	88.11	87.31
RF	93.64	87.72	95.64	87.20	87.46
NB	90.91	87.13	92.19	79.08	82.91
LINEAR SVM	86.52	83.54	87.52	69.40	75.82
LOGISTIC	88.79	84.73	90.16	74.47	79.27
DT	87.50	81.14	89.66	72.65	76.66
BN	83.71	83.23	83.87	63.62	72.11

Table 4.17 : Evaluation of classification performance of different classifiers for ISIC 2019 dataset

CLASSIFIER	Acc	Sen	Spec	Prec	F1
PROPOSED	**98.04**	96.67	**98.52**	**95.82**	**96.24**
YOLO	97.92	**97.11**	98.20	95.00	96.04
KNN	97.11	95.33	97.73	93.67	94.49
MLP	95.49	93.56	96.17	89.57	91.52
MG SVM	94.10	91.33	95.08	86.71	88.96
RF	94.05	94.67	93.83	84.36	89.21
NB	87.40	89.11	86.80	70.35	78.63
LINEAR SVM	90.58	93.56	89.53	75.86	83.78
LOGISTIC	90.52	88.44	91.25	78.04	82.92
DT	89.31	90.89	88.75	73.96	81.55
BN	84.80	87.33	83.91	65.61	74.93

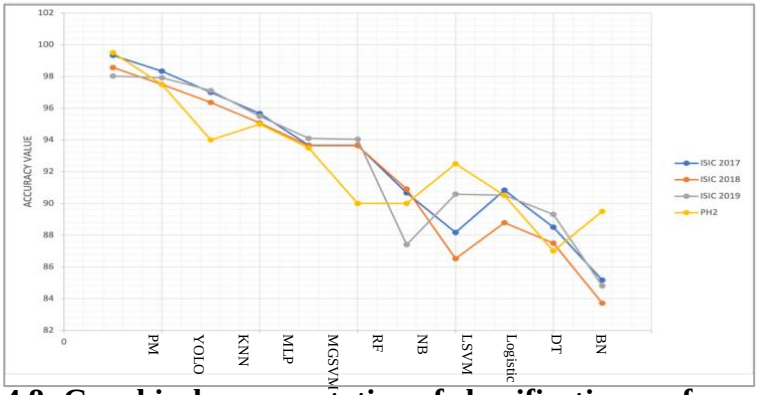

Figure 4.8: Graphical representation of classification performance

The supremacy of proposed classifier is evidently illustrate by the comparisons with well-known classifiers for accurate identification of skin lesion. Proposed classifier yields high score for all the evaluation parameters when compared with recently developed and extensively used classifiers. Due to its ability to distinguish minor difference of pixel coloration for classification, Inception and residual block stands to be most efficient and trustworthy for classification of dermoscopic images. This study also focuses on importance of adequate pre-processing method for removal of artefacts from the acquired image and thereafter enhancing the image, which will help the classifier to fetch such high values of accuracy. Notwithstanding the fact that segmentation of skin lesion using neutroscopy and third order determinant also helps to achieve high value of classification. Complete work flow is represented in Figure 4.9, where each step is pictorially represented. Dermoscopic images from each dataset is chosen to represent the work flow.

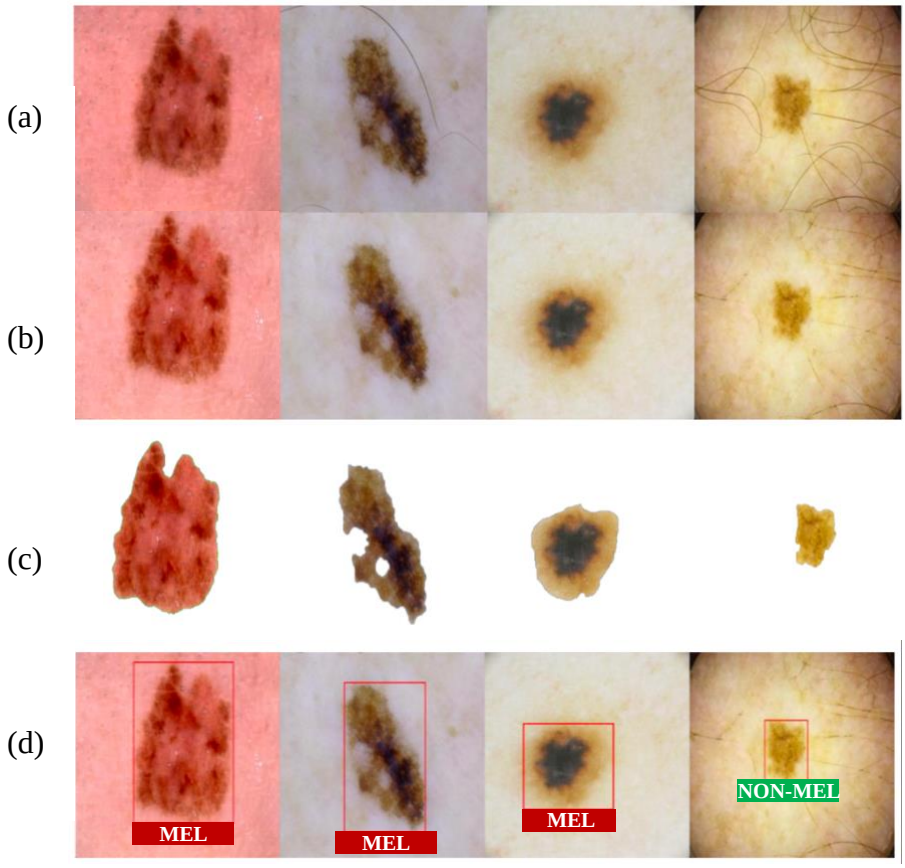

Figure 4.9: Detailed work flow of proposed system (a) Image acquisition (b) Pre-processing (c) Segmentation (d) Classification

4.5 Smart phone app: DermoApp

The dissertation proposes a smartphone application for digital diagnosis of skin lesion. The proposed system is enables image acquisition of suspected lesion through smartphones with the help of digital camera. Furthermore the image is being classified by proposed classifier to detect the type of lesion. Acquired melanoma image is shown in figure 4.10, which shows a lesion with external background feature like skin hairs. The snapped image from the smartphone is pre-processed by the proposed method of noise removal and histogram equalisation, thereafter the digital hair removal algorithms are employed. Henceforth the image is segmented in the background with the process of fuzzy thresholding method. The segmented images is processed for feature extraction, meanwhile the image is classified by proposed classifier. Thereafter the classification result is further matched and confirmed by the feature extraction techniques like ABCD rule and Menzies method. Features like asymmetric nature of lesion, uneven border, variable colour and a diameter of more than 6mm are the

set of signs for a lesion to be classified as melanoma. Features of input images are being extracted and matched with classified result, thereby assuring and increasing the rate of detection. Complete flowchart of the proposed method is described in figure 4.11.

Figure 4.10: Acquired image of melanoma lesion

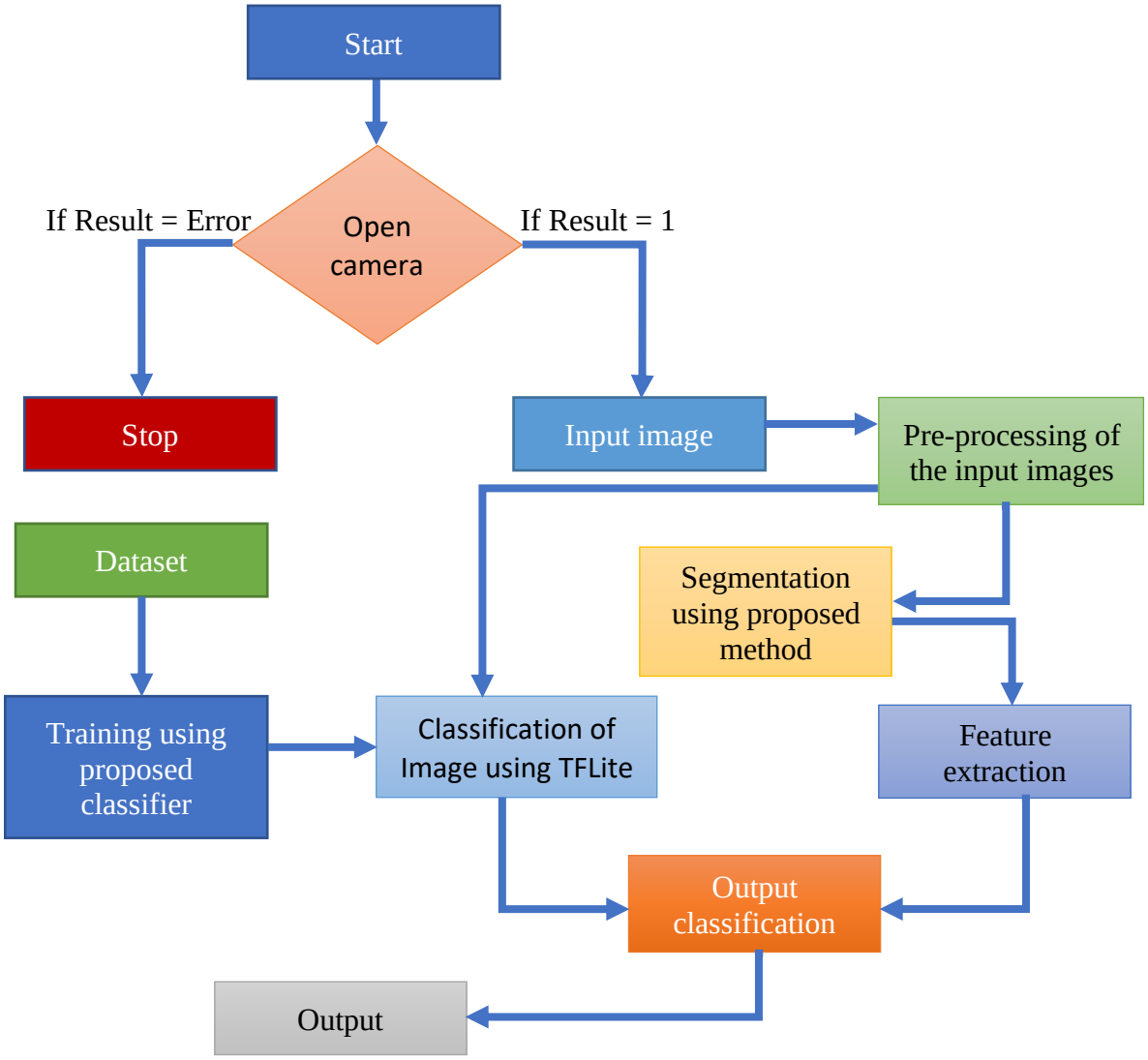

Figure 4.11: Flowchart of proposed smartphone application for diagnosis of lesion

As shown in figure 4.11, the input image is pre-processed by novel techniques and the pre-processed image is further send for segmentation, it is important stage of CAD system as the proposed system uses smartphone for capturing lesion images which is more prone of capturing undesirable noise and artifacts which might affect the classification results. The lesion image is segmented, such that only lesion pixels are sent for feature extraction. Thereby this process proves to be much effective and increases the accuracy mark from 82.79% to 91.33% for image classification. The pre-processed image is being sent for classification using a modified TensorFlow Lite classifier, which is designed to work on smartphones, however the datasets are trained over proposed classifier on remote computer with high end configuration. Advanced mathematics calculations are used for extraction of feature such as Asymmetry, border, colour and diameter, thereafter the results for both feature extraction and classification are classified. The output classification is done on the bayes theorem, the output classification example is illustrated in table 4.18 in detail. Thereafter output for the image lesion is generated with the accuracy result of 96.8%. The complete processing is done by a smartphone application, the images are being processed locally, thus enabling the users from remote location, to use this application without the need of proper network connection, thus they can use the application for quick and easy diagnosis of skin lesion. The application is designed for capturing image lesion with mere smartphone camera, thereafter the image is modified and classified to show the result of diagnosis over the smartphone, this process not only eases and simplifies the diagnosis but also produces diagnosis results within few seconds, moreover this advance computer vision technique is a non-invasive mode of diagnosis which will promote users to diagnose every single-minute lesion present on their body.

Table 4.18: Output classification based of maximum probability

Classification result	Feature Extraction result	Final output
True; Probability = 90%	True; Probability = 85%	Melanomatic lesion
False; Probability = 78%	True; Probability = 37%	Non-Melanomatic lesion
False; Probability = 95%	False; Probability = 98%	Non-Melanomatic lesion
True; Probability = 84%	False; Probability = 12%	Melanomatic lesion

The complete process of diagnosis is performed over a smartphone, which eases the whole process of diagnosis. Figure 4.12 depicts the screenshots of the smartphone application, where a lesion is diagnosed and step wise results are fetched. Accuracy have significantly being increased with the user of novel methods and function that are proposed in the prototype. Accuracy mark from 78.12% for input image classification have jumped to 96.80% for the proposed prototype, which is a significant achievement in the field of computer vision based diagnosis.

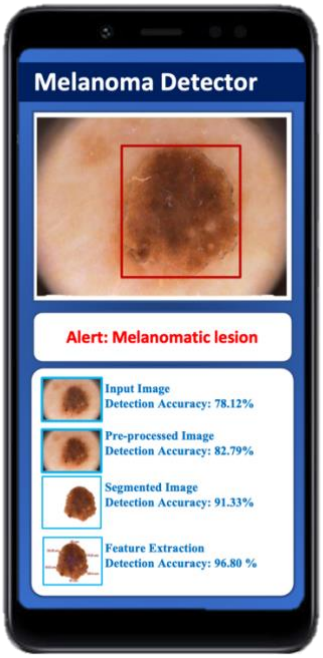

Figure 4.12: Screenshot of proposed smartphone application

We have developed the system while analysing of the disadvantages and limitations of prior diagnostic system. We have briefly inspected all the possible ways available and tried to resolve most of the limitations and even put on some additional attributes. In addition to that we have developed the device in a simple and easy to use manner, such that even non-technical individual can also use the application with same comfort and ease as others.

Here are the list advantages of our system over the prior state-of-art:-

1. **Fast :-** Diagnosis speed have been increased immensely with the use of modern technologies and algorithms. Result of diagnosis is return within few seconds unlike primitive invasive method.

2. **Accurate: -**The proposed device return accurate detection results without the presence of skilled professional. Diagnosis of melanoma lesion produces an accuracy mark of 96.8%, which is more than existing invasive and modern methods.
3. **Non-invasive: -** The proposed method is non-invasive in nature, which indicates that it does not require any painful operation. The method uses a defined dramatology and smartphone for melanoma detection by clicking images through smartphone. These images are been processed by neural network to find malignant melanoma.
4. **Easily Accessible: -** Smartphones are the most widespread and easily accessible device, thus making the proposed prototype easily available for common masses even in remote location, thus enabling them to diagnose skin lesion easily with their comfort.

A smartphone application like this, will not only ease the diagnosis process but also assist an expert dermatologist in the process of decision making. An accurate and easily available tool will increase the rate of diagnosis thereby decreasing the chances of mortality as melanoma can be cured in its situ.

4.6 Discussion

The prevalence of melanoma has been increased consistently in the last few decades and is projected to rise across the globe in near future. It has been noticed that the death rate from melanoma is influenced by the factors like geographical boundaries, nationality, age and gender. There have been manifold attempts to upgrade the accuracy of melanoma diagnosis and thus the development of ingenious ideas have fostered to handle the mortality rate of the disease. In this study, an effective pre-processing model was proposed in order to digitally remove the artefacts present in the acquired image, thereby refining the image for up next segmentation phase, mathematical based algorithm using third-order determinant and neutrosophic is demonstrated to achieve enhanced segmentation results. Henceforth the segmented image is classified using proposed classifier. The studies have been implemented on four widely acceptable datasets such as PH2, ISIC 2017, ISIC 2018 and ISIC 2019.

Moreover, the results of the tests ranging over a numerous criterions claim that the proposed method achieved optimistic end results in comparison to other deep learning-based methodologies. Here, we have analysed the computational steps to eventually scrutinize cancer by the use of different digital and dermatological images from the previously mentioned datasets. The proposed segmentation technique which employs determinant for calculating the mean pixel value of 3×3 matrix and neutrosophic for calculation of uncertain threshold value, have amplified the segmentation results which led to impact the recognition process classification with precision. The proposed characteristics of this study have furnished an appreciable effectiveness to the comprehensive process of cancer diagnosis though there's a lot more to be unveiled, examined and realized in this field. In the future extensive training of the system with a varied range of datasets having several lesions and classification of lesion by upgraded CAD techniques or clinical testing can help to achieve more pronounced output.

Chapter 5: Conclusions and future work

5.1 Summary of achievements and contribution

The dissertation starts with the brief Introduction about the topic in Chapter 1, where the importance and significance of the topic is explained. The evolution of diagnosing techniques over ages are summarized in this section. Furthermore, we have explained the utmost need of computer aided diagnosis for identification of melanoma lesion with proper statistical representation. This section also introduces the novelty of the dissertation, where the proposed methodology for pre-processing, segmentation, feature extraction and classification are explained in brief.

We have reviewed the literature of existing state-of-art technologies in Chapter 2, where we have described various methods for each phase of CAD. Various existing methods for pre-processing and refinement of skin lesion are mentioned in this section. Furthermore, this section throws the light over conventional and modern methods for segmentation and portrays the effectiveness of both the techniques. These methods and approaches are later contrasted against our proposed method, and our method proves to be much more efficient in terms of accuracy score. Traditional methods of classification using Swarm intelligence, genetic algorithms, fuzzy based and decision tree, whereas modern methods such as ANN, KNN, SVM and different models of CNN's are illustrated. Different types of datasets that are used for training the classifier and testing its accuracy is summarized in this section, along with evaluation parameters for each phase of the CAD system. Accuracy and need of each phase are shown in our research work.

Our proposed method was illustrated in Chapter 3 and Chapter 4, where the acquired image follows the CAD steps for accurate classification. In Chapter 3, novel methods of dynamic thresholding by using standard deviation followed by threshold calculation by LR Fuzzy logic is employed for accurate segmentation of skin lesion, which further enhances the classification results. The segmented image is then classified using Yolo v3, which is trained over ISIC 2017 and ISIC 2018. The proposed system yields a mark of 94%, 91% and 90% of IoU metric for PH2, ISIC 2017

and ISIC 2018 dataset respectively. The proposed segmentation method has fetched an accuracy, sensitivity and specificity of 96.50%, 97.50% and 96.25% for PH2; 96.16%, 91.88% and 98.26% for ISIC 2017; 95.91%, 91.62% and 97.37% for ISIC 2018 dataset respectively, this indicates the supremacy of threshold-based segmentation using appropriate mathematical logic. Classification of melanoma lesion for the test images seems to yield an accuracy, sensitivity, and specificity mark of 98.16%, 95.43%, 99.50% respectively. The proposed method also compares the classification performance with and without undergoing segmentation phase, and it results to outperform when segmentation phase is executed. In depth analysis of classification results and comparison of performance with other well-known classifiers have been made to showcase the accuracy of modified classifier. Chapter 4 of this dissertation represents a novel method of pre-processing and digitally removal of artefacts (like hair follicles and blood vessels) present in acquired image. Thereafter, a third-order determinant is used to calculate the average weight of 5×5 matrix which is discard or considered into a segmentation mark based on threshold value which is generated by neutroscopy (a mathematical decision-making tool). Novel and advanced mathematical concepts of neutrosophy enables the system to segment the skin lesion image with an accuracy, sensitivity, and specificity mark of 99.00%, 97.50%, 99.38% for PH2; 98.83%, 98.48%, 99.01% for ISIC 2017; 98.56%, 98.50%, 98.58% for ISIC 2018; and 97.86%, 97.56%, 97.97% for ISIC 2019 dataset respectively. Modified segmentation has also contributed to the classification phase, which is carried out by a proposed classifier using inception and residual blocks with softmax layer after each residual block. Furthermore, data augmentation is performed by addition of artefacts and noise to the training dataset and rotating the images at an angle of 65^0, 135^0, and 215^0 such that the training dataset is increased to 92838 from 30946 images. Training data is increased by data augmentation, where external artefacts such as hair follicles and noise are added to the image and they are rotated at an angle of 65^0, 135^0, and 215^0, thus the training data is increased and it enables the classifiers is able to achieve an accuracy, sensitivity and specificity mark of 99.50%, 100%, 99.38% for PH2; 99.33%, 98.48%,

99.75% for ISIC 2017; 98.56%, 97.61%, 98.88% for ISIC 2018 and 98.04%, 96.67%, 98.52% for ISIC 2019 dataset respectively.

The above mentioned methods are encapsulated and deployed into a smart phone application for easy, reliable, and effective way of a cancer diagnosis. This modern and effective application is not only accessible but also able to detect skin lesions in real-world scenarios with an accuracy of 94.56%. The developed system will be one of the milestones in the process of diagnosis of a malignant lesion. Image can be easily acquired for testing by using high-resolution cameras on smartphones, thereafter the image is automatically processed and with the help of deep learning, the lesion will be classified into malignant or non-malicious. The proposed characteristics of this study have furnished appreciable effectiveness to the comprehensive process of cancer diagnosis though there's a lot more to be unveiled, examined and realized in this field. In the future, extensive training of the system with a varied range of datasets having several lesions and classification of lesions by upgraded CAD techniques or clinical testing can help to achieve a more pronounced output.

5.2 Future work

We aim to develop a fully functional mobile application and a dermoscopy device, which can easily fit on smartphone. The dermoscopic device will magnify and illuminate the skin lesion image while the process of image acquisition, thereby assisting the classifier to produce enhanced classification results as the features of skin lesion will be represented with more precision. We need to design and develop a 3D model which will not only fit a convex lens but also help the flashlight of smart phone to project its light on the surface of skin lesion, thereby properly illuminating the skin surface. The device should be flexible enough such that it could be used by multi sized smartphones with multiple cameras.

Our primary objective is to deploy the proposed system into an easily accessible smartphone application, which can be used for the accurate diagnosis of the lesion. We also aim to increase the

training data by acquiring dermoscopic images from various cancer cure hospitals under the guidance of expert dermatologists, who will further suggest the ground truth results and segmentation mask for the image. These datasets will be acquired at various angles, such that the classifier will be well trained to produce correct classification results in a real-life scenario where individuals might input test images at certain angles. Additionally, increasing the data size will enhance the quality of training which might help in the classification of visually identical generic benign and malignant lesions. The system will also be equipped to for detection of multiple cancerous lesions along with melanoma, which will increase its diversity and usability.

References

1. Saba T, Khan MA, Rehman A et al (2019) Region extraction and classifcation of skin cancer: a heterogeneous framework of deep CNN features fusion and reduction. J Med Syst 43:289. https:// doi.org/10.1007/s10916-019-1413-3
2. Feng, J.; Isern, N.G.; Burton, S.D.; Hu, J.Z. Studies of secondary melanoma on C57BL/6J mouse liver using 1H NMR metabolomics. *Metabolites* **2013**, *3*, 1011–1035.
3. Karimkhani, C.; Green, A.; Nijsten, T.; Weinstock, M.; Dellavalle, R.; Naghavi, M.; Fitzmaurice, C. The global burden of melanoma: Results from the Global Burden of Disease Study 2015. *Br. J. Dermatol.* **2017**, *177*, 134–140.
4. H.L Kaufman, The Melanoma Book: A Complete guide to prevent and treatment, vol. 1, Gotham Books, New York, USA, 2005.
5. American Society of Clinical Oncology. *Melanoma*. 2015: <http://www.cancer.net/cancer-types/melanoma/view-all/>
6. Gandhi, S.A.; Kampp, J. Skin Cancer Epidemiology, Detection, and Management. *Med. Clin. N. Am.* **2015**, *99*, 1323–1335.
7. Mayer, J.E.; Swetter, S.M.; Fu, T.; Geller, A.C. Screening, early detection, education, and trends for melanoma: Current status (2007–2013) and future directions Part II. Screening, education, and future directions. J. Am. Acad. Dermatol. 2014, 71, e1–e611.
8. Rigel, D.S.; Russak, J.; Friedman, R. The evolution of melanoma diagnosis: 25 years beyond the ABCDs. *CA Cancer J. Clin.* **2010**, *60*, 301–316.
9. Lodha, S.; Saggar, S.; Celebi, J.T.; Silvers, D.N. Discordance in the histopathologic diagnosis of difficult melanocytic neoplasms in the clinical setting. *J. Cutan. Pathol.* **2008**, *35*, 349–352.
10. D.S. Rigel, R.J. Friedman, The rationale of the ABCDs of early melanoma. 29 (6) (1993) 1060_/1061.
11. Di Leo G, Paolillo A, Sommella P, Fabbrocini G (2010) Automatic diagnosis of melanoma: a software system based on the 7-point checklist. In: Proc. Annu. Hawaii Int. Conf. Syst. Sci., pp 1–10
12. Madooei A, Drew MS, Sadeghi M, Atkins MS (2013) Automatic detection of blue-white veil by discrete colour matching in dermos- copy images. Lect. Notes Comput. Sci. (including Subser. Lect. Notes Artif. Intell. Lect. Notes Bioinformatics), vol. 8151, no. August 2015
13. MAJ J. Scott Henning, DO, US Army,[a,b] Stephen W. Dusza, MPH,[a] Steven Q. Wang, MD,[a] Ashfaq A. Marghoob, MD,[a] Harold S. Rabinovitz, MD,[c]David Polsky, MD, PhD,[a] and Alfred W. Kopf, MD[a] New York, New York; Fort Sam Houston, Texas; and Plantation, Florida. "The CASH (color, architecture, symmetry, and homogeneity) algorithm for dermoscopy" . 2007 by the American Academy of Dermatology, Inc. doi:10.1016/j.jaad.2006.09.003
14. Miller, A.J., Mihm, M.C., Melanoma, 2006. N Engl J Med 355 (1), 51–65.
15. American Cancer Society (2017) Cancer Facts and Figures 2017. Genes Dev 21(20):2525–2538
16. Siegel RL, Miller KD, Jemal A (2018) Cancer statistics, 2018. CA Cancer J Clin 68(1):7–30
17. Jemal, A.; Siegel, R.; Ward, E.; Hao, Y.; Xu, J.; Thun, M.J. Cancer statistics, 2019. *CA Cancer J. Clin.* **2019**, *69*, 7–34.
18. F.R. Liu, Practical Skin Science, People Health Press, Beijing, 2005.
19. Cancer Research UK, Cancer statistic report on skin cancer, <http://www.cancerresearchuk.org/health-professional/ skin-cancer-statistics/>, 2013 (accessed 08.10.15).
20. INCA, Estimativa 2014: Incidência de câncer no Brasil, INCA, Rio de Janeiro, 2014.
21. Giotis, I.; Molders, N.; Land, S.; Biehl, M.; Jonkman, M.F.; Petkov, N. MED-NODE: A computer-assisted melanoma diagnosis system using non-dermoscopic images. *Expert Syst. Appl.* **2015**, *42*, 6578–6585.
22. Al-Masni MA, Al-antari MA, Choi M-T, Han S-M, Kim T-S (2018) Skin lesion segmentation in dermoscopy images via deep full resolution convolutional networks. Comput Methods Programs Biomed 162:221–231
23. Adegun, A., Viriri, S. (2020) Deep learning technique for skin lesion analysis and melanoma cancer detection: a survey of state-of-the-art; Artificial Intelligence Review; https://doi.org/10.1007/s10462-020-09865-y
24. Afza F, Khan MA, Sharif M, Rehman A (2019) Microscopic skin laceration segmentation and classification: a framework of statistical normal distribution and optimal feature selection. Microsc Res Tech. https://doi.org/10.1002/jemt.23301
25. Deepika K, Bhisham S (2019) Advanced neutrosophic set-based ultrasound image analysis. Neutrosophic set in medical image analysis. Academic Press, Cambridge, pp 51–73
26. Ünver HM, Ayan E (2019) Skin lesion segmentation in dermoscopic images with combination of YOLO and grabcut algorithm. Diagnostics 9(3):72

27. Beuren AT, Janasieivicz R, Pinheiro G, Grando N, Facon J (2012) “Skin melanoma segmentation by morphological approach.” In: Proceedings of the international conference on advances in computing, communications and informatics, pp 972-978
28. Zaqout I (2019) Diagnosis of skin lesions based on dermoscopic images using image processing techniques. In: Pattern recognition-selected methods and applications, IntechOpen
29. Andreas, B.; Giacomel, J. Tape dermatoscopy: Constructing a low-cost dermatoscope using a mobile phone, immersion fluid and transparent adhesive tape. *Derm. Pr. Concept* **2015**, *5*, 87–93.
30. Koehoorn,J.,Sobiecki,A.,Boda,D.,Diaconeasa,A.,Doshi,S.,Paisey,S.,Jalba,A.,Telea,A.:Automateddigitalhairremoval by threshold decomposition and morphological analysis. In: Proc. ISMM. pp. 324–335 (2015)
31. Lee T, Ng V, Gallagher R, Coldman A, McLean D. DullRazor: a software approach to hair removal from images. Comput Biol Med. 1997 Nov;27(6):533-43. doi: 10.1016/s0010-4825(97)00020-6. PMID: 9437554.
32. Xie,F.,Qin,S.,Jiang,Z.,Meng,R.:PDE-basedunsupervisedrepairofhair-occludedinformationindermoscopyimagesof melanoma. Comp. Med. Imag. Graph. 33(4), 275–282 (2009)
33. Kiani, Kimia & Sharafat, Ahmad Reza. (2011). E-shaver: An improved DullRazor (R) for digitally removing dark and light-colored hairs in dermoscopic images. Computers in biology and medicine. 41. 139-45. 10.1016/j.compbiomed.2011.01.003.
34. Abbas, Q., Celebi, M.E., García, I.F.: Hair removal methods: A comparative study for dermoscopy images. Biomed Signal Proc Control 6(4), 395–404 (2011)
35. Fiorese,M.,Peserico,E.,Silletti,A.:VirtualShave:automatedhairremovalfromdigitaldermatoscopicimages.In:Proc .IEEE EMBS. pp. 5145–5148 (2011)
36. Huang, A., Kwan, S., Chang, W., Liu, M., Chi, M., Chen, G.: A robust hair segmentation and removal approach for clinical images of skin lesions. In: Proc. EMBS. pp. 3315–3318 (2013)
37. Joost Koehoorn, André Sobiecki*, Paulo Rauber, Andrei Jalba, and Alexandru Telea, “Efficient and Effective Automated Digital Hair Removal from Dermoscopy Images”; De Gruyter open. DOI 10.1515/mathm-2016-0001
38. Nasir M, Khan MA, Sharif M, Lali IU, Saba T, Iqbal T (2018) An improved strategy for skin lesion detection and classification using uniform segmentation and feature selection-based approach. Microsc Res Tech 18(6):528–543
39. N. Otsu, A threshold selection method from gray-level histograms, IEEE Trans. Syst. Man Cybern. 9 (1) (1979) 62–66.
40. P. Sahoo, C. Wilkins, J. Yeager, Threshold selection using Renyi’s entropy, Pattern Recognit. 30 (1) (1997) 71–84.
41. D. Bradley, G. Roth, Adaptive thresholding using the integral image, J. Graphics Tools 12 (2) (2007) 13–21.
42. H.J. Trussell, Comments on picture thresholding using an iterative selection method, IEEE Trans. Syst. Man Cybern. 9 (5) (1979) 311.
43. L.-K. Huang, M.-J.J. Wang, Image thresholding by minimizing the measures of fuzziness, Pattern Recognit. 28 (1) (1995) 41–51.
44. K. Fukunaga, L. Hostetler, The estimation of the gradient of a density function, with applications in pattern recognition, IEEE Trans. Inf. Theory 21 (1) (1975) 32–40.
45. D. Comaniciu, P. Meer, Mean shift: A robust approach toward feature space analysis, IEEE Trans. Pattern Anal. Mach. Intell. 24 (5) (2002) 603–619.
46. J. MacQueen, et al., Some methods for classification and analysis of multivariate observations, in: Proceedings of the Fifth Berkeley Symposium on Mathematical Statistics and Probability, vol. 1, Oakland, California, United States, 1967, pp. 281–297.
47. D.E. Ilea, P.F. Whelan, Color image segmentation using a spatial k-means clustering algorithm, in: International Machine Vision and Image Processing Conference, Dublin, Ireland, 2006.
48. Bi L, Kim J, Ahn E, Kumar A, Fulham M, Feng D (2017) Dermoscopic image segmentation via multistage fully convolutional networks. IEEE Trans Biomed Eng 64(9):2065–2074
49. Y. Yuan, M. Chao, Y. Lo, Automatic skin lesion segmentation using deep fully convolutional networks with Jaccard distance, IEEE Trans. Med. Imaging 36 (9) (2017) 1876–1886.
50. Y. Yuan, Y. Lo, Improving dermoscopic image segmentation with enhanced convolutional-deconvolutional networks, IEEE J. Biomed. Health Inform. 23 (2) (2019) 519–526.
51. S. Baghersalimi, B. Bozorgtabar, P. Schmid-Saugeon, H.K. Ekenel, J.-P. Thiran, Dermonet: densely linked convolutional neural network for efficient skin lesion segmentation, EURASIP J. Image Video Process. 2019 (1) (2019) 71.
52. Vesal S, Ravikumar N, Maier A (2018) “Skinnet: a deep learning framework for skin lesion segmentation.” In: 2018 IEEE nuclear science symposium and medical imaging conference proceedings (NSS/MIC). IEEE, pp 1–3

53. Barata C, Emre Celebi M, Marques JS (2018) A survey of feature extraction in dermoscopy image analysis of skin cancer. IEEE J Biomed Health Inf 23(3):1096–1109
54. Oliveira RB, Pereira AS, Tavares JMRS (2018) Pattern recognition in macroscopic and dermoscopic images for skin lesion diag- nosis. Lect Notes Comput Vis Biomech 27:504–514
55. Abbes W, Sellami D (2016) Control, and E. E. Departmement. High- level features for automatic skin lesions neural network-based classification. Int Image Process Appl Syst Conf, pp 1–7
56. Ma Z, Tavares JMRS (2017) Effective features to classify skin lesions in dermoscopic images. Expert Syst Appl 84:92–101
57. Shoieb DA, Youssef SM, Aly WM (2016) Computer-aided model for skin diagnosis using deep learning. J Image Gr 4(2):122–129
58. Pathan S, Prabhu KG, Siddalingaswamy PC (2018) Techniques and algorithms for computer aided diagnosis of pigmented skin lesions—a review. Biomed Signal Process Control 39(October):237–262
59. Barata C, Ruela M, Mendonça T, M arques JS (2014) A bag-of-features approach for the classification of melanomas in dermoscopy images: the role of color and texture descriptors
60. Hameed N, Ruskin A, Hassan KA, Hossain MA (2016) A comprehen- sive survey on image-based computer aided diagnosis systems for skin cancer. In: 10th international conference on software, knowledge, information management & applications (SKIMA)
61. Chatterjee S, Dey D, Munshi S (2018) Optimal selection of features using wavelet fractal descriptors and automatic correlation bias reduction for classifying skin lesions. Biomed Signal Process Control 40:252–262
62. Woo S, Lee C (2018) Incremental feature extraction based on decision boundaries. Pattern Recognit 77:65–74
63. Abbas Q, Celebi M E, Serrano C, Fondo I (2013) Pattern classifica- tion of dermoscopy images: a perceptually uniform mod," vol 46, pp. 86–97
64. Hasan MJ, Uddin J, Pinku SN (2017) A novel modified SFTA approach for feature extraction. In: 2016 3rd Int. Conf. Electr. Eng. Inf. Commun. Technol. iCEEiCT 2016, pp. 1–5
65. Haji MS, Alkawaz MH, Rehman A, Saba T (2019) Content-based image retrieval: a deep look at features prospectus. Int J Comput Vision Robot 9(1):14–38
66. Oliveira RB, Filho ME, Ma Z, Papa JP, Pereira AS, Tavares JMRS (2016b) Computational methods for the image segmentation of pigmented skin lesions: a review. Compute Methods Programs Biomed 131:127–141
67. Isasi AG, Zapirain BG, Zorrilla A (2011) Melanomas non-invasive diagnosis application based on the ABCD rule and pattern recognition image processing algorithms. Comput Biol Med 41(9):742–755
68. Iqbal S, Khan MUG, Saba T, Mehmood Z, Javaid N, Rehman A, Abbasi R (2019) Deep learning model integrating features and novel classifiers fusion for brain tumor segmentation. Microsc Res Tech. https://doi.org/10.1002/jemt.23281
69. Capdehourat G, Corez A, Bazzano A, Musé P 2009 Pigmented skin lesions classification using dermatoscopic images. Lect. Notes Comput. Sci. (including Subser. Lect. Notes Artif. Intell. Lect. Notes Bioinformatics), vol. 5856 LNCS, pp 537–544
70. Ruela M, Barata C, Marques JS, Rozeira J (2017) A system for the detection of melanomas in dermoscopy images using shape and symmetry features. Comput Methods Biomech Biomed Eng Imaging Vis 5(2):127–137. https://doi.org/10.1080/21681 163.2015.1029080
71. Goceri E (2019) "Analysis of deep networks with residual blocks and different activation functions: classification of skin diseases." In: 2019 Ninth international conference on image processing theory, tools and applications (IPTA), pp 1-6. IEEE
72. Jamil U, Khalid S (2014) "Comparative study of classification techniques used in skin lesion detection systems." In: 17th IEEE international multi topic conference 2014, pp 266-271. IEEE
73. Khan MQ, Hussain A, Rehman SU, Khan U, Maqsood M, Mehmood K, Khan MA (2019) Classification of melanoma and nevus in digital images for diagnosis of skin cancer. IEEE Access 7:90132–90144
74. Krizhevsky A, SI, Hinton GE (2012) Imagenet classification with deep convolutional neural networks. Adv Neural Inf Process Syst, pp 1097–1105
75. Simonyan K, Zisserman A (2014) "Very deep convolutional networks for large-scale image recognition." arXiv preprint arXiv:1409.1556
76. Chollet F (2017) Xception: deep learning with depthwise separable convolutions. In: Proceedings of the IEEE conference on computer vision and pattern recognition, pp 1251–1258
77. Wu S, Zhong S, Liu Y (2018) Deep residual learning for image steganalysis. Multimed Tools Appl 77(9):10437–10453
78. Xie S, Girshick R, Dollár P, Tu Z, He K (2017) "Aggregated residual transformations for deep neural networks." In: Proceedings of the IEEE conference on computer vision and pattern recognition, pp 1492-1500.

79. Francois-Lavet V, Henderson P, Islam R, Bellemare MG, Pineau J (2018) “An introduction to deep reinforcement learning.” arXiv preprint arXiv:1811.12560
80. Huang G, Liu Z, Van Der ML, Weinberger KQ (2017) Densely connected convolutional networks. In: Proceedings of the IEEE conference on computer vision and pattern recognition, pp 4700–4708
81. Ratul AR, Hamed MM, Lee W-S, Parimbelli E (2019) “Skin lesions classification using deep learning based on dilated convolution.” bioRxiv, 860700
82. Gessert N, Nielsen M, Shaikh M, Werner R, Schlaefer A (2020) “Skin lesion classification using ensembles of multi-resolution EfficientNets with meta data.” MethodsX, p 100864
83. Brinker TJ, Hekler A, Enk AH, Klode J, Hauschild A, Berking C, Schilling B et al (2019) Deep learning outperformed 136–157 dermatologists in a head-to-head dermoscopic melanoma image classification task. Eur J Cancer 113:47–54
84. Alqudah AM, Alquraan H, Qasmieh IA (2019) “Segmented and non-segmented skin lesions classification using transfer learning and adaptive moment learning rate technique using pretrained convolutional neural network.” In: Journal of Biomimetics, Biomaterials and Biomedical Engineering, (Vol 42, pp 67-78) Trans Tech Publications Ltd
85. Akram T, Junaid Lodhi HM, Naqvi SR, Naeem S, Alhaisoni M, Ali M, Haider SA, Qadri NN (2020) A multilevel features selection framework for skin lesion classification. Human-centric Computer Inf Sciences 10:1–26
86. Guha SR, Haque SMR (2020) “Performance comparison of machine learning-based classification of skin diseases from skin lesion images.” In: International conference on communication, computing and electronics systems, pp 15–25, Springer, Singapore
87. El-Khatib H, Popescu D, Ichim L (2020) Deep learning-based methods for automatic diagnosis of skin lesions. Sensors 20(6):1753
88. Almaraz-Damian J-A, Ponomaryov V, Sadovnychiy S, Castillejos-Fernandez H (2020) Melanoma and nevus skin lesion classification using handcraft and deep learning feature fusion via mutual information measures. Entropy 22(4):484
89. Zhang G, Shen X, Chen S, Liang L, Luo Y, Jie Y, Jianwei L (2019) DSM: a deep supervised multi-scale network learning for skin cancer segmentation. IEEE Access 7:140936–140945
90. L. Ballerini, R.B. Fisher, B. Aldridge, J. Rees, A color and texture based hierarchical k-nn approach to the classification of non-melanoma skin lesions Color Medical Image Analysis, vol. 6, 2013, pp. 63–86.
91. T. Mendonc ¸a, P.M. Ferreira, J.S. Marques, A.R. Marcal, J. Rozeira, Ph 2-a dermoscopic image database for research and benchmarking, in: International Conference of the IEEE Engineering in Medicine and Biology Society, Osaka, Japan, 2013, pp. 5437–5440.
92. G. Argenziano, H. Soyer, V. De Giorgi, D. Piccolo, P. Carli, M. Delfino, Interactive Atlas of Dermoscopy (Book and CD-ROM), EDRA Medical Publishing & New Media, Milan, 2000.
93. Tschandl P, Rosendahl C, Kittler H (2018) The HAM10000 dataset, a large collection of multi-source dermatoscopic images of common pigmented skin lesions. Sci Data 5:180161
94. D. Gutman, N.C.F. Codella, E. Celebi, B. Helba, M. Marchetti, Nabin Mishra, and A. Halpern. "Skin lesion analysis toward melanoma detection: A chal- lenge at the international symposium on biomedical imaging (ISBI) 2016, hosted by the international skin imaging collaboration (ISIC)." arXiv preprint arXiv:1605.01397 (2016)
95. N.C. Codella, D. Gutman, M.E. Celebi, B. Helba, M.A. Marchetti, S.W. Dusza and A. e. a. Kalloo, "Skin lesion analysis toward melanoma detection: a challenge at the 2017 International Symposium on Biomedical Imaging (ISBI), hosted by the International Skin Imaging Collaboration (ISIC)," arXiv: 1710.05006, 2017.
96. Codella NCF, Gutman D, Celebi ME, Helba B, Marchetti MA, Dusza SW, Kalloo A et al. (2018) “Skin lesion analysis toward melanoma detection: a challenge at the 2017 international symposium on bio- medical imaging (isbi), hosted by the international skin imaging collaboration (isic).” In: 2018 IEEE 15th international symposium on biomedical imaging (ISBI 2018), pp 168-172. IEEE
97. Marc Combalia, Noel C. F. Codella, Veronica Rotemberg, Brian Helba, Veronica Vilaplana, Ofer Reiter, Allan C. Halpern, Susana Puig, Josep Malvehy: “BCN20000: Dermoscopic Lesions in the Wild”, 2019; arXiv:1908.02288.
98. Rotemberg, V., Kurtansky, N., Betz-Stablein, B., Caffery, L., Chousakos, E., Codella, N., Combalia, M., Dusza, S., Guitera, P., Gutman, D., Halpern, A., Helba, B., Kittler, H., Kose, K., Langer, S., Lioprys, K., Malvehy, J., Musthaq, S., Nanda, J., Reiter, O., Shih, G., Stratigos, A., Tschandl, P., Weber, J. & Soyer, P. A patient-centric dataset of images and metadata for identifying melanomas using clinical context. Sci Data 8, 34 (2021). https://doi.org/10.1038/s41597-021-00815-z
99. Redmon, J.; Farhadi, A. Yolov3: An incremental improvement. arXiv 2018, arXiv:1804.02767.

100. Yen, K.K.; Ghoshray, S.; Roig, G. A linear regression model using triangular fuzzy number coefficients. Fuzzy Sets Syst. 1999, 106, 166–167.
101. R. Joseph and A. Farhadi, "YOLO9000: better faster stronger", Proceedings of the IEEE Conference on Computer Vision and Pattern Recognition, pp. 7263-7271, 2017.
102. Bi, L.; Kim, J.; Ahn, E.; Kumar, A.; Feng, D.; Fulham, M. Step-wise integration of deep class-specific learning for dermoscopic image segmentation. Pattern Recognit 2019, 85, 78–89.
103. Ünver, H.M.; Ayan, E. Skin Lesion Segmentation in Dermoscopic Images with Combination of YOLO and GrabCut Algorithm. Diagnostics 2019, 9, 72.
104. Hasan, K.M.; Dahal, L.; Samarakoon, N.P.; Tushar, I.F.; Martí, R. DSNet: Automatic dermoscopic skin lesion segmentation. Comput. Biol. Med. 2020, 120, 1–10.
105. Xie, Y.; Zhang, J.; Xia, Y.; Shen, C. A Mutual Bootstrapping Model for Automated Skin Lesion Segmentation and Classification. IEEE Trans. Med Imaging 2020, 39, 2482–2493.
106. Yuan, Y. Automatic skin lesion segmentation with fully convolutional-deconvolutional networks. arXiv 2017, arXiv:1703.05165.
107. Bi, L.; Kim, J.; Ahn, E.; Feng, D. Automatic skin lesion analysis using large-scale dermoscopy images and deep residual networks. arXiv 2017, arXiv:1703.04197.
108. Li, Y.; Shen, L. Skin Lesion Analysis towards Melanoma Detection Using Deep Learning Network. Sensors 2018, 18, 556. [CrossRef]
109. Sarker et al. SLSDeep:Skin lesion segmentation based on Dilated residual and pyramid pooling networks. International conference on Medical Image Computing and Computer-Assisted Intervention- MICCAI 2018, 2018, Vol 11071.
110. Soudani, A.; Barhoumi, W. An image-based segmentation recommender using crowdsourcing and transfer learning for skin lesion extraction. Expert Syst. Appl. 2019, 118, 400–410.
111. Akram, T.; Lodhi, J.M.H.; Naqvi, R.S.; Naeem, S.; Alhaisoni, M.; Ali, M.; Haider, A.S.; Qadri, N.N. A multilevel features selection framework for skin lesion classification. *Hum. Cent. Comput. Inf. Sci.* **2020**, *10*, 1–26.
112. Al-masni, A.M.; Kim, D.; Kim, T. Multiple skin lesions diagnostics via integrated deep convolutional networks for segmentation and classification. Comput. Methods Programs Biomed. 2020, 190, 1–12.
113. A. H. Shahin, K. Amer and M. A. Elattar, "Deep Convolutional Encoder-Decoders with Aggregated Multi-Resolution Skip Connections for Skin Lesion Segmentation," *2019 IEEE 16th International Symposium on Biomedical Imaging (ISBI 2019)*, 2019, pp. 451-454, doi: 10.1109/ISBI.2019.8759172.
114. Ji Y, Li X, Zhang G, Lin D, Chen H (2018) Automatic skin lesion segmentation by feature aggregation convolutional neural network. ISIC
115. Koohbanani NA, Jahanifar M, Tajeddin NZ, Gooya A(2018) "Leveraging transfer learning for segmenting lesions and their attributes in dermoscopoy images", ISIC
116. Qian C, Jiang H, Liu T (2018)"Skin lesion analysis" ISIC
117. Chakraborty. A., Mondal, S. P., Mahata, A., & Alam, S. (2021). Different linear and non-linear form of trapezoidal neutrosophic numbers, de-neutrosophication techniques and its application in time-cost optimization technique, sequencing problem. RAIRO-Operations Research, 55, S97-S118.
118. Moolayil. J, John S," Learn Keras for Deep Neural Networks", Apress, Berkeley, CA. https://doi.org/10.1007/978-1-4842-4240-7
119. Banerjee, S., Singh, S. K., Chakraborty, A., Das, A., & Bag, R. (2020). Melanoma diagnosis using deep learning and fuzzy logic. Diagnostics, 10(8), 577.
120. Tang, P., Yan, X., Liang, Q., & Zhang, D. (2021). AFLN-DGCL: Adaptive Feature Learning Network with Difficulty-Guided Curriculum Learning for skin lesion segmentation. Applied Soft Computing, 110, 107656.
121. Khan, M. A., Sharif, M., Akram, T., Damaševičius, R., & Maskeliūnas, R. (2021). Skin lesion segmentation and multiclass classification using deep learning features and improved moth flame optimization. Diagnostics, 11(5), 811.
122. Hosny, K. M., Kassem, M. A., & Fouad, M. M. (2020). Classification of skin lesions into seven classes using transfer learning with AlexNet. Journal of digital imaging, 33(5), 1325-1334.
123. Azad, R., Asadi-Aghbolaghi, M., Fathy, M., & Escalera, S. (2019). Bi-directional ConvLSTM U-Net with densley connected convolutions. In Proceedings of the IEEE/CVF International Conference on Computer Vision Workshops (pp. 0-0).